Western University
Scholarship@Western

Digitized Theses | Digitized Special Collections

1989

Chemical Durability Of Simulated Nuclear Waste Glasses And Their Natural Analogues In Submarine Conditions

Zhihong Zhou

Follow this and additional works at: https://ir.lib.uwo.ca/digitizedtheses

Recommended Citation
Zhou, Zhihong, "Chemical Durability Of Simulated Nuclear Waste Glasses And Their Natural Analogues In Submarine Conditions" (1989). *Digitized Theses*. 1859.
https://ir.lib.uwo.ca/digitizedtheses/1859

This Dissertation is brought to you for free and open access by the Digitized Special Collections at Scholarship@Western. It has been accepted for inclusion in Digitized Theses by an authorized administrator of Scholarship@Western. For more information, please contact tadam@uwo.ca, wlswadmin@uwo.ca.

National Library of Canada
Bibliothèque nationale du Canada

Canadian Theses Service
Service des thèses canadiennes

Ottawa, Canada
K1A 0N4

NOTICE

The quality of this microform is heavily dependent upon the quality of the original thesis submitted for microfilming. Every effort has been made to ensure the highest quality of reproduction possible.

If pages are missing, contact the university which granted the degree.

Some pages may have indistinct print especially if the original pages were typed with a poor typewriter ribbon or if the university sent us an inferior photocopy.

Reproduction in full or in part of this microform is governed by the Canadian Copyright Act, R.S.C. 1970, c. C-30, and subsequent amendments.

AVIS

La qualité de cette microforme dépend grandement de la qualité de la thèse soumise au microfilmage. Nous avons tout fait pour assurer une qualité supérieure de reproduction.

S'il manque des pages, veuillez communiquer avec l'université qui a conféré le grade.

La qualité d'impression de certaines pages peut laisser à désirer, surtout si les pages originales ont été dactylographiées à l'aide d'un ruban usé ou si l'université nous a fait parvenir une photocopie de qualité inférieure.

La reproduction, même partielle, de cette microforme est soumise à la Loi canadienne sur le droit d'auteur, SRC 1970, c. C-30, et ses amendements subséquents.

NL-339 (r. 88/04) c

Canada

CHEMICAL DURABILITY OF SIMULATED NUCLEAR WASTE GLASSES AND THEIR NATURAL ANALOGUES IN SUBMARINE CONDITIONS

by

ZHIHONG ZHOU

Department of Geology

Submitted in partial fulfilment
of the requirements for the degree of
Doctor of Philosophy

Faculty of Graduate Studies
The University of Western Ontario
London, Ontario
April 1989

© Zhihong Zhou 1989

National Library of Canada
Bibliothèque nationale du Canada

Canadian Theses Service
Service des thèses canadiennes

Ottawa, Canada
K1A 0N4

The author has granted an irrevocable non-exclusive licence allowing the National Library of Canada to reproduce, loan, distribute or sell copies of his/her thesis by any means and in any form or format, making this thesis available to interested persons.

L'auteur a accordé une licence irrévocable et non exclusive permettant à la Bibliothèque nationale du Canada de reproduire, prêter, distribuer ou vendre des copies de sa thèse de quelque manière et sous quelque forme que ce soit pour mettre des exemplaires de cette thèse à la disposition des personnes intéressées.

The author retains ownership of the copyright in his/her thesis. Neither the thesis nor substantial extracts from it may be printed or otherwise reproduced without his/her permission.

L'auteur conserve la propriété du droit d'auteur qui protège sa thèse. Ni la thèse ni des extraits substantiels de celle-ci ne doivent être imprimés ou autrement reproduits sans son autorisation.

ISBN 0-315-51759-X

Canada

ABSTRACT

Glass corrosion in MCC-1 tests at 90°C was characterized by dissolution of glass and formation of surface layers. All three glasses studied showed greater durability in seawater (SW) than in distilled and deionized water (DDW). In DDW, the amount of dissolution was 4.40 and 5.38 μm in 360 days for ABS-113 and basaltic glasses respectively, and was 33.30 μm in 180 days for PNL 76-68 glass. The amount of dissolution in the same period was about three times smaller in SW for all the glasses.

Among three types of glass, PNL 76-68 was least stable in both DDW and SW. ABS-118 glass and basaltic glass showed comparable dissolution rates. The rate of glass dissolution decreases with reaction time (progress). The " final rate" of dissolution of ABS-118 and basaltic glasses in SW is about 0.76 μm/y; that of PNL 76-68 glass is about one order magnitude greater.

Glass corrosion proceeded much slower at 30°C than 90°C. The mechanisms of glass corrosion at the two temperature scales are similar. The glass specimen corroded in oceanic muds exhibit even less change.

The composition of surface layers depends both on glass and leachant compositions. In DDW, they were enriched in insoluble elements such as Fe, Al, Zn, REE, etc.; surface layers developed in SW were enriched in Mg and Cl, but also Fe, Al, and Zn. The surface layers in both leachants were very

poor in crystallinity. In SW, Mg enriched layer silicate(s) was the dominant component in surface layers of all the three glasses. A reaction zone was found between surface layer and unaltered glass. This was usually less than 1000 Å and depleted in soluble elements such as B, Na, and Mo. For PNL 76-68 glass, Si was also depleted in this zone. When SW was used as leachant, Mg was found to diffuse through the reaction zone.

Glass corrosion consists of three successive stages: (1) ion-exchange between alkalis in glass and H_3O^+ (and/or Mg^{2+}) in leachant; (2) formation of a reaction zone depleted in B, Na, Li, Mo, and Si; and (3) slow dissolution of the reaction zone at solid/solution interface accompanied by diffusion of ions from the fresh glass boundary, and subsequent precipitation of hydroxides and silicates. The dissolution reaction slows down when silicate phases attain saturation. Mg diffusion through the reaction zone and rapid saturation of Mg layer silicate contribute to the enhanced stability of the glasses in SW.

Palagonitization of basaltic glass from DSDP Site 335 bears remarkable similarities to the corrosion processes in the laboratory conditions. The changes in composition of palagonite with physicochemical conditions was assumed to reflect the thermodynamic control on its formation. This argument, together with the authigenic minerals precipitated in the vicinity of palagonite, suggested that the release of major constituents will be controlled by solubilities of

phases formed from the elements involved.

The dissolution rate of basaltic glass at Site 335 was found to be 1 μm/ky. Glass shards in pelagic clays have much slower dissolution rate. The explosive textures of the glass shards are well preserved and suggested that little alteration has taken place. After temperature correction, the laboratory determined dissolution rate was found to be the same order as those of basaltic glass from Site 335. At 90°C, the glasses studied would dissolved at a rate of a few to a few tens of micrometers per year. The basaltic and simulated ABS-118 glasses would have a dissolution rate of a few micrometers per thousand years at 10°C. The rate for PNL 76-68 glass should be an order of magnitude greater.

ACKNOWLEDGEMENTS

I am sincerely grateful to Dr. W.S. Fyfe for suggesting this topic, providing research funds and inspiration throughout the course of this work. I also appreciate Dr. Fyfe for his humanistic help whenever I needed it. I thank Dr. F.L. Sayles of the Woods Hole Institution of Oceanography for his constructive input at the planning stage of this study and for providing natural seawater and oceanic muds. The DSDP samples were provided by U.S. National Science Foundation and the Department of Geology, Dalhousie University. Dr. W. Church of this department kindly provided the basalt samples.

I thank Dr. K. Tazaki for her instruction on using electron microscopes and Dr. S.J. van der Gaast of The Netherlands Institute for Sea Research for his assistance with low-angle XRD analysis. I sincerely thank Dr. I. Muir of the Chemistry Department for his extremely kind assistance with glass making and SIMS analysis. I thank Mr. J. Forth for his remarkable patience in cutting and polishing hundreds of glass beads and many other delicate samples, Mr. G. Wood and Mr. R. Shirran for their assistance with setting up the experimental apparatus, Mr. R.L. Barnett and D. Kingston for their time spent on non-routine probe analyses, Mr. D.A. Tel of the Department of Land Resources, University of Guelph and Dr. C. Hu of Plant Sciences, UWO for their assistance with photospectroscopy analysis, Dr. A. Crowe of The National Water Research Institute and Dr. B. Grambow of The Hahn-Meitner

Institute of West Germany for letting me use their PC-PHREEQE computer programs, and Dr. E.J. Reardon of the University of Waterloo for his help with PHREEQE computer program.

I also thank my fellow graduate students George and Kathy Albino, Roba Gaba, Mike Powell, Bill Shotyk and Steve Talman for their friendship and various kinds of help. Among many other things, Steve led me to the world of reaction kinetics; Bill, George and Kathy spent countless hours on improving my skill in English writing and patiently taught me the Canadian culture. My life at the university was also made easier by the professional administration of Dr. R.W. Hodder and Ms. J. Ainge. Drs. R. Dayal and A.T. Jukabick of Ontario Hydro are acknowledged for their support during the course of my thesis writing. I thank R. Tsang and A. Vorauer for their help with computer drafting. Most of all, I would like to thank my parents who, for more than thirty years, have always tried to offer me the very best regardless of the cost of themselves. Finally I have to say that it was not a laughing matter for me to start working before completing my thesis. I was able to do both at the same time only because I have a wonderful wife who shared the difficult time with me and helped me through.

TABLE OF CONTENTS

List of Tables

List of Figure

List of Plates

The author of this thesis has granted The University of Western Ontario a non-exclusive license to reproduce and distribute copies of this thesis to users of Western Libraries. Copyright remains with the author.

Electronic theses and dissertations available in The University of Western Ontario's institutional repository (Scholarship@Western) are solely for the purpose of private study and research. They may not be copied or reproduced, except as permitted by copyright laws, without written authority of the copyright owner. Any commercial use or publication is strictly prohibited.

The original copyright license attesting to these terms and signed by the author of this thesis may be found in the original print version of the thesis, held by Western Libraries.

The thesis approval page signed by the examining committee may also be found in the original print version of the thesis held in Western Libraries.

Please contact Western Libraries for further information:
E-mail: libadmin@uwo.ca
Telephone: (519) 661-2111 Ext. 84796
Web site: http://www.lib.uwo.ca/

CHAPTER 1 - INTRODUCTION

1.1 Opening Statement

The nuclear industry has produced and will continue to produce large amounts of radioactive wastes. Such wastes usually contain tens of radionuclides with half lives ranging from less than one second to more than several million years, and will remain harmful to human beings for hundreds of thousands of years. Safe disposal of radioactive wastes is to isolate them from the human environment (biosphere) in such a way that no further surveillance will be required, and that the environmental impact of these disposed wastes on future generations will be within present-day acceptable limits. Most of the world's high level radioactive waste is incorporated into borosilicate glass. Thus it is evident that the long-term stability of nuclear waste glass is one of the critical aspects of nuclear waste management.

The current strategy for disposal of nuclear waste is to seal it in vaults constructed within stable geological formations in continents (Brookins, 1984). Although scientific research on the continent disposal of radwaste has made measurable progress in the past thirty years, the political and social problems caused by the disposal strategy are worrisome (Kullenberg, 1986). An alternative option to this strategy is to dispose the wastes in sub-seabed sediments (Hollister et al., 1981). The latter concept is attractive because two thirds of the Earth's surface is covered by

seawater, and abyssal clay formations (oxidized red clay) covers nearly 30 percent of the sea floor and hence 20 percent of the earth's surface. The pelagic clays are vertically and laterally uniform, with low permeability, very high cation retention capacity, and exhibit a potential for self-healing when disturbed (Hollister et al., 1981). All of these qualities are desirable for the safe disposal of nuclear wastes.

With respect to the strategy of sub-seabed disposal of nuclear wastes, the isolation of nuclear wastes relies on a series of barriers to prevent radionuclide release to the accessible environment. This is the so-called Multiple-Barrier Principle which includes both the near-field and far-field barriers. The near-field barriers include the waste form, canister, and the sediments within the maximum extent of the 100°C isotherm. The far-field barrier is the thermally unaltered sediments outside the 100°C isotherm.

One of the unresolved problems inherent in sub-seabed disposal of radwaste glass is the corrosion behaviour and long-term stability of the glass in this environment. A thorough understanding of the problem is essential in assessing the concept of sub-seabed disposal of nuclear wastes. Laboratory corrosion tests on radwaste glass have been carried out extensively during the past years using distilled and simulated ground waters. However, the chemistry of sediment pore water is significantly different from that of distilled and ground waters and solution chemistry is known

to affect glass corrosion. It is thus necessary to conduct corrosion tests using seawater or sedimentary pore water in order to obtain relevant information for subseabed disposal of nuclear wastes.

Most durability data of radwaste glass are from laboratory tests of simulated waste glass, which may be adequate for evaluating the relative merits/shortcomings of various waste form compositions and for assessing critical environmental parameters controlling corrosion. However these data alone can not yield reliable rate constant over long-term corrosion. The long-term stability of radwaste glass must be predicted from extrapolations of short-term laboratory data and then verified. Such verification is only possible by comparing the glasses with their closest natural analogues (Lutze et al., 1986). Volcanic glasses of known geological history are suitable for this purpose, because they have existed in natural environments for millions of years, and are structurally similar to radwaste glass. The validity of volcanic glasses as natural analogues to radwaste glass has been discussed by Ewing (1979), Allen (1982), Ewing and Jercinovic (1987), Lutze et al.(1988), Byers et al.(1987). Lutze et. al. (1986) and Zhou et al.(1988) demonstrated experimentally the similarity in corrosion behaviour between volcanic glasses and waste glasses. A careful examination of the natural alteration process is also required in order to improve our confidence in using volcanic glass as valid analogues.

The mechanism and kinetics of waste glass corrosion must be known in order to make reliable predictions of its long-term stability. This is not a simple task, but can be closely approximated by careful analysis of the corrosion data from laboratory tests and natural environments. Recently, there have been many arguments that diffusion controlled leaching is not a rate controlling step in glass dissolution, and that surface reactions dominate the kinetics of glass corrosion (e.g. Grambow, 1985; Bunker, 1987). Most of these models are based solely on solution chemistry and sometimes only on data of silica release. However, owing to similarities in the functional form of the integrated rate equation for different kinetic constraints, the nature of the rate-limiting step in glass corrosion processes cannot be deduced with confidence solely from observations of changes in solution composition as function of time. In fact, experimental uncertainties and ambiguities commonly permit alternate interpretation of such data in terms of first order, second order, logarithmic, parabolic, or linear rate laws.

On the other hand, recent studies on feldspar dissolution indicate that characteristics of leached mineral can provide constraints on dissolution kinetics (Berner and Holdren, 1977; Nesbitt and Muir, 1988; Muir et al., 1989; Banfield and Eggleton, 1989). It was our intention in this study to combine solution chemistry with material characterization on corroded glass. Attention was also paid to chemical and physical properties of the reaction front. Although this front is no

more then a few hundreds of angstroms in thickness, it is this portion of glass which undergoes dissolution reactions. Clearly, kinetic models of glass corrosion must consider both the solution chemistry and the effects of corroded glass.

1.2 Purposes and Methodology of This Study

This study was initiated to investigate the corrosion behaviour of nuclear waste glass in marine environments, to evaluate the validity of natural analogues, and to predict the long-term stability of radwaste glass in marine environments. The approach taken here is more empirical than theoretical. Two steps were taken to achieve these objectives. First, laboratory corrosion tests were conducted on both simulated radwaste and volcanic glasses. The goal here was to document the corrosion behaviours of the glasses in seawater and oceanic sediments at room and elevated temperatures. This allows an assessment of most important environmental parameters in glass corrosion, and, most importantly, ensures that the corrosion mechanism and reaction kinetics are the same or at least comparable for volcanic glasses and borosilicate radwaste glasses. The relative stability among and between waste and natural glasses may be deduced from the testing data, and this comparison may lend confidence to the use of volcanic glasses as natural analogues of radwaste glasses.

In the second step, the alteration of volcanic glasses from mid-ocean ridges and pelagic sedimentary environments

were studied. The alteration rate of glasses from such environments can provide the best implication for the long-term durability of radwaste glasses in marine sediments. By characterizing the alteration process and products, we are able to compare them with those in laboratory tests. If a positive correlation is found, information gained in laboratory would be useful in modelling the long-term performance of waste glass under field.

It should be emphasized that glass corrosion is a complex process and many physicochemical parameters may affect the rate of glass dissolution. Many of these such as pH, pressure, radiation, and so on, are not addressed in this study. The corrosion tests at 30°C were conducted only to see if the mechanism of glass corrosion would be changed with temperature but were not designed to derive the activation energy.

1.3 Organization

This chapter introduces the problems, provide some general background information, and defines the objectives of the research. There are two major parts in this thesis. The first part deals with the experimental studies and includes three chapters (Chapters 2, 3, & 4). The experimental and analytical methods are described in Chapter 2. Chapter 3 reports the experimental results. This chapter also includes a section on geochemical modelling using a computer program PHREEQE. The discussion and conclusion on experimental results is presented in Chapter 4.

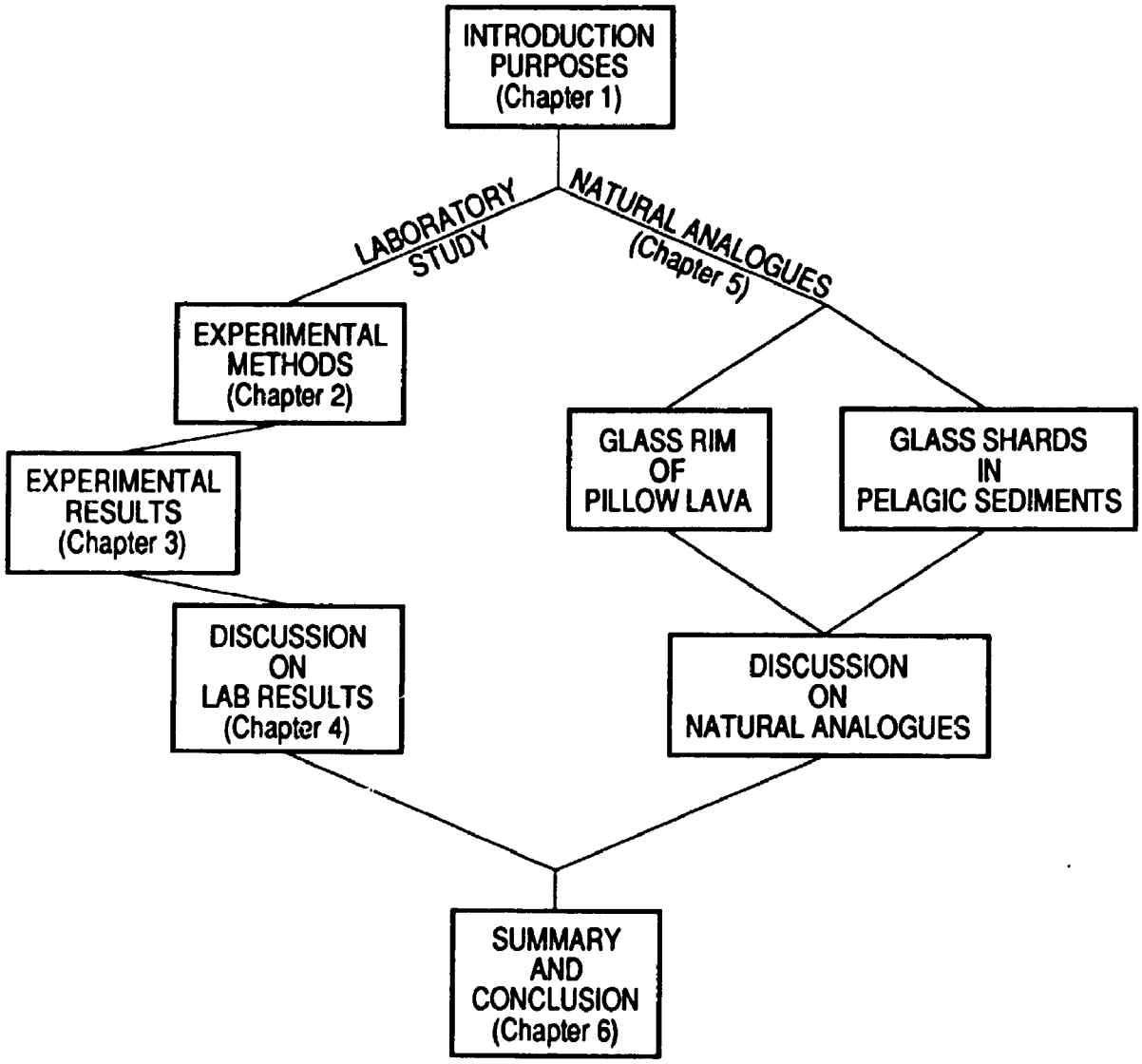

FIGURE 1.1 Organization chart of this study

The second part of this thesis (Chapter 5) is on the low-temperature alteration of volcanic glasses in marine environments. The validity of natural analogues is also discussed and the rate of alteration of natural glass is compared with the laboratory data. Finally chapter 6 presents the conclusions of this study. The organization of the thesis is summarized in Figure 1.1.

1.4 Nomenclature

Some technical terms used in this thesis have been used in a different context in the literature. Therefore, it is necessary to define these terms within the context of this study. The following definitions of technical terms are only for the purpose of this thesis.

Alteration, corrosion, dissolution, and leaching have all been used to describe the interactions between glass and aqueous solution. Leaching refers to the process in which selected constituents are extracted from the glass when it is exposed to water. It is generally accepted that this involves an exchange of hydrogen or hydronium ions from the solution for mobile ions such as Na in the glass. Dissolution or network dissolution is due to the attack on the glass structures. Network dissolution is congruent when all constituent are extracted into solution in the same ratio as they are present in the glass. Corrosion is often used in the recent literature and refers to the general set of surface changing reactions which a glass undergoes when exposed to

solution. Alteration is often used in the geochemical literature and applies to changes of the solid phase in the natural conditions. In this thesis corrosion is used to include all the processes involved in water/glass interactions, whereas dissolution will be used when kinetics are considered. It is understood that "the rate of glass corrosion" is an inappropriate term because corrosion includes more than one process and that "the rate of glass dissolution" is a more appropriate term and should be used.

Leachant and leachate both refer to the aqueous solution used in glass corrosion. The leachant is the starting solution while the leachate is the solution which results after attacking the glass and now contains glass constituents, either in solution or colloidal suspension.

Radwaste is an abbreviation for radioactive waste and used in same meaning as nuclear waste in this thesis and most of the literature. Nuclear waste glass refers to the glass containing radioactive wastes and is made from vitrification of high-level liquid wastes. It is commonly borosilicate glass. High-level waste (HLW) is defined by U.S. federal government as "aqueous waste resulting from the operation of the first cycle solvent extraction system, or equivalent, in a facility for reprocessing irradiated reactor fuel"(Brookins, 1984). HLW consists of fission products as well as some actinides and radiogenic actinide-daughter elements.

CHAPTER 2 - EXPERIMENTAL METHODS

2.1 Sample Preparation

Glasses chosen for this study include simulated PNL76-68, ABS-118, and basalt. PNL76-68 glass is a simulated waste glass, developed at the Pacific Northwest Laboratory (PNL) of the U.S. Department of Energy. In this formula, actinide radionuclides are substituted by non-radioactive rare earth elements (REE) for the purpose of research. ABS-118 glass is a French commercial waste glass, developed at PIVER, the Marcoule Nuclear Centre, France (Sombret, 1985). Both PNL76-68 and ABS-118 glasses used in the experiments were made from mixed oxide powders according to their formula (Grauer, 1985). High-level waste oxides in ABS-118 were not included. Basaltic glass (BG) was made from natural basalt to which about one weight percent of U_3O_8 was added. The powdered samples were fused at 1400°C in Pt crucibles for 30-45 minutes, then poured into a stainless steel mould and air quenched. To ensure homogeneity, glass pellets from the first fusion were ground and fused for a second time. The glass pellets of the second fusion were annealed at 550°C for three hours, then cut into discs (about 1.5 mm thick, 11.0mm in diameter).

All glass discs were polished with diamond powder and ultrasonically cleaned in an acetone bath. The actual compositions of the glasses were determined by electron microprobe and inductively coupled argon plasma spectroscopy (Table 2.1).

The leachants used in the experiments were distilled and deionized water (DDW) and natural seawater (SW). Natural seawater was collected from Massachusetts Bay, USA, by Dr. F.L. Sayles of Woods Hole Institution of Oceanography. The composition of DDW and SW was determined by inductively coupled argon plasma spectroscopy (Table 2.2).

2.2 Corrosion Tests

A. MCC-1 Corrosion Tests in DDW and SW

Most of the corrosion tests were conducted following the MCC-1 procedures (Strachen et al., 1981). Glass discs were placed on Teflon grids near the centre of Teflon vials, and leachants were added to yield a glass surface area to leachant volume ratio of 10 m^{-1}. Vials were placed in a conventional oven operating at 90°C ± 0.5°C. Nalgene Polyethylene bottles were used for the 30°C tests. All other corrosion conditions are the same. MCC-1 type of experiments is a static corrosion test. The justification of this method in study corrosion behaviour of nuclear waste glasses is given elsewhere (Strachen et al., 1981). Reaction times varied from 10 days to 360 days. A test matrix for MCC-1 experiments is given in Tables A1.1 and A1.2 in Appendix 1. Only limited number of triplicates was conducted (Table A1.1).

B. Corrosion Tests in Oceanic Muds

In a simulated submarine environment at room temperature, oceanic muds were placed in a 20 litre plastic cylinder, and

Table 2.1 Glass composition

Oxide	Basalt[a]	ABS-118		PNL 76-68	
		Intended	Analyzed[b]	Intended	Analyzed[b]
SiO2	48.79	51.00	54.54	40.17	40.25
Al2O3	15.39	5.53	5.59	-	-
Fe2O3	10.32[c]	3.27	3.30	11.15	11.02
MgO	8.19	-	-	-	-
CaO	11.32	4.52	3.87	2.01	1.68
Na2O	2.94	11.05	10.47	12.96	10.87
K2O	0.40	-	-	0.10	0.09
TiO2	1.12	-	-	3.01	3.14
MnO2	0.19	-	-	-	-
P2O5	0.12	0.34	0.44	0.50	0.58
UO3	1.00	1.40	d	-	-
B2O3	-	15.68	d	9.54	d
Li2O	-	2.26	d	-	-
Cs2O	-	-	-	1.10	d
BaO	-	-	-	0.60	0.70
SrO	-	-	-	0.40	0.40
NiO	-	0.45	0.41	0.60	0.36
ZnO	-	2.82	2.90	5.02	0.05
Cr2O3	-	0.56	0.68	0.40	0.32
ZrO2	-	1.12	1.14	1.91	1.88
MoO3	-	-	-	2.41	d
CeO2	-	-	-	3.01	d
La2O3	-	-	-	3.11	d
Eu2O3	-	-	-	1.00	d
Yb2O3	-	-	-	1.00	d
Total	99.09	100.00		100.00	

[a]Analyzed by electron microprobe; [b]analyzed by inductively coupled argon plasma; [c]total iron is given as Fe2O3; [d]not analyzed

covered by a seawater reservoir. Nylon threads were attached to glass discs buried in the mud.

Type A tests were conducted to compare the long-term corrosion behaviour of radwaste and volcanic glasses, and to compare the effect of seawater relative to deionized water; Types B tests were to study the effect of the presence of sediments. Most of experimental work has been done using Type A tests, and therefore our discussion will focus on this type of corrosion tests.

2.3 Analytical Methods

After the allotted corrosion time (10, 30, 90, 180, and 360 days), both the solution and surface chemistry of corroded glasses were studied.

2.3.1 Solution Analysis

At the end of each run, a subsample of leachate was taken for pH analysis. The rest of the leachate was acidified and stored in a cold room for other chemical analysis. Solute concentrations of leachates were analyzed using atomic absorption spectroscopy (for Zn, Fe), by photospectroscopy (for Si and B), and by neutron activation (for U). The instruments used and their operating conditions for the analysis are given in Appendix 2.

2.3.2 Solid Analysis

The corroded glass surfaces were first investigated by

optical microscopy, and the material on one face of each glass disc was scraped off, and analyzed using X-ray diffractometer (XRD), transmission electron microscopy (TEM), and scanning transmission electron microscopy (STEM). The other face of each glass disc was coated with gold or carbon, then observed by scanning electron microscopy (SEM) with energy dispersive X-ray analyzer (EDX), and further studied by secondary ion mass spectrometry (SIMS), and electron microprobe (EMP). The thickness of the surface layers of corroded glasses was measured on the glass surface using a Dektak IIA profilometer. The instruments and their working conditions used for solid analysi re given in Appendix 2.

Because surface layers can grow to more than 25 μm in thickness after 360 days , use of surface analysis instruments can be extremely time-consuming and very costly. Therefore, it became desirable to have corroded glasses sectioned in order to document the chemical and physical characteristics of glass surfaces. Despite the efforts, successes were obtained infrequently, and only with great difficulty. Nevertheless, valuable information was made available by those few samples which were sectioned successfully.

Table 2.2 Concertration of major cations in seawater (SW) and distilled and deionized water (DDW)[a,b]

	Na	K	Mg	Ca	Sr	B	Si
DDW	<1	<1	<0.1	<0.05	<0.001	0.012	0.10
SW	10900	431	1170	364	6.62	4.70	0.40

[a]Analyzed by inductively coupled argon plasma spectrscopy

[b]Concentration in mg/l

CHAPTER 3 - EXPERIMENTAL RESULTS

3.1 MCC-1 Tests in DDW and SW at 90°C

3.1.1 Leachate Composition

Only selected constituents in the leachates were analyzed and the results are shown in Tables A3.1 - A3.3. Leachate pHs from tests in SW showed very small variations whereas in DDW, leachate pH increased quickly (Figure 3.1). For example, leachate pH from tests of PNL 76-68 glass in DDW rose to 9.2 after 10 days. The elemental releases from the corrosion of ABS-118, PNL 76-68, and basaltic glasses are shown in Figures 3.2, 3.3, 3.4, respectively. The corrosion results are plotted as normalized elemental mass loss per unit area and were calculated using the equation

$$NL_i = M_i/F_i * SA$$

where

NL_i= normalized elemental loss (release),

M_i = mass of element i in the leachate,

F_i = mass fraction of element i in the glass, and

SA = geometric surface area of glass specimen.

For all three types of glasses, the amount of release in SW is much less than in DDW. Normalized boron(B) release from ABS-118 in SW was half of that in DDW after one year; silicon(Si) release in SW was one fourth of that in DDW after six months and even declined thereafter (Figure 3.2). Normalized Zn and U release in SW is remarkably low. The slope

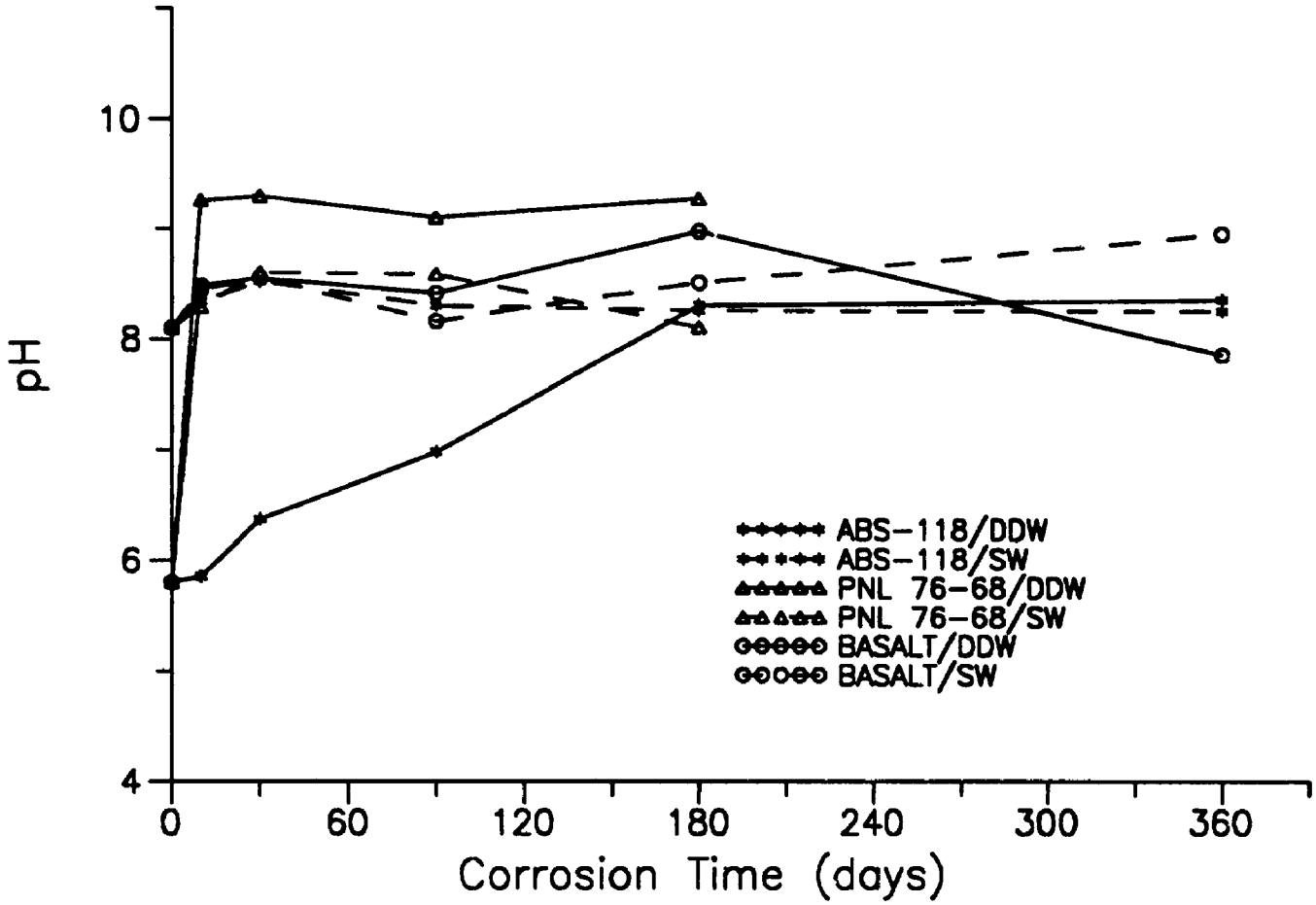

FIGURE 3.1 Leachate pH of MCC-1 corrosion tests at 90° C

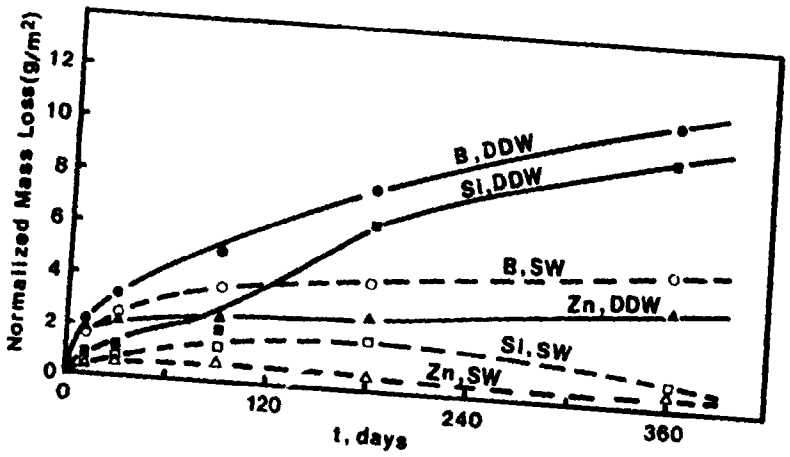

FIGURE 3.2 Normalized elemental release during corrosion of ABS-118 glass in distilled water(DDW) and seawater(SW).

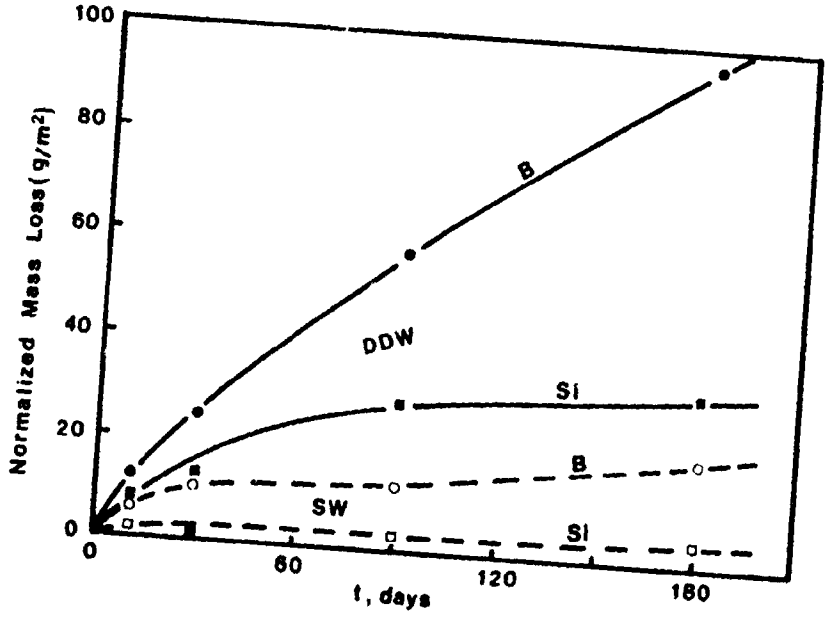

FIGURE 3.3 Normalized elemental release during corrosion of PNL 76-68 glass in distilled water(DDW) and seawater(SW).

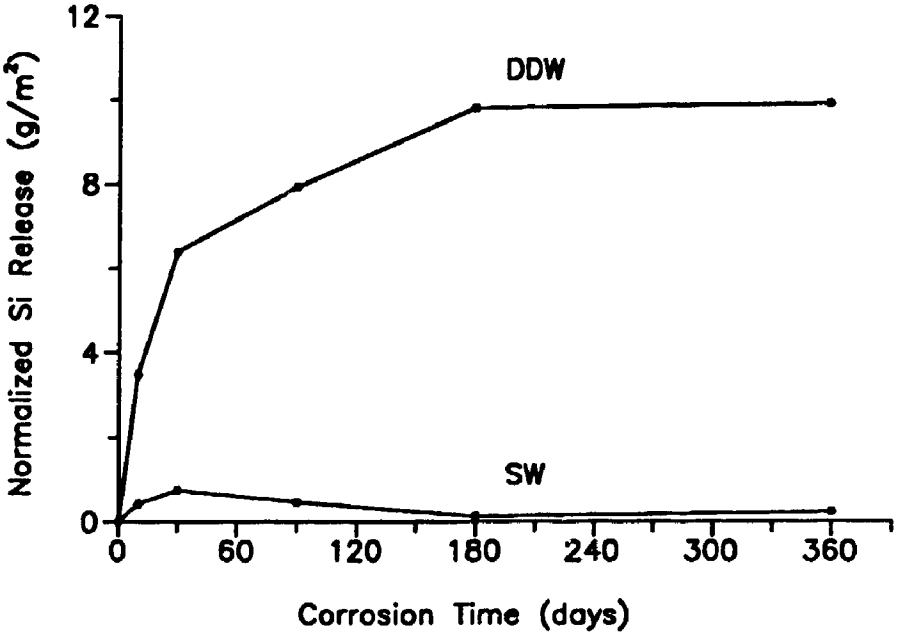

FIGURE 3.4 Normalized Si release during corrosion of basaltic glass

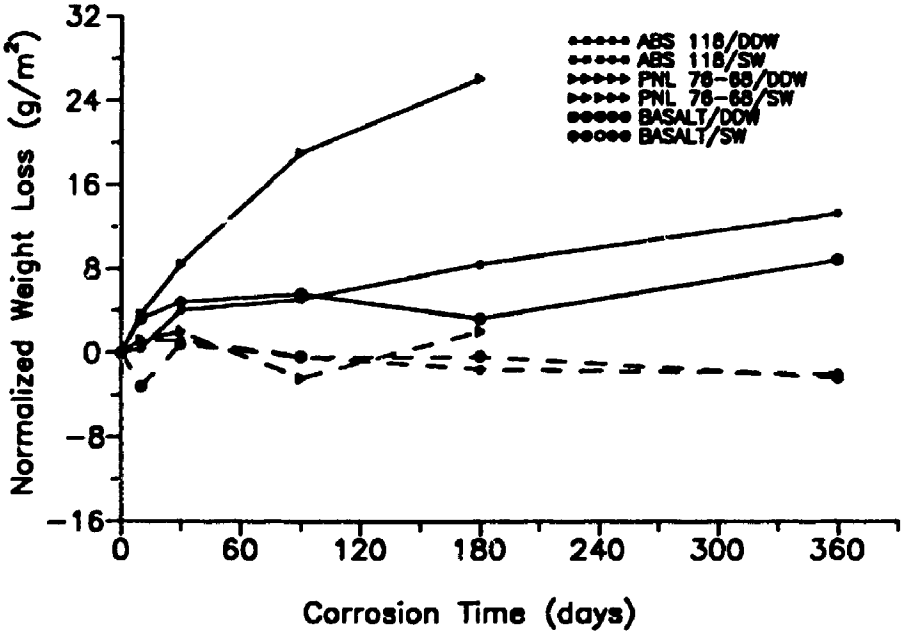

FIGURE 3.5 Normalized weight loss during glass corrosion

of the B release curve in SW is less than that of in DDW. The normalized release of B and Si in DDW is very similar and this indicates that congruent dissolution is predominant.

For PNL 76-68 glass, the normalized B and Si release in SW was also significantly lower than in DDW (Figure 3.3). The curves of boron release over time is very flat and suggests much lower dissolution rate than in DDW. Normalized B release in DDW increased almost linearly with corrosion time, even though Si release appeared to slow down after 90 days. In both SW and DDW, normalized Si release was always smaller than the normalized B release.

The releases of Si, Fe, and U were monitored for basaltic glass. However, the leachates contained only very low concentrations of Fe and U and no apparent trend can be identified. Therefore, only the normalized Si release is shown in Figure 3.4. The Si release in SW was very low and Si concentration appeared to be stable after 10 days. In DDW, however, normalized Si release was an order of magnitude higher and Si reached stable concentration after 180 days.

3.1.2 General Observations on Corroded Glasses

After the glass samples were retrieved from the test tubes at the end of the tests, the glass surface dehydrated very quickly, and a thin, brownish surface film became visible on PNL 76-68 and basaltic glasses in DDW. For ABS-118 glass, this type of film was observed only after 180 days in DDW. The surface film readily flaked off upon dehydration. Glass

Table 3.1 Thicknes of surface layers from 90°C tests

Corrosion Time (days)	ABS-118		PNL-76-68		Basalt	
	DDW	SW	DDW	SW	DDW	SW
10	a	0.7	a	2.7	a	a
30	a	1.0	8.2	a	1.7	a
90	a	a	18.8	14.8	3.7	0.8
180	0.7	2.3	30.0	28.4	4.1	1.2
360	1.3	a	-	-	4.9	a

Note: thickness in micrometer; a: not available

corroded in SW had a greenish surface and the surface film was more cohesive. Table 3.1 shows the thickness of the surface layers developed during corrosion of the glasses. Measurement of surface film thickness using a profilometer depends on micro-elevation of the surface film relative to the glass surface underneath. Therefore, such measurement is only possible when a patch of surface film peels off and the rest stays on the glass surface. Not all measurements are available, especially for those developed in SW whose surface layers are very adhesive. Values reported in Table 3.1 are not accurate and an error of 20 percent can be expected. Surface films of PNL 76-68 glass in both SW and DDW grew to 30 μm in thickness after six months, which was about one order of magnitude greater than those of ABS-118 and basaltic glasses. The surface layer built up slower during the corrosion of ABS-118 glass in DDW than in SW; for basaltic glass, the surface layer developed faster in DDW than in SW.

The weight loss of the glasses during corrosion are very small in SW compared with that in DDW (Figure 3.5). Actually, weight gain was observed for the glasses corroded in SW due to hydration of the glass and Mg addition to the glass surface (see following electron microprobe analysis). In DDW, all the glasses experienced weight loss and PNL 76-68 glass suffered the greatest weight loss among three types of glass.

3.1.3 Characteristics of Surface Layers Developed in DDW

The nature of surface layers developed in DDW depends on

FIGURE 3.6 SEM morphology of the surface layers developed in DDW. A. ABS-118 glass; B. PNL 76-68 glass; C. basaltic glass.

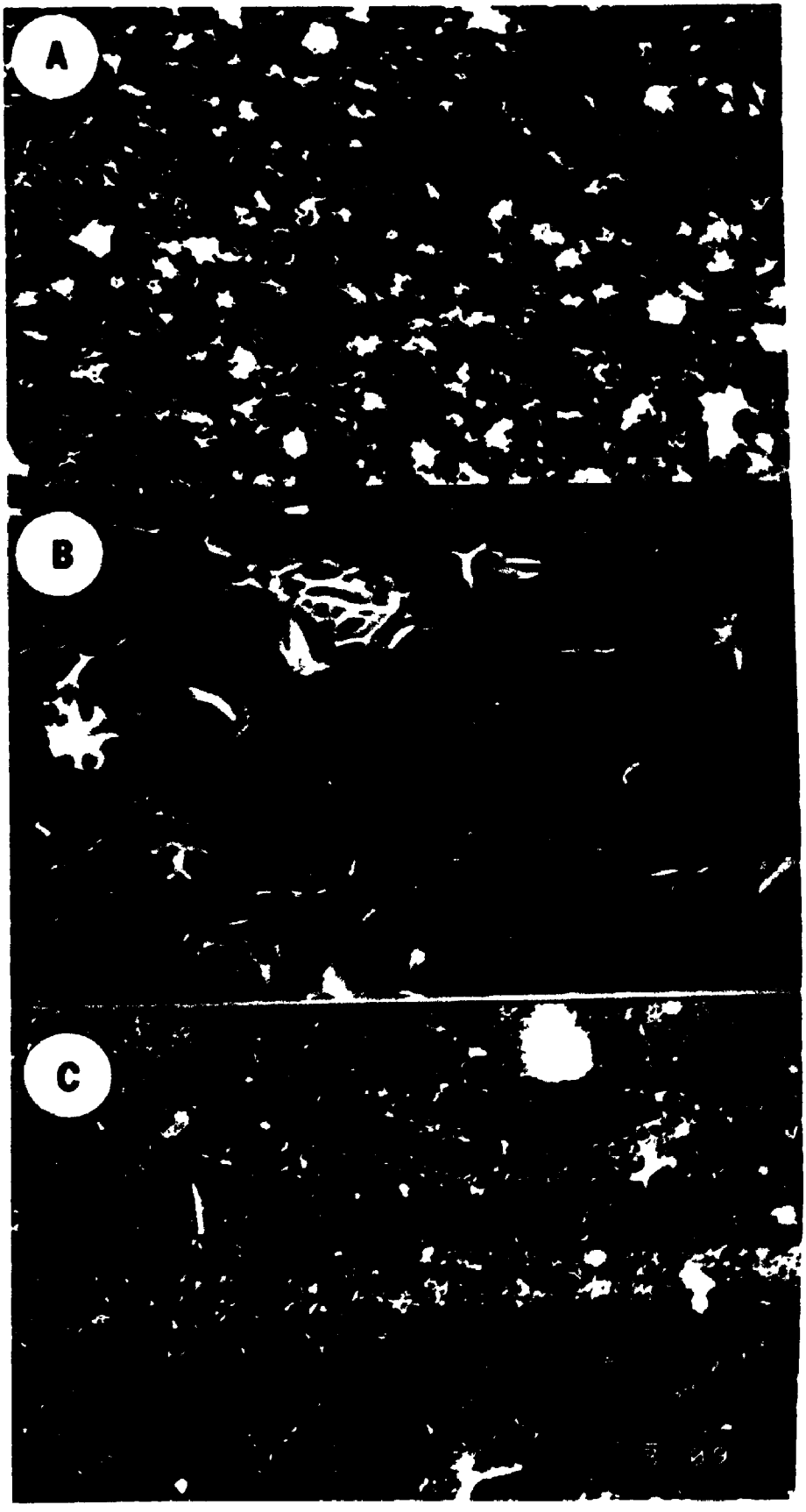
A
B
C

the composition of glass. Surface layers of both ABS-118 and basaltic glasses appear as aggregates of acicular particles which are less than 1 μm in size (Figure 3.6a,c), whereas those of PNL 76-68 glass are honeycomb like and with very large specific surface area (Figure 3.6b). The surface layers often display a multi-layer structure. Figure 3.7a shows the multi-layer structure on basaltic glass surface. The composition of the two surface layers are similar. The glass surface underneath the surface layer has a very smooth surface, indicating no preferential dissolution (except along polishing scratch). This is in contrast to dissolution of crystalline silicate minerals in which dissolution is along cleavages or other defects in the mineral crystals (Berner and Holdren, 1977). Figure 3.7b is a cross-section through the surface of corroded PNL 76-68 glass. Two sub-layers are displayed. The outmost layer is extremely rich in Zn. The inner layer is very rich in Fe and shows a continuous change in the chemical composition as indicated by the EDX analysis.

The materials in the surface layers are either amorphous or poorly crystalline as shown by Gandolfi powder XRD. Intensity of X-ray diffraction appears to increase with corrosion time. However, even after 360 days of corrosion, identification of crystalline phase in surface layers is not possible using X-ray diffraction data. TEM analysis confirmed the XRD results. The surface layer is composed mostly by flocculated sub-micron amorphous particles (Figure 3.8). They have diffused electron diffraction rings or weak and irregular

FIGURE 3.7 The multi-layer structure of the surface layers developed in DDW. A. Basaltic glass, 360 days. The glass surface underneath the surface layer is smooth and indicates uniform dissolution. Prefrential dissolution only occurs along polishing scratches (lower right corner); B. PNL 76-68 glass, 180 days (cross-section). **OL**: outer layer, enriched in Zn; **IL**: inner-layer, enriched in Fe and REE; **G**: glass.


A

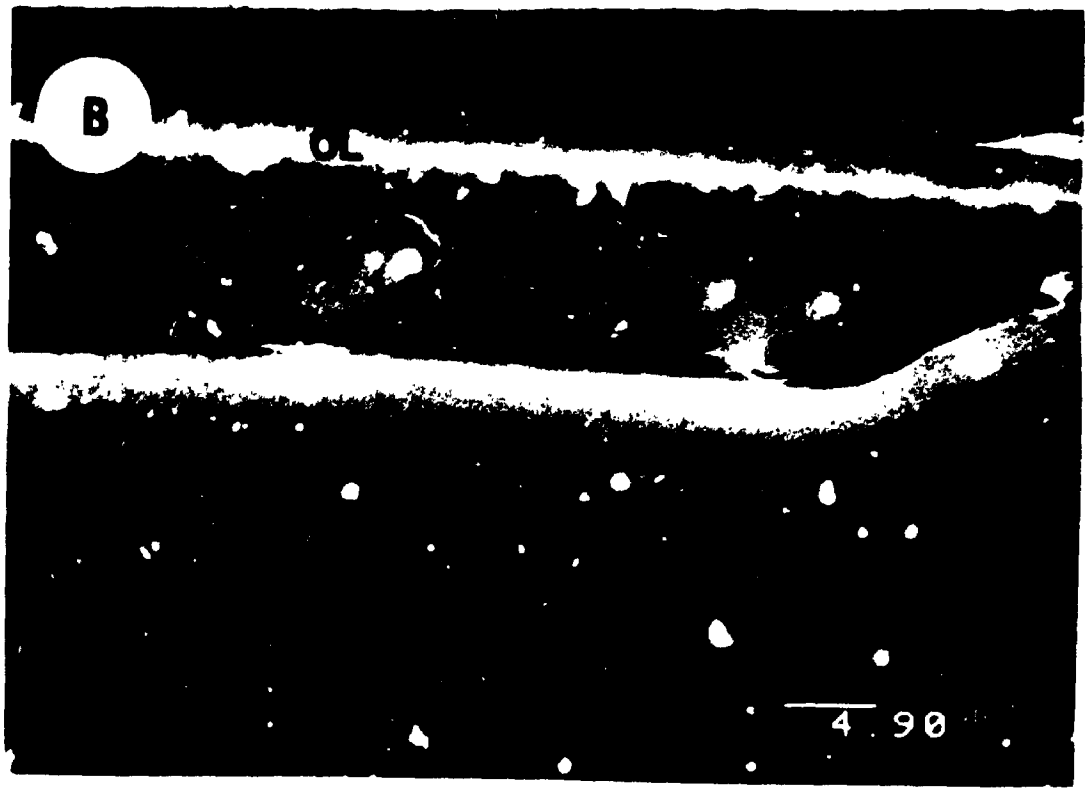
B
OL
4.90

electron diffraction patterns, which are typical of amorphous and poorly crystalline materials. Incipient crystallization is manifested by the line structures in Figure 3.8. Most of the electron diffraction patterns obtained were too poor to identify the crystalline materials present. However, Fe hydroxides and alumino-silicate clay minerals were identified as major crystalline phases in the surface layers. Despite the poor crystallinity, a Zn-silicate has a well- defined chemical composition (Figure 3.9b).

The chemical composition of the surface layers was determined using an electron microprobe (Tables 3.2 - 3.4). As a reference, the unleached glasses (labelled as "parent" in the tables) were also probed. The compositions of the parent glasses shown are slightly different from those in Table 2.1 but within the typical reproducibility of the electron microprobe. Because B and Li can not be determined by electron microprobe and some other elements were not analyzed, the totals are low for ABS-118 and PNL 76-68 glasses. It should be noted that electron microprobe analysis only gives the bulk composition in an electron excited field (a hemisphere with radius of about 2 μm) but the composition of the surface layers can change in sub-micron orders. Therefore, such analysis can not resolve the compositional changes within the surface layers. In addition, when a surface layer is less than 2 μm in thickness (e.g. surface layer of ABS-118 in DDW), the instrument may also receive X-ray signals from the glass underneath the surface layer and therefore the

FIGURE 3.8 TEM micrograph and electron diffraction pattern of amorphous material in the surface layer of basaltic glass formed in DDW. Incipient crystallization is indicated by the line structures distributed randomly over the area.

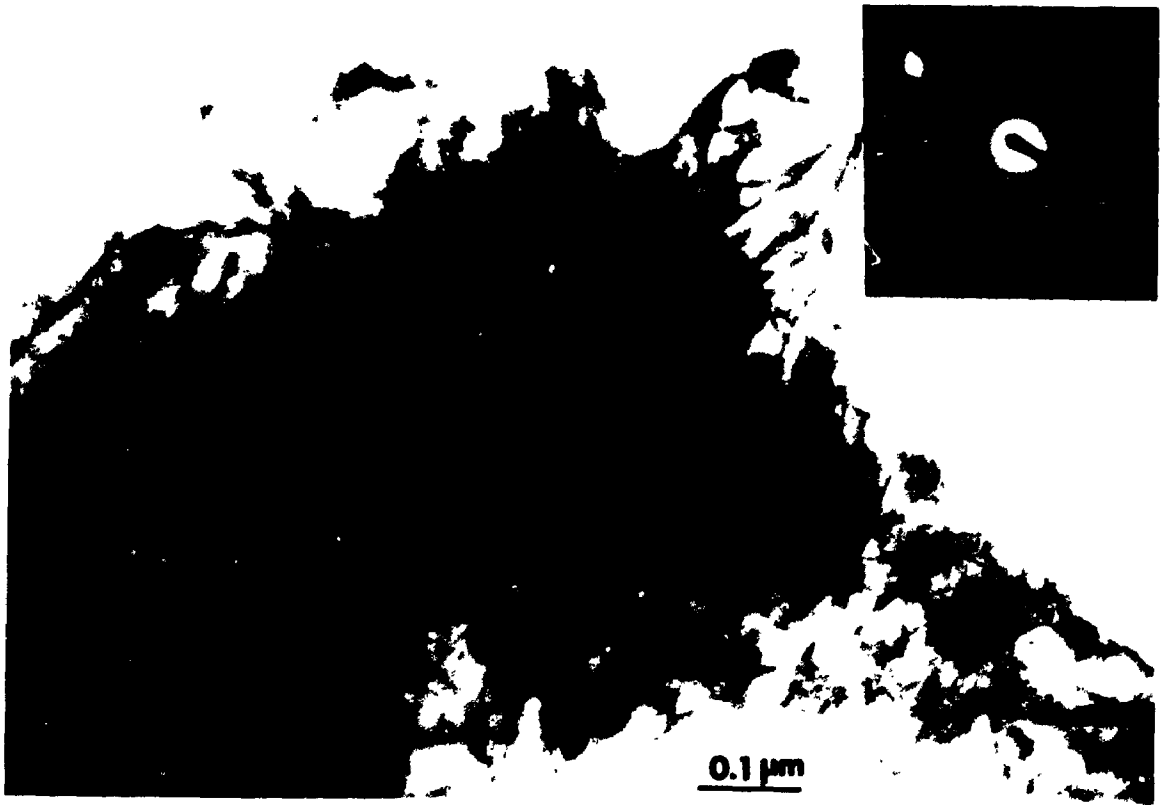
0.1 μm

FIGURE 3.9 TEM micrographs of crystalline material present in the surface layers formed in DDW. A. Illite(?) present in the surface layer of basaltic glass; B. Zn-silicate present in the surface layer of PNL 76-68 glass; C. Fe- hydroxides present in the surface layer of basaltic glass.

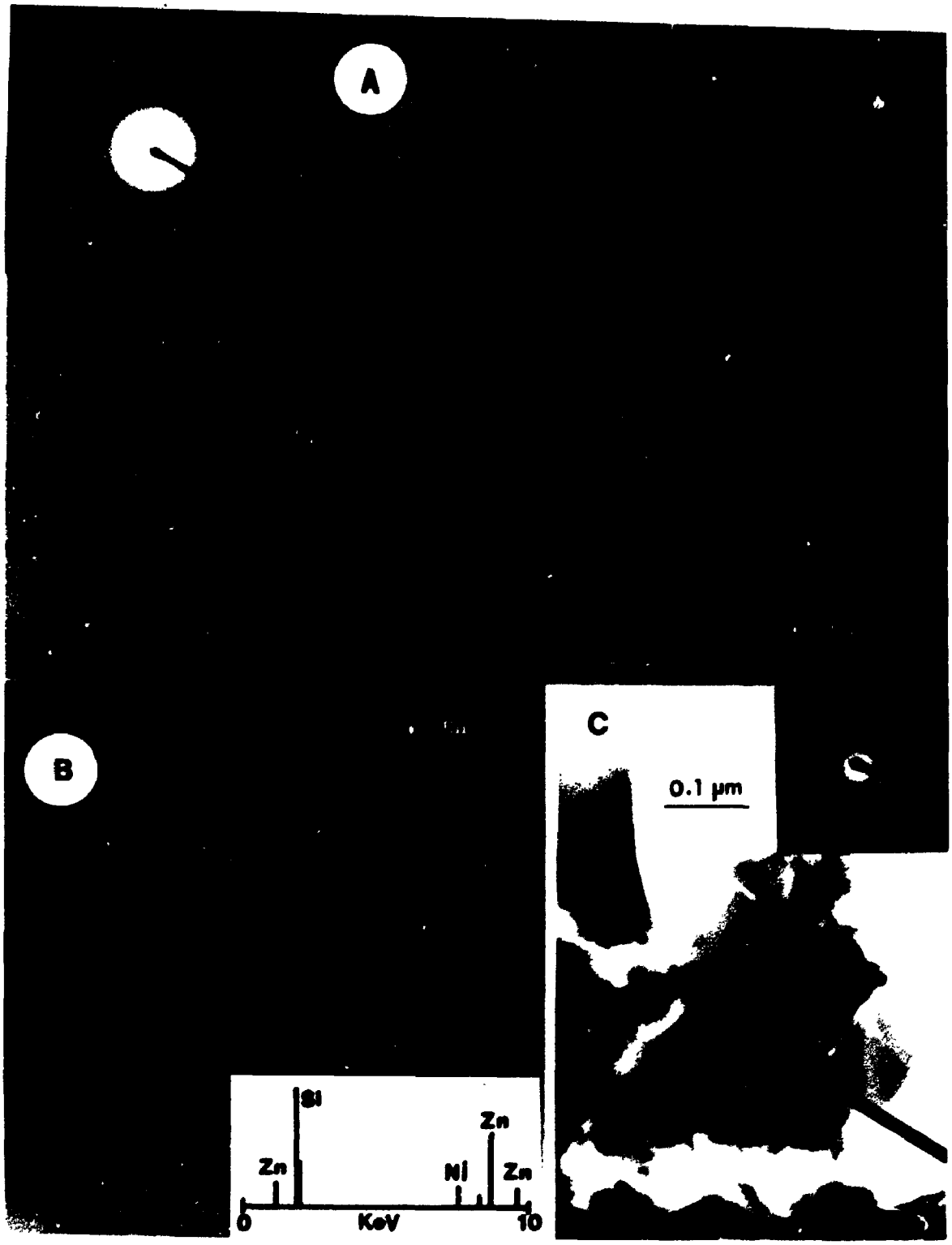
A
B
C
0.1 μm
Si
Zn
Zn
Ni
Zn
0
KeV
10

compositions are not truly representative of the surface layer but a composite one of the surface layer and underlying unaltered glass. Despite all of these limitations, the data should still indicate the trend in composition changes from parent glasses to surface layers.

Surface layers of ABS-118 glass in DDW are enriched in Fe, Zn, Zr, U, Ni, Cr, and Al, relative to the unleached glass (Table 3.2). This enrichment represents a passive accumulation resulting from the loss of other elements such as Na, B, Li, and Si. The depletion of B and Li in surface layer is deduced from solution analysis and confirmed by SIMS analysis of the surface layers. Aluminum and Ca are also lost to solution during corrosion of the glass. This is indicated by a decrease in the ratio of Al/Fe and Ca/Fe. Because the solution analysis indicated very little release of Fe to the solution during corrosion, Fe can be assumed as an immobile element. If the ratio of an element to Fe is lower in the surface layer than that in glass, the element must be lost during corrosion.

Surface layers formed in early stages of PNL 76-68 corrosion in DDW are very rich in Fe. Rare earth elements (REE), Zr, and Ti are also enriched in this Fe-rich layer (Table 3.3). Among REE, only La and Ce were determined quantitatively and Eu and Yb were not determined by electron microprobe. However, Eu and Yb have similar behaviour to La and Ce according to the qualitative EDX spectrum. A Zn-rich surface layer formed on the top of a Fe-rich layer after 90 days of corrosion (Table 3.3). This is best illustrated by a

Table 3.2 Surface layer composition of ABS-118 glass in DDW

	Parent	30 D	90 D	180 D	360 D
SiO2	53.32	56.33	60.90	46.23	32.51
Al2O3	5.80	6.18	7.20	7.80	8.99
FeO	3.35	4.01	4.83	7.84	12.49
ZnO	3.00	2.02	3.12	6.07	7.99
CaO	4.24	3.42	3.63	3.95	3.37
ZrO2	1.40	1.41	1.94	3.07	4.60
NiO	0.52	0.39	0.51	0.72	1.14
Na2O	9.34	4.07	3.89	6.28	1.86
UO3	1.55	1.63	2.18	2.60	3.47
Cr2O3	0.53	0.69	0.82	1.40	2.02
Total	83.05	80.15	89.02	85.96	78.44
Si/Fe	15.92	14.05	12.61	5.90	2.60
Al/Fe	1.73	1.54	1.49	0.99	0.72
Zn/Fe	0.90	0.50	0.65	0.77	0.64
Ca/Fe	1.27	0.85	0.75	0.50	0.27
Zr/Fe	0.42	0.35	0.40	0.39	0.37
Ni/Fe	0.16	0.10	0.11	0.09	0.09
Na/Fe	2.79	1.01	0.81	0.80	0.15
U/Fe	0.46	0.41	0.45	0.33	0.28
Cr/Fe	0.16	0.17	0.17	0.18	0.16

Table 3.3 Surface layer compositionof PNL 76 glass in DDW

	Parent	30 D	90 D	180 D (O)	180 D (I)
SiO2	41.46	23.82	31.41	36.87	26.86
TiO2	2.95	5.78	1.24	0.55	5.02
FeO	11.49	22.82	9.19	2.71	15.93
ZnO	5.35	14.50	26.81	29.25	5.48
CaO	1.82	1.80	0.98	0.51	2.74
SrO	0.35	0.40	0.18	0.00	0.49
ZrO2	1.86	3.11	0.94	0.46	2.67
MoO3	1.81	0.00	0.00	0.00	0.03
Na2O	11.95	0.15	0.61	0.82	0.05
La2O3	3.86	5.95	2.57	0.87	4.96
CeO2	3.37	6.28	2.06	0.72	5.25
Total	86.27	84.61	75.99	72.76	69.48
Si/Fe	3.61	1.04	3.42	13.61	1.69
Ti/Fe	0.26	0.25	0.13	0.20	0.32
Zn/Fe	0.47	0.64	2.92	10.79	0.34
Zr/Fe	0.16	0.14	0.10	0.17	0.17
Na/Fe	1.04	0.01	0.07	0.30	0.00
La/Fe	0.34	0.26	0.28	0.32	0.31
Ce/Fe	0.29	0.28	0.22	0.27	0.33

Table 3.4 Surface layer composition of basaltic glass in DDW

	Parent	30 D	90 D	180 D	360 D
SiO2	48.74	28.24	25.40	24.69	24.31
Al2O3	15.03	15.55	13.78	17.53	13.87
FeO	9.56	24.49	24.20	18.50	26.09
TiO2	1.14	2.82	3.34	2.09	3.44
CaO	11.90	5.44	5.32	4.23	4.07
MgO	7.88	6.32	5.58	8.01	4.19
MnO	0.12	0.38	0.35	0.43	0.38
Na2O	2.94	0.62	0.27	0.09	0.05
K2O	0.42	0.01	0.00	0.00	0.00
Cr2O3	0.08	0.02	0.09	0.03	0.19
P2O5	0.18				0.22
UO3	1.17	3.28	4.42	2.06	3.93
Total	99.16	87.23	82.75	77.71	80.74
Si/Fe	5.10	1.15	1.05	1.33	0.93
Al/Fe	1.57	0.63	0.57	0.95	0.53
Ti/Fe	0.12	0.12	0.14	0.11	0.13
Ca/Fe	1.24	0.22	0.22	0.23	0.16
Mg/Fe	0.82	0.26	0.23	0.43	0.16
Na/Fe	0.31	0.03	0.01	0.00	0.00
U/Fe	0.12	0.13	0.18	0.11	0.15

cross section through the surface layer (Figure 3.7). The compositions of the Fe- and Zn-rich layers are also shown in Table 3.3. The "180 days (O)" represents the outer surface layer and contains about 24 percent of ZnO. The "180 days (I)" represents the inner surface layer and the glass and contains about 20 percent of FeO. In both Fe-rich and Zn-rich surface layers, Na, B, and Sr are depleted relative to parent glass.

For basaltic glass, surface layers developed in DDW are enriched in Fe, U, Ti, Al, and Mn, and depleted in Na, K, Ca, Si, and Mg, relative to the parent glass (Table 3.4). Iron, U, Ti, and Mn appear to be constant, but Al is partly lost during the corrosion. The greater loss of Na and Si causes the apparent increase of Al.

3.1.4 Characteristics of Surface Layers Developed in SW

The morphology of the surface layers developed in SW is remarkably similar for the three types of glasses. At high magnification, the surface layers appear as aggregates of rice-shaped grains (Figure 3.10). The surface layers were patchy at the beginning and then became continuous after 10 days for PNL 76-68 or 30 days for ABS-118 and basaltic glasses. After one layer formed, a second layer may deposit on the top of the first one. Euhedral carbonate crystals were found on the surface layers of ABS-118 and basaltic glasses (Figure 3.11). These crystals, according to limited XRD and electron diffraction data, are tentatively identified as aragonite.

FIGURE 3.10 SEM micrographs and EDX spectrum of the surface layers developed in SW. A. ABS-118 glass; B. PNL 76-68 glass; C. Basaltic glass. For comparison, the EDX of the surface layers(S) is superimposed on that of parent glasses(P). The enrichment of Mg and Cl is clearly demonstrated by the EDX data.

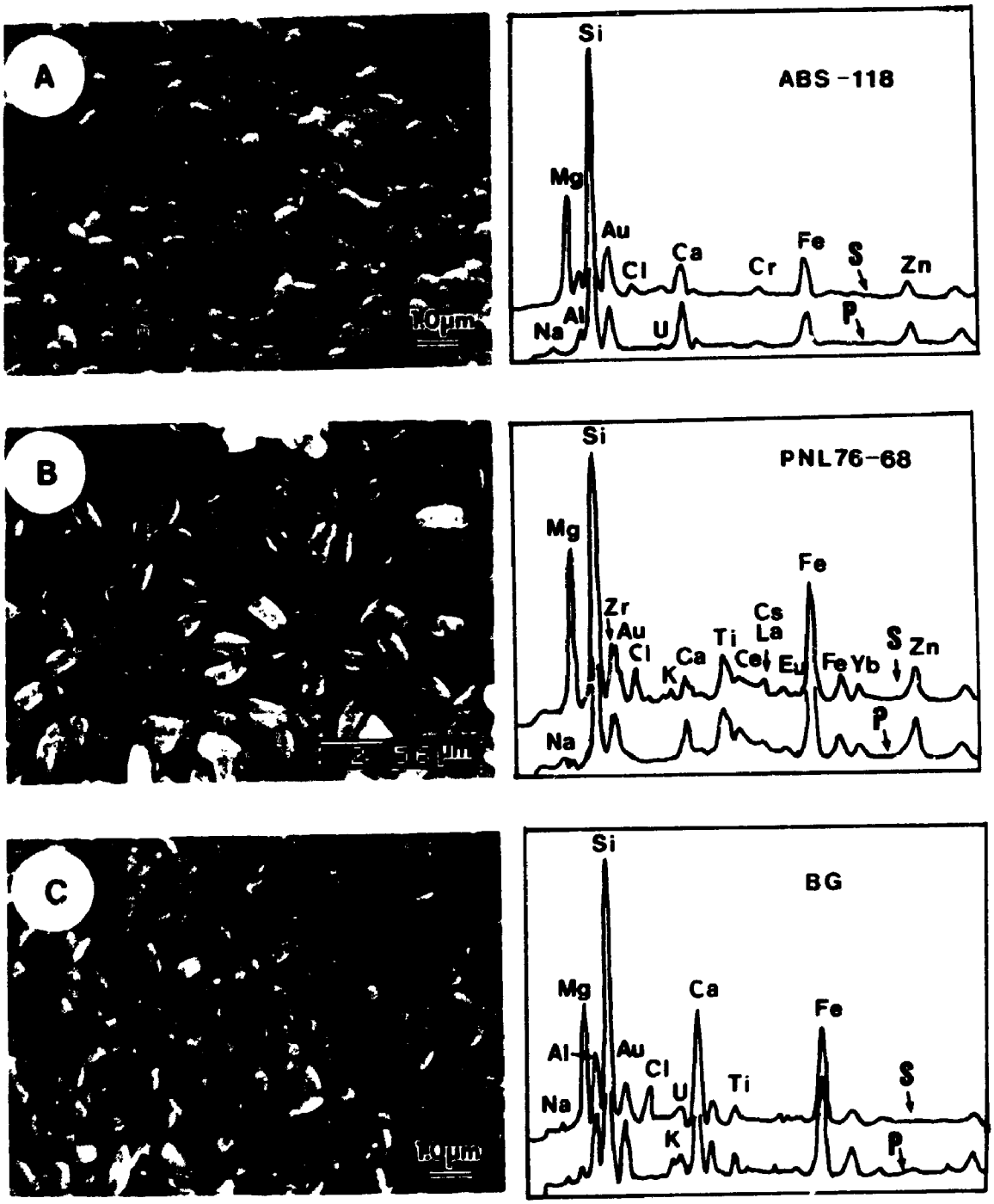
A
1.0μm
Si
ABS-118
Mg
Au
Cl
Ca
Cr
Fe
S
Zn
Na
Al
U
P
B
PNL76-68
Zr
Cs
La
Ti
K
Eu
Yb
C
BG

FIGURE 3.11 Calcium carbonate precipitates in the surface layers developed in SW. A. ABS-118; B. Basaltic glass.

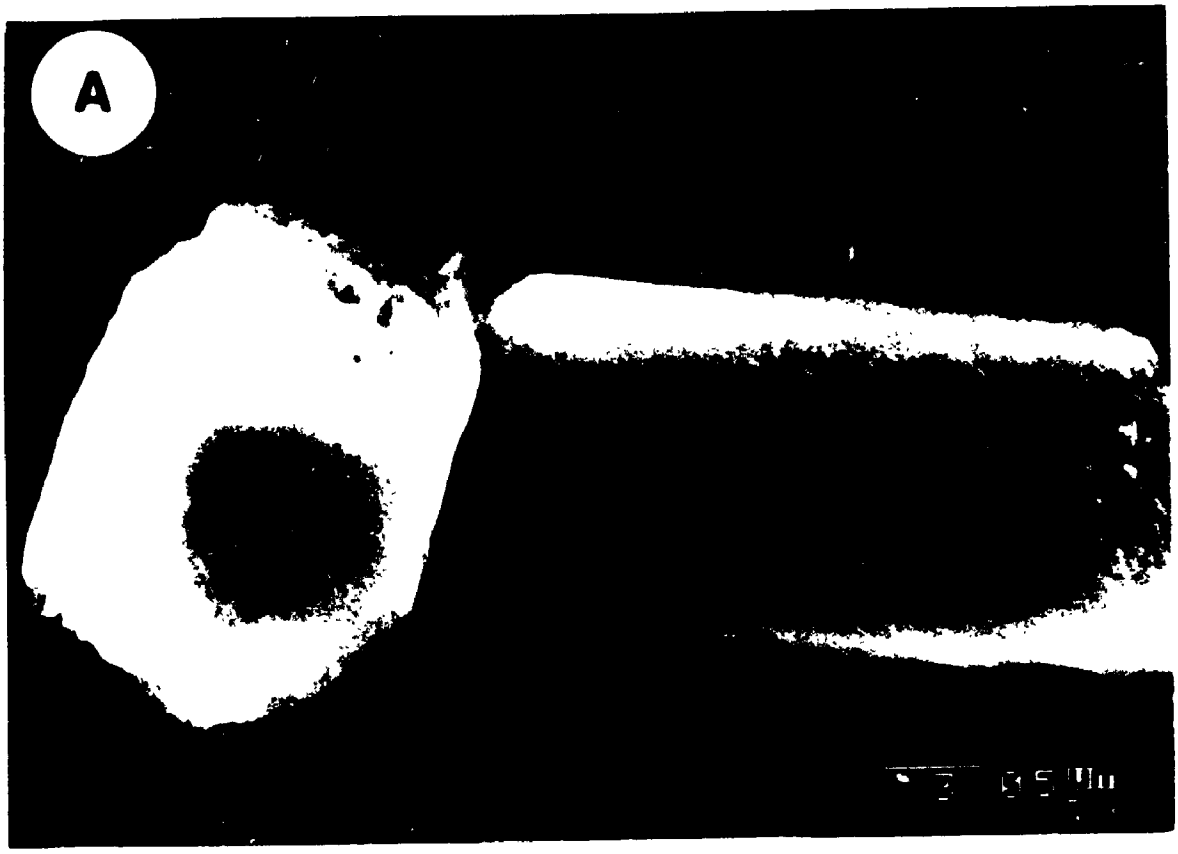
A


B

The surface layers developed in SW are also poor in crystallinity. Powder XRD from the Gandolfi camera show only weak diffraction lines which correspond to those of aragonite but also include 4.5, 2.6, and 1.4 Å. TEM analysis indicated that crystalline and weakly crystalline materials were abundant but characterization of these materials was complicated by the structural damage induced by high voltage electron beams. Among phases identified were serpentine and talc (Figure 3.12). Kaolinite and illite are also present when the parent glasses contain substantial amount of Al.

As indicated by the EDX analysis, surface layers are extremely rich in Mg, with lesser amounts of Cl. Electron microprobe analyses confirmed these results (Tables 3.5 - 3.7). The surface layers of ABS-118 in SW contain about 25 percent MgO. All other components were depleted in surface layers, relative to the parent glass (Table 3.5). However, for Al, Zr, U, Ni, and Zn, the depletion can be well accounted by dilution effects. That is, these elements were not lost to solution and the decrease of their abundances in surface layers is due to the addition of Mg, Cl, and H_2O into the glass surface. The Cl was not determined by EMP due to some operational difficulties but its enrichment in surface layers were clearly shown by EDX analysis (see Figure 3.10). The loss of Si is small as indicated by the small decrease in the Si/Fe ratio from glass to surface layer. The elements lost during corrosion are Na, B, Li, and to less degree, Ca.

For PNL 76-68 glass, the surface layers also contain

FIGURE 3.12 TEM micrographs and EDX microanalysis of amorphous and crystalline material present in the surface layers formed in SW. A. An amorphous particle present in the surface layer of basaltic glass; B. Talc present in the surface layer of PNL 76-68 glass; C. Lizardite present in the surface layers of basaltic glass.

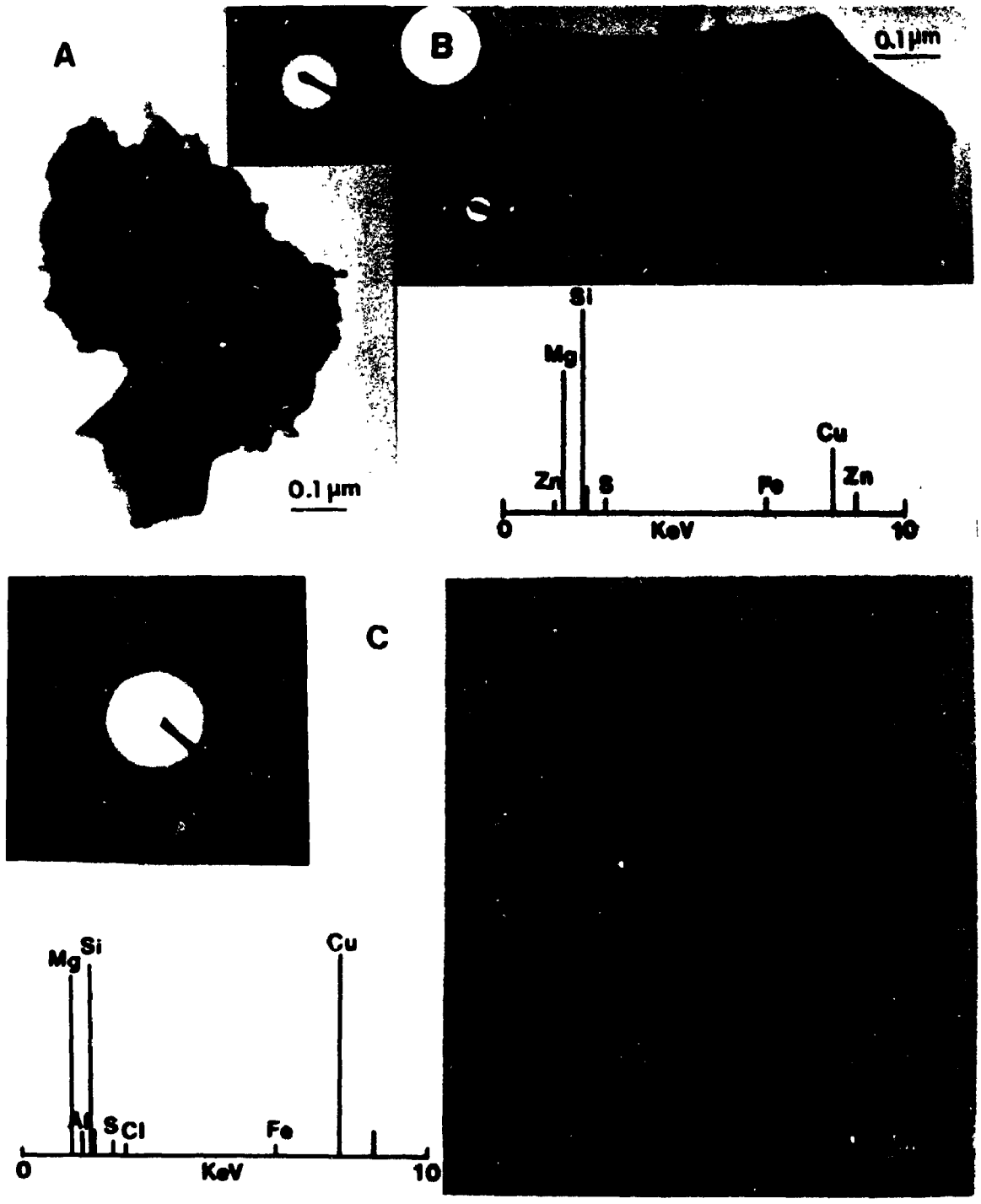
A
B
0.1 µm
0.1 µm
Si
Mg
Cu
Zn
S
Fe
Zn
0
KeV
10
C
Mg
Si
Cu
Al
S
Cl
Fe
0
KeV
10

Table 3.5 Surface layer composition of ABS-118 glass in SW

	Parent	30 D	90 D	180 D	360 D
SiO2	53.32	36.86	36.10	29.33	36.28
Al2O3	5.80	6.18	5.65	5.94	4.73
FeO	3.35	3.02	2.99	3.14	2.71
ZnO	3.00	2.75	2.27	2.54	1.99
CaO	4.24	2.01	2.04	2.11	1.79
ZrO2	1.40	1.29	1.05	0.96	1.00
NiO	0.52	0.37	0.43	0.45	0.36
Na2O	9.34	2.85	1.71	0.83	1.85
UO3	1.55	1.22	1.53	1.51	1.04
Cr2O3	0.53	0.46	0.53	0.59	0.49
MgO	0.01	22.81	27.31	28.72	24.81
Total	83.05	79.82	81.61	76.12	77.05
Si/Fe	15.92	12.21	12.07	9.34	13.39
Al/Fe	1.73	2.05	1.89	1.89	1.75
Zn/Fe	0.90	0.91	0.76	0.81	0.73
Ca/Fe	1.27	0.67	0.68	0.67	0.66
Zr/Fe	0.42	0.43	0.35	0.31	0.37
Ni/Fe	0.16	0.12	0.14	0.14	0.13
Na/Fe	2.79	0.94	0.57	0.26	0.68
U/Fe	0.46	0.40	0.51	0.48	0.38
Cr/Fe	0.16	0.15	0.18	0.19	0.18
Mg/Fe	0.00	7.55	9.13	9.15	9.15

Table 3.6 Surface layer composition of PNL 76-68 glass in SW

	Parent	30 D	90 D	180 D
SiO2	41.46	24.60	27.08	33.88
TiO2	2.95	2.16	2.19	4.81
FeO	11.49	9.58	7.98	18.68
ZnO	5.35	3.25	2.66	5.65
MgO	0.08	26.66	24.31	2.29
CaO	1.82	1.15	1.38	1.19
SrO	0.35	0.00	0.05	0.14
ZrO2	1.86	1.56	1.58	3.37
MoO3	1.81	0.00	0.15	0.00
Na2O	11.95	0.00	1.28	0.00
La2O3	3.86	3.04	2.40	5.28
CeO2	3.37	2.91	2.54	3.49
Total	86.35	74.91	73.60	78.78
Si/Fe	3.61	2.57	3.39	1.81
Ti/Fe	0.26	0.23	0.27	0.26
Zn/Fe	0.47	0.34	0.33	0.30
Ca/Fe	0.16	0.12	0.17	0.06
Zr/Fe	0.16	0.16	0.20	0.18
La/Fe	0.34	0.32	0.30	0.28
Ce/Fe	0.29	0.30	0.32	0.19

Table 3.7 Surface layer composition of basaltic glass in SW

	Parent	30 D	180 D	360 D
SiO2	48.74	36.93	28.53	33.15
Al2O3	15.03	12.00	7.48	10.17
FeO	9.56	7.06	4.56	6.40
TiO2	1.14	0.83	0.55	0.78
CaO	11.90	7.73	3.45	5.85
MgO	7.88	22.60	32.20	25.48
MnO	0.12	0.08	0.08	0.05
Na2O	2.94	1.59	0.71	1.98
K2O	0.42	0.25	0.08	0.21
Cr2O3	0.08	0.03	0.03	0.03
P2O5	0.18	a	a	0.17
UO3	1.17	0.85	0.40	0.70
Cl	a	2.26	a	a
Total	99.16	92.21	78.07	84.97
Si/Fe	5.10	5.23	6.26	5.18
Al/Fe	1.57	1.70	1.64	1.59
Ti/Fe	0.12	0.12	0.12	0.12
Ca/Fe	1.24	1.09	0.76	0.91
Mg/Fe	0.82	3.20	7.06	3.98
Na/Fe	0.31	0.23	0.16	0.31
U/Fe	0.12	0.12	0.09	0.11

a: not measured

about 25 percent MgO. The surface layer of 180 day experiment is Fe-rich, while the MgO content decreases to about two percent. REE, Ti, Zn, and Zr are closely associated with Fe and are poor in Mg-rich layers. Sodium, Mo, B, and Sr, and to a less degree, Si and Ca, are lost to solution during corrosion(Table 3.6).

Surface layers of basaltic glass also contains significant amount of MgO. Silicon, Al, Ti, U, and Mn are all conservative during the corrosion (Table 3.7). This is consistent with solution analysis which show that Si and U in leachates were remarkably low. Sodium and Ca were lost during corrosion.

3.1.5 SIMS Depth Profiles of Reaction Zones

Using SEM and EMP, no changes in either morphology or composition can be detected between unreacted glass and the glass underneath the surface layers. This does not confirm that the glass underneath the surface layers is pristine and has an identical structure and same composition to the unreacted glass, simply because both SEM and EMP can not resolve morphological and compositional changes at sub-micron levels. The region underneath the surface layers is physically a reaction front of glass corrosion and its characteristics are of great importance in understanding the mechanism of glass corrosion. To characterize this region (which will be termed the reaction zone in the following text), the depth profile capability of the SIMS technique was used.

Because only the characteristics of the reaction zone were of interest, the surface layers on the corroded glass were mechanically removed prior to SIMS analysis. Figure 3.13 shows the SIMS depth profiles of an unreacted (reference) glass and a PNL 76-68 glass corroded in SW for 180 days. Selected isotopes (^{11}B, ^{23}Na, ^{24}Mg, ^{28}Si, ^{54}Fe, ^{64}Zn, and ^{98}Zr) were counted. The count intensity of the isotopes from the reference glass show minor changes with sputtering time(depth). Most obvious changes are Na rise towards the surface and Zn and Zr rise towards the interior of the glass. These changes are considered as instrumental variations rather than true compositional changes in the glass. The depth profile of the reference glass serves as a basis for normalization for corroded glasses.

Because the intensities of secondary ions are affected by many instrumental conditions, certain normalization procedures are required to minimize the effects of instrumental variations on count rates (Abrajano and Bates, 1987; Muir et al., 1989). The normalization procedures adopted here were proposed by Muir et al.(1989) and involve three steps. The first step in the normalization involves ratioing the counts (observed secondary ion intensity) from the element of interest (^{11}B, ^{23}Na, ^{24}Mg, ^{64}Zn) to that of ^{28}Si (or ^{54}Fe). Here, ^{28}Si (or ^{54}Fe) is used as an internal standard, and by ratioing to ^{28}Si (or ^{54}Fe) any variation in sputtering yields during the analyses are minimized. ^{28}Si was chosen as the internal standard because the Si is a network builder in the

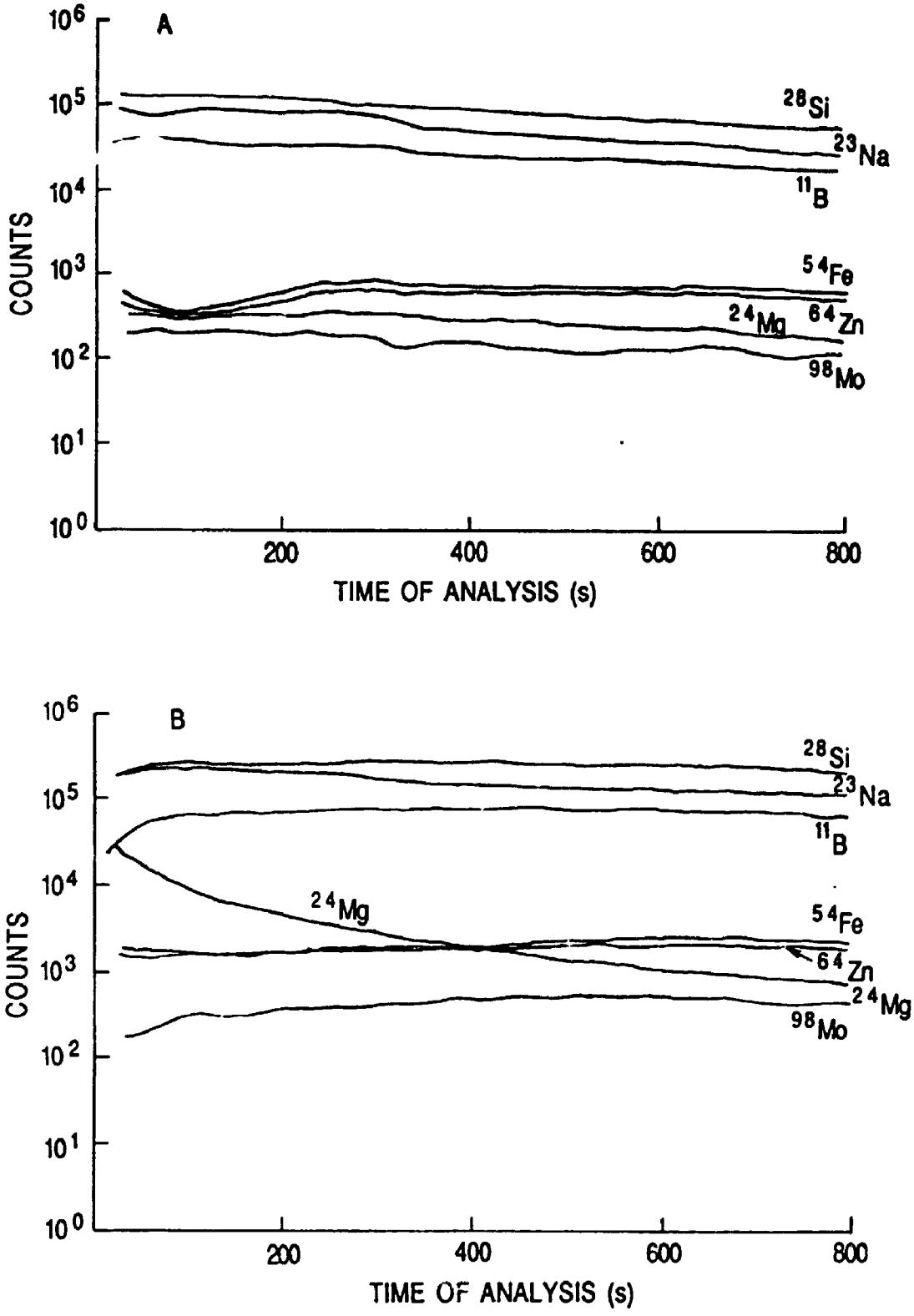

FIGURE 3.13 SIMS depth profiles of non-corroded (A) and SW-corroded (B) PNL76-68 glass

glass structure. However, in some cases, Si was extracted from the reaction zone in preference to Fe, and therefore can not be used as internal standard. In this case, ^{54}Fe was used as internal standard. In the second step the data from each point (cycle) of the profile are normalized to the average of the later cycles (last few hundred seconds) in the profile. The data from the deepest part of the profiles are assumed to represent the original (bulk) composition of the glass. Thus the difference in the secondary ion intensity resulting from the dissolution process may be calculated. The third step is a repeat of the second step for the reference specimen which has been analyzed during the same session to keep the operating parameters of SIMS instrument constant. This step is used in an attempt to reduce any effect(s) on the secondary ion signals due to surface and/or surface charging. The average of the data from the reference glass is then subtracted from the reacted sample (each point of analysis) to give the difference in observed secondary ion intensity due to the formation of leached layers during corrosion. The difference is expressed as a percent. This normalization procedure may be expressed by the following equation:

$$\left\{ \left[\frac{(^{11}B/^{28}Si)surf.}{(^{11}B/^{28}Si)bulk} \right]_{Corroded} \times \left[\frac{(^{11}B/^{28}Si)surf.}{(^{11}B/^{28}Si)bulk} \right]_{Reference} - 1 \right\} \times 100$$

where ^{11}B is replaced with ^{23}Na, ^{24}Mg, etc. for each point of

analysis for the corroded glass. The correction factor from the reference glass is obtained from the average of two analyzed spots.

The depth profiles of PNL 76-68 glass corroded for 180 days in DDW and SW were first normalized to ^{28}Si. The results showed that Fe is enriched in the reaction zone relative to Si. Because there was no source for iron other than in the glass, the increase in the Fe/Si ratio must result from the loss of Si. Thus, Si is not suitable for internal standard in this case, and Fe was used instead.

Figures 3.14 and 3.15 represent Fe-normalized profiles for the PNL 76-68 glass corroded in DDW and in SW for 180 days, respectively. In each figure, the data for elements of the corroded glass have been plotted as open circles and were best fitted using a polynomial expression (solid lines); data for the unreacted reference glass have been plotted as "+" and were best fitted using a linear equation (dashed lines). The normalization procedure for the reference samples is identical to that for the corroded samples described above.

For the glass corroded in DDW, B, Na, as well as Si are depleted in the reaction zone. Mo is also depleted and has a similar shape to the profile of B. The depth profile of Zn/Fe is not significantly different to that of reference glass, indicating that Zn behaves similarly to Fe. Profiles of Mo/Fe and Zn/Fe are not plotted. For the glass corroded in SW, B (and Mo), Na, and Si are also depleted in the reaction zone. Mg is enriched in reaction zone. The percent change in Mg/Fe

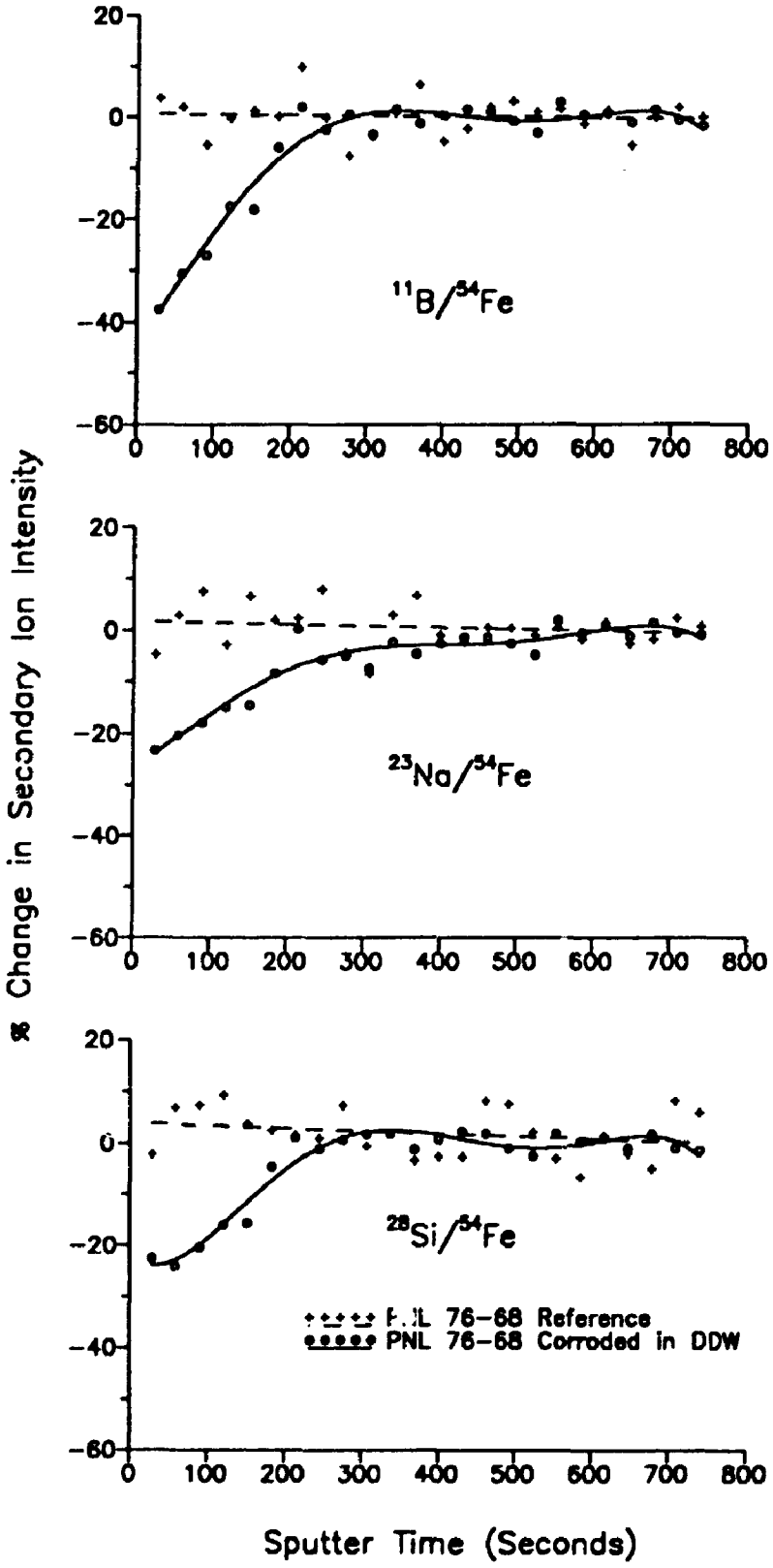

FIGURE 3.14 SIMS depth profiles of PNL 76-68 glass corroded in DDW.

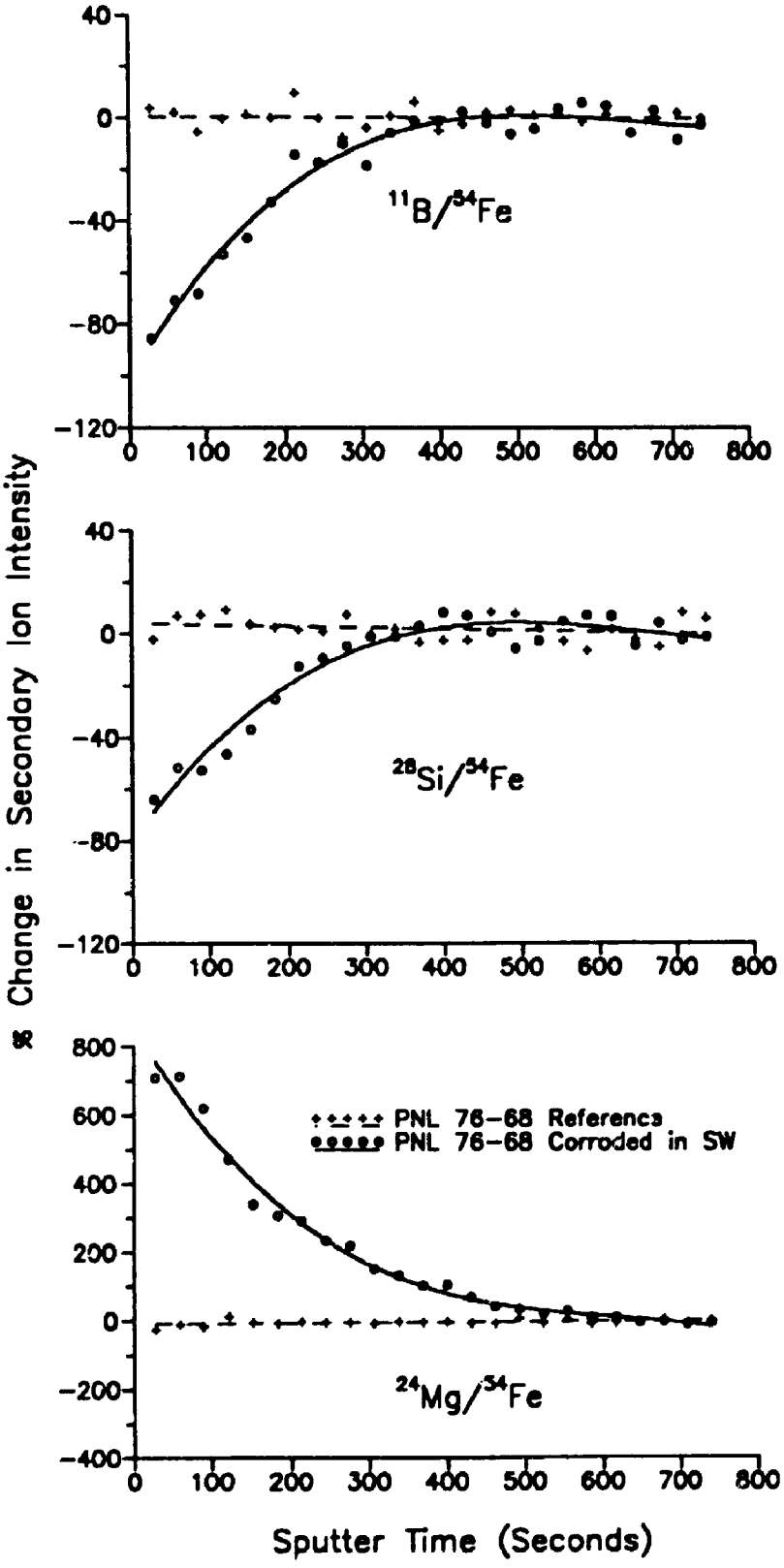

FIGURE 3.15 SIMS depth profiles of PNL 76-68 glass corroded in SW.

is much greater than 100, which indicates that Mg in SW has diffused into the reaction zone.

The depth of depletion is taken from the surface (beginning of the profile) to the depth where the secondary ion signals of the reacted and non-reacted specimens became somewhat similar. The correlation of analysis time with the depth of penetration by the primary beam was achieved by determining the sputtering rate from the reference glass. The sputtering rate was found to be about 2.5 Å per second per 200 nA of primary beam current. This translates to 700 Å for the sample corroded in DDW and 1000 Å for the sample corroded in SW. For the specimen corroded in DDW, the degree of near surface depletion of B is greater than that of Si although the depths of depletion of the two are the same. The degree of Na depletion is also smaller than B. However the Na depth profile may be disturbed by charge induced migration during probe analysis (Muir et al., 1989). Actually, the depth of Na depletion is greater than B (and Mo) depletion, although the percent changes in Na/Fe ratios are very small in the region below B depletion.

In SW, the degree and depth of Si depletion are slightly smaller than those of B depletion. The Mg enrichment penetrates about 400 Å deeper than B depletion. It should be emphasized, however, that Mg is a trace element in PNL 76-68 glass and therefore its enrichment below 1000 Å is not significant. Overall, the degree and depth of B and Si depletions of SW-corroded specimen are greater than those of

DDW-corroded ones.

The fact that B and Si are depleted in the reaction zone indicates that the processes in the reaction zone include not only cation exchange but also network dissolution. This is consistent with Bunker's (1983) high resolution TEM observation that the corroded glass surface is porous. It is not certain, however, if rearrangement of glass structure is involved. It should be noted that both Mg enrichment and Na depletion penetrated to greater depth than Si and B depletion. The cation exchange process thus most likely takes place prior to the network dissolution.

3.2 MCC-1 Tests in DDW and SW at 30°C

3.2.1 General Observations

Corrosion reactions of the glasses proceed much slower at 30 °C than at 90°C. As shown in Tables A3.4 and A3.5, the amount of release of major components from ABS-118 and basaltic glasses is very small. The relationship between the amount of the release and corrosion time are not well defined. This is, at least partly, due to the fact that the amount of released elements in the leachates were close to sensitivities of the analytical methods employed (photospectrometric methods for Si and B, and atomic absorption for Fe and Zn). There was no noticeable difference between samples corroded in SW and those corroded in DDW. Leachate pHs were lower than their corresponding leachants but again, no clear trend with corrosion time was indicated. Normalized weight losses were

penetration of EMP analysis is about 2 μm. Therefore the compositions determined by EMP are composite ones of surface layers and the underlying glass substrate.

3.2.2 SIMS Depth Profiles

The depth profiles of ABS-118 glass in DDW are shown in Figure 3.17. The data were normalized to Si. The Fe/Si ratios showed only very small change from the reference glass. This justifies the normalization against Si. In the top surface of the reaction zone, almost all of B and perhaps all of Na is extracted from the glass. The sputtering rate was found to be about 1.5 Å per second per 200 nA of prime beam current. So, the depletion penetrated to about 600 Å. It should be emphasized that the data were normalized to Si and therefore depletion of B and Na are relative to Si. This indicates that, at low temperature, the silica dominated matrix may be not disturbed in the reaction zone. The SIMS depth profiles of ABS-118 glass corroded in SW are complicated by the surface layer on the glass surface. Because the layer is very adhesive, no method can separate it from the reaction zone and the unaltered glass.

3.3 Corrosion Test in Oceanic Muds

Glass samples corroded in oceanic muds underwent the least change among all tests conducted in this study. Both ABS-118 and basaltic glasses were used in this test. Changes in leachate compositions were not monitored because


A
2 μm

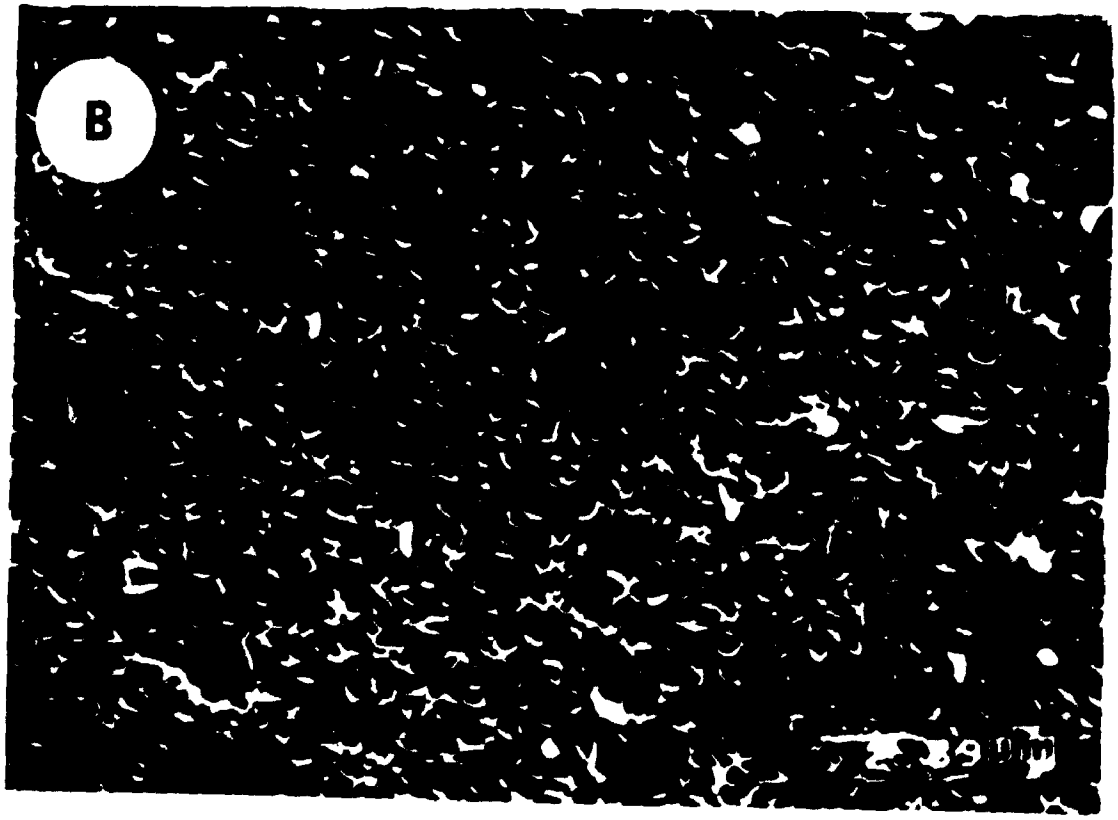
B
2 μm

Table 3.8 Surface layer composition of ABS-118 glass corroded at 30°C

	Parent	DDW	SW	MUDS
SiO2	54.60	54.71	44.26	54.25
Al2O3	5.75	5.65	6.25	5.40
Cr2O3	0.54	0.62	0.72	0.54
FeO	3.43	3.48	4.12	3.06
NiO	0.47	0.45	0.56	0.48
ZnO	3.06	2.85	3.33	2.89
MgO	0.05	0.05	7.61	0.03
CaO	4.15	4.00	3.32	4.02
Na2O	9.45	8.80	8.04	10.00
P2O5	0.50	0.51	0.50	0.52
ZrO2	1.18	1.25	1.32	1.07
UO2	1.51	1.57	1.20	1.53
Total	84.68	83.95	81.22	83.80
Si/Fe	15.91	15.74	10.74	17.73
Al/Fe	1.68	1.62	1.52	1.76
Cr/Fe	0.16	0.18	0.17	0.18
Ni/Fe	0.14	0.13	0.14	0.16
Zn/Fe	0.89	0.82	0.81	0.94
Mg/Fe	0.01	0.01	1.85	0.01
Ca/Fe	1.21	1.15	0.81	1.31
Na/Fe	2.75	2.53	1.95	3.27
P/Fe	0.15	0.15	0.12	0.17
Zr/Fe	0.34	0.36	0.32	0.35
U/Fe	0.44	0.45	0.29	0.50

Table 3.9 Surface layer composition of basaltic glass corroded at 30°C

	REF	DDW	SW	MUDS
SiO2	47.74	49.09	34.02	48.43
TiO2	1.05	1.07	1.01	1.03
Al2O3	14.66	14.74	13.44	14.56
Cr2O3	0.05	0.00	0.00	0.00
MnO	0.18	0.18	0.09	0.17
MgO	7.97	7.85	16.05	7.93
FeO	8.88	8.50	8.37	8.81
CaO	11.21	10.98	8.07	11.05
Na2O	3.00	3.07	2.58	3.07
K2O	0.49	0.44	0.33	0.49
P2O5	0.12	0.11	0.10	0.12
U3O8	1.79	1.61	1.50	1.81
Total	97.13	97.63	85.57	97.45
Si/Fe	5.38	5.77	4.07	5.50
Ti/Fe	0.12	0.13	0.12	0.12
Al/Fe	1.65	1.73	1.61	1.65
Mg/Fe	0.90	0.92	1.92	0.90
Ca/Fe	1.26	1.29	0.96	1.25
Na/Fe	0.34	0.36	0.31	0.35
K/Fe	0.06	0.05	0.04	0.06
U/Fe	0.20	0.19	0.18	0.21

also very small (Tables A3.4 and A3.5).

Although surface layers were not visible for all the glasses corroded at 30°C, SEM observations indicate that after 360 days of corrosion in SW, the surfaces of both ABS-118 and basaltic glasses are covered by very thin surface layers (Figure 3.16). These surface layers are similar to those formed at 90 °C. They are aggregates of very small elongated grains of less than one micron metre in size. The surface layer as a whole is very porous. For those corroded in DDW at 30°C, even less changes were detected using SEM. Only scattered particles of less than 0.5 μm in size were noticed on the surface of basaltic glass after 360 days corrosion in DDW. No changes were detected for ABS-118 glass in DDW even after 360 days.

The above observations were further confirmed by EMP analysis of the corroded samples. The compositions reported in Tables 3.8 and 3.9 are averages of 3 to 5 point analyses, and the compositions of reference glasses were determined in the same analytical session as the corroded samples (The surface composition of the glasses corroded in oceanic muds are also shown in Tables 3.8 and 3.9). There are no significant differences in compositions of unreacted reference glass and the samples corroded in DDW. In SW, surface layers of ABS-118 and basaltic glasses are rich in Mg. The degree of the Mg enrichment is not as great as those of surface layers formed at 90°C. This is because the surface layers developed at 30°C are less than 0.5 μm in thickness and electron

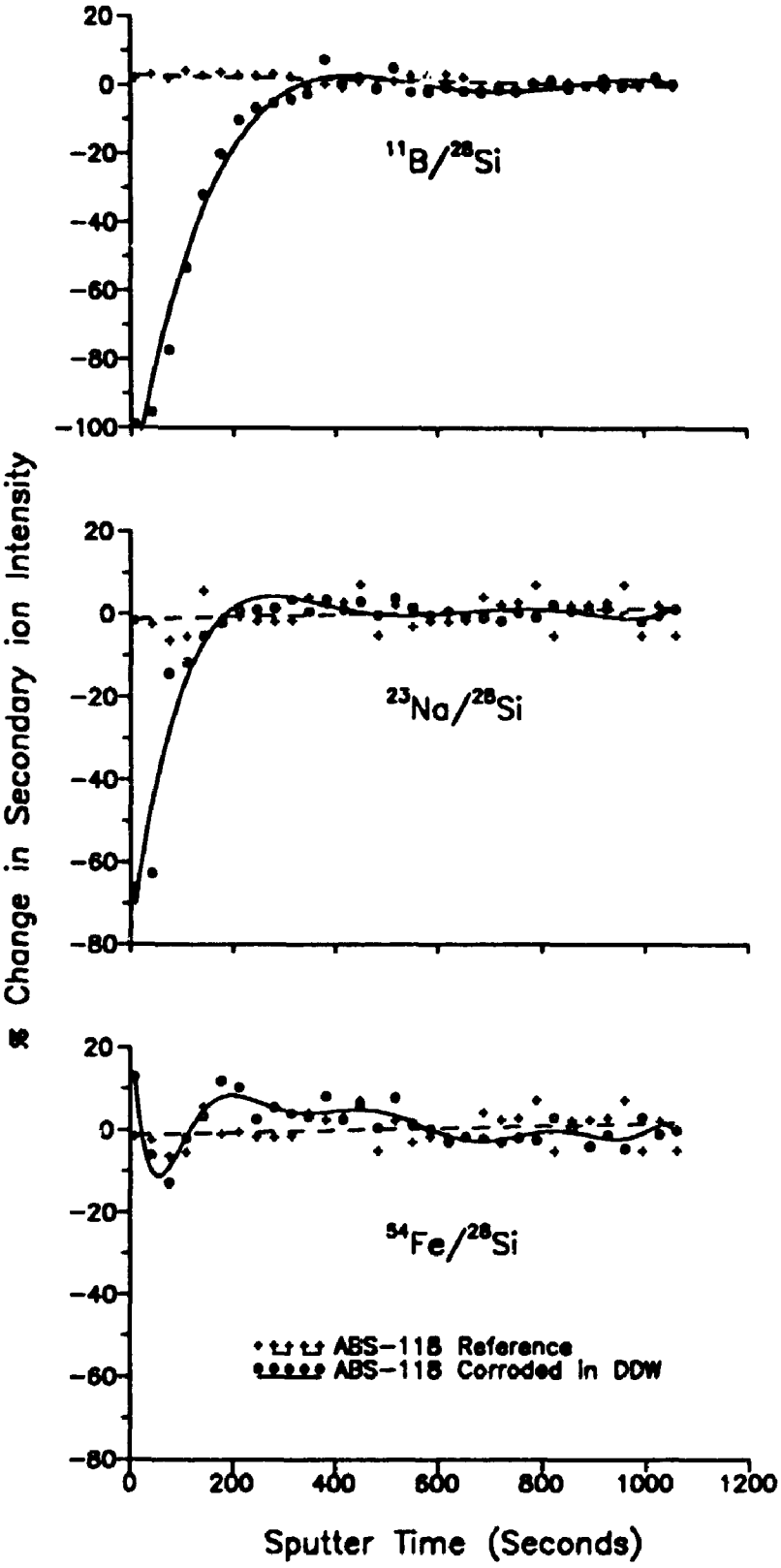

FIGURE 3.17 SIMS depth profiles of ABS-118 glass corroded in DDW.

penetration of EMP analysis is about 2 μm. Therefore the compositions determined by EMP are composite ones of surface layers and the underlying glass substrate.

3.2.2 SIMS Depth Profiles

The depth profiles of ABS-118 glass in DDW are shown in Figure 3.17. The data were normalized to Si. The Fe/Si ratios showed only very small change from the reference glass. This justifies the normalization against Si. In the top surface of the reaction zone, almost all of B and perhaps all of Na is extracted from the glass. The sputtering rate was found to be about 1.5 Å per second per 200 nA of prime beam current. So, the depletion penetrated to about 600 Å. It should be emphasized that the data were normalized to Si and therefore depletion of B and Na are relative to Si. This indicates that, at low temperature, the silica dominated matrix may be not disturbed in the reaction zone. The SIMS depth profiles of ABS-118 glass corroded in SW are complicated by the surface layer on the glass surface. Because the layer is very adhesive, no method can separate it from the reaction zone and the unaltered glass.

3.3 Corrosion Test in Oceanic Muds

Glass samples corroded in oceanic muds underwent the least change among all tests conducted in this study. Both ABS-118 and basaltic glasses were used in this test. Changes in leachate compositions were not monitored because

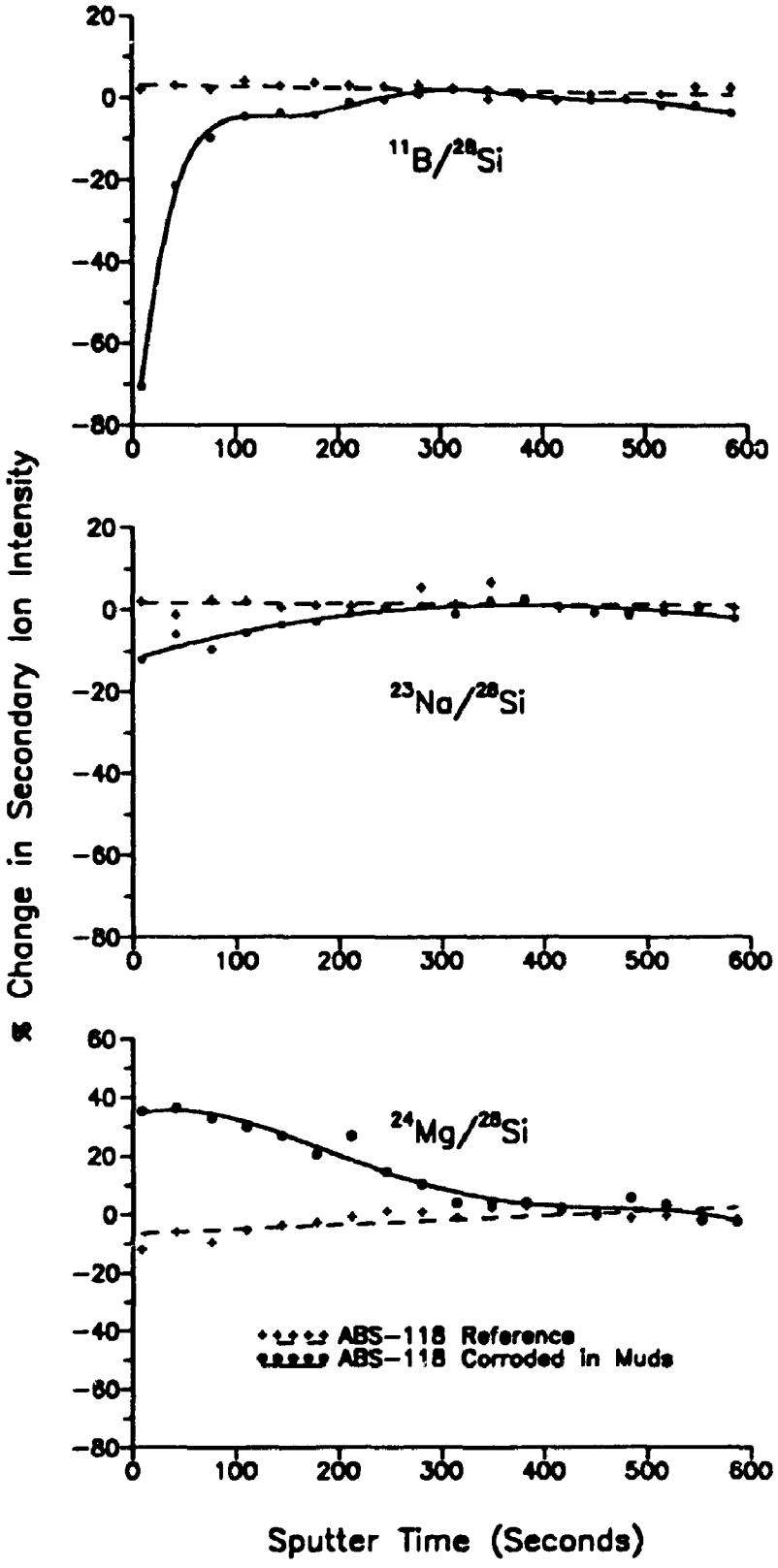

FIGURE 3.18 SIMS depth profiles of ABS–118 glass corroded in oceanic muds.

SA(glass)/V(SW) ratio was very small and any change in leachate composition was expected to be much less than the sensitivity of analytical methods. SEM observations indicate that no changes in surface morphology can be detected for ABS-118 and basaltic glasses after 360 days corrosion. Similarly, no compositional changes were found using EMP (Tables 3.8 and 3.9). SIMS analysis was also used to study the changes in surface chemistry. Figure 3.18 shows depth profiles of ABS-118 glass after one year corrosion in the muds. A thin (about 300 Å) reaction zone is present as indicated by depletion of B and Na. Compared with B, the degree of Na depletion is small, so as the degree of Mg enrichment. By any measure, the rate of glass corrosion in the oceanic muds are small.

3.4 Geochemical Modelling of Reaction Path

The experimental results presented in the preceding sections indicate very complicated reaction patterns. To better understand these results, geochemical modelling was performed. In general, chemical modelling encompasses the speciation of elements in solution and the degree of saturation of an aqueous media with regard to metastable and stable solids (Jenne, 1979). The purpose here is to trace the reaction pathways of glass corrosion. This can not only elucidate the mechanism of leachate evolution but also help one to predict the long-term behaviours of radwaste glass under repository conditions (Crosivier et al. 1986; Grambow, 1984).

The computer code PHREEQE was chosen because of its ability to calculate the speciation of a given solution and to calculate mass transfer as a function of reaction progress. PHREEQE uses ion-association models and mass balance principle and can calculate masses of phase dissolved or precipitated and associated solution composition resulting from user specified reaction steps and phase assemblages. The assumptions and limitations of PHREEQE program were explained in detail by Parkhurst et al.(1980).

The corrosion processes of ABS-118 glass in DDW and SW were simulated. The reaction path may be followed by inverse modelling in which analytical data of the leachate compositions are used as input data. However, this requires a complete analysis of major components in leachates and our leachate data are not complete and thus not adequate for inverse modelling. Therefore forward modelling method was used. In this approach, the amount of dissolution and precipitating solid phases were specified in the input data file. The simulation was based on congruent dissolution of glass matrix and subsequent precipitation of selected low-soluble phases. This is justified by the experimental observations presented in the preceding sections. The reaction path in forward modelling is not mathematically unique, and often the same chemical changes can be modelled exactly by two or more reaction paths. It is felt, however, that the reaction path presented here is the best to simulate the system under consideration.

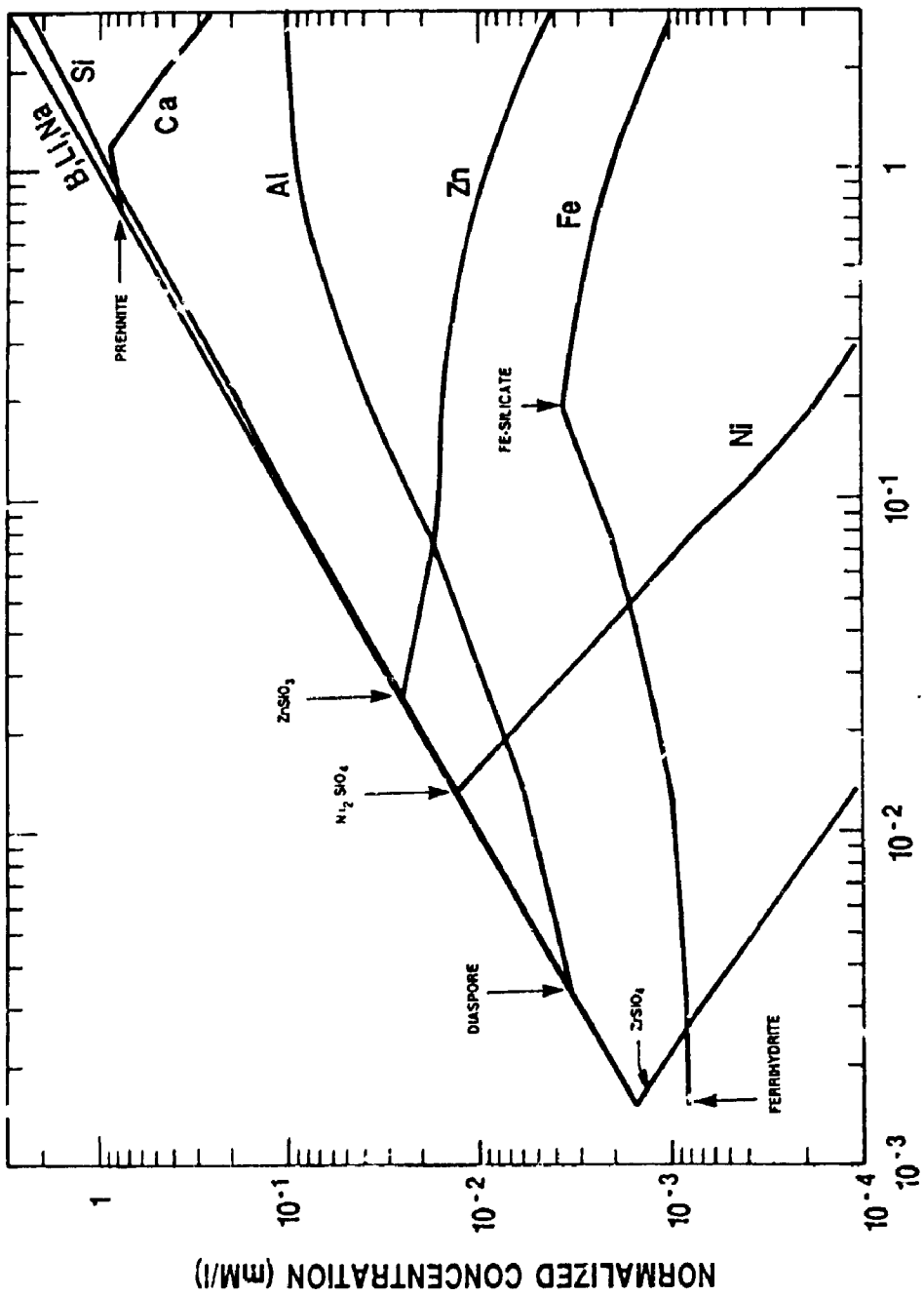

FIGURE 3.19 Simulated reaction path for corrosion of ABS-118 glass in DDW at 90°c

Figure 3.19 shows the results of reaction path modelling for ABS-118 glass with DDW at 90°C. The solid phases used for modelling and their sequence of precipitation are shown in the figure. The total concentration calculated for the element i in solution was expresses as $C_i/V_{i,g}$ and the reaction progress as C_g. Here C_i is the concentration of element i in solution. The $V_{i,g}$ is the number of moles of element i in 100 gram of glass. The C_g is moles of glass dissolution in a litre of solution. One mole of glass is defined as 100 gram. For the line with slope equal to 1, $C_i/V_{i,g} = C_g$. Any conservative element which is not consumed by precipitation fell on this line. B and Li are such examples and their concentration in solution are directly proportional to amount of glass dissolved. Concentration of other elements may be less than the amount of stoichiometric release.

There are intersections at various stages of reaction progress, the curves representing the saturation concentration of certain elements with respect to their solid phases. Beyond each intersection, the solution concentration is controlled by solubility limit; thus $C_i/V_{i,g}$ become less than C_g. The concentrations of various elements at any stage of reaction progress can be obtained from Figure 3.19, using the $V_{i,g}$ values.

The modelling results indicate that Fe- and Al-hydroxides are among the first phases to precipitate. This is followed by the saturation of Zn-, Ni-, and Zr- silicates. These elements would be kept low in leachates. It also

predicts that Fe-hydroxide would be replaced by Fe- silicate (hisingerite) as the activity of silica increases. Both ferrihydrite and hisingerite are very poor in crystallinity and this is consistent with experimental observation. As the reaction progress increases, a Ca-aluminosilicate (prehnite or Ca-zeolite) may form and will remove Ca from solution. The modeled pH values are slightly higher than measured ones. This is because the modelling was performed by assuming that the system is isolated from atmospheric CO_2(gas) but the ingression of CO_2 into the test tubes is almost certain and this will lower the leachate pH.

Among the solid phases used in the modelling, Fe-hydroxide and Fe-layer silicates were confirmed in experiments. Diaspore was chosen over kaolinite because Si concentration would not fit the experimental values as well should kaolinite be used as control for Al. The ZrSiO4 and Ni2SiO4 may not reflect actual precipitating forms of Zr and Ni. Fortunately, both elements have small molar fractions in the glass and would not affect overall leachate chemistry significantly. Analysis of precipitates in surface layer indicated that Zn occurs as hydrated Zn-silicates. However, no such mineral with documented thermodynamic properties is available to our knowledge and therefore more accurate modelling is not possible.

The modelling of glass dissolution in SW is more complicated and less reliable because of the high ionic strength. PHREEQE uses ion association models to calculate

individual ion activity coefficients and both the Davis and Extended Debye-Huckel equations are only applicable to solution with ionic strength around 0.5 M or less (Stumm and Morgan, 1981). Because SW has ionic strength of 0.7 M or so, modelling of glass dissolution in SW will inevitably include some degree of uncertainty. Caution thus should be taken to the modelling results of SW/glass reaction reported in literature (e.g. Crosivier et al., 1986). Therefore the detailed results may be less important but a general discussion can be made.

Modelling results of ABS-118 glass in SW indicate that the reaction path is different from that of DDW in that Mg-silicate (saponite) is a principal solid phase controlling the dissolved silica. Also calcium carbonate (aragonite) is oversaturated from the very beginning. The modeled silica concentration fits the observed values very well by saponite (or sepiolite) control at reaction progress less than 0.30 mM/l. Beyond this point Fe-saponite seems fit the data better. However, saponite can not account for the decrease in silica concentration observed during the experiments (Figure 3.2). The formation of talc or lizardite may account for this behaviour. Both minerals were observed in the surface layers and have much smaller solubility than saponite.

In summary, although very much speculative at this point, the changes in leachate chemistry and precipitating solids with corrosion time (reaction progress) can be simulated by PHREEQE. The oxides, hydroxides, and silicates of major

constituents in glass are saturated at very small reaction progress, and this is justified by the formation of surface layers. The silica concentration in DDW leachates appear to be controlled by ferric- and alumino- layer silicates. In SW, on the other hand, Si concentration is regulated mainly by Mg-layer silicates. This leads to lower Si concentration in SW leachate than in DDW leachates.

CHAPTER 4 - DISCUSSION ON EXPERIMENTAL RESULTS

The experimental results presented in the last section will be discussed in two different contexts. From an empirical point of view, the experiments provided a basis for the comparison of a) relative stability of radwaste glasses and basaltic glass, and b) SW leachant vs. DDW leachant. From theoretical point of view, the experiments provided constraints on the mechanisms of glass dissolution. Because more systematic information was obtained from the tests at 90°C than 30°C, the following discussion will emphasize the test results of 90°C.

4.1 The Amount and "Final Rate" of Glass Dissolution

Before any discussion, the amount of dissolution for each glass in specific corrosion conditions has to be clearly established. This is complicated by the fact that not only dissolution but also secondary precipitation is involved during glass corrosion. Thus the amount of dissolution cannot be judged by the elemental release during glass corrosion. That is, the NL_i of most elements is not directly related to the amount of glass dissolution. For example, the NL_i of Si does not indicate the degree of dissolution because precipitation during the corrosion consumes dissolved Si. The NL_i of Na cannot be used as an indicator of glass dissolution because Na is a modifier in the glass structure and its

extraction from glass may not destroy the network of the glass. In this respect, the NL_i of B is probably most meanful because B is a network builder and its precipitation during glass corrosion is negligible (Scheetz et al., 1981, 1985). Thus NL_i of B may be used as a direct measure of degree of dissolution of borosilicate glass. The amount of dissolution is numerically equal to NL_B because the release of B is normalized. Furthermore, by knowing the density of glass, the amount of dissolution may be transferred to depth of dissolution according to following equation:

$$T_d = NL_B/d_g \qquad \text{.....4.1}$$

where T_d is the depth of dissolution (μm),

NL_B is normalized B release (g/m^2), and

d_g is the density of the glass (g/cm^3).

The densities of the glasses are readily calculated by measuring the geometry and mass of the glass specimens, and found to be 2.5, 2.9, and 2.8 g/cm^3 for ABS-118, PNL 76-68, and basaltic glasses respectively.

For the glass which does not contain B, e.g. basaltic glass, it is even more difficult to establish an indicator for degree of glass dissolution. Furnes (1975) used the thickness of the surface layer to calculate the rate of alteration of basaltic glass. However, as will be shown later, the thickness of surface layers is not equal to the dissolution depth, and thus it is not appropriate to calculate the rate of dissolution based on the surface layer thickness. Zhou et al.(1987) suggested that both surface layer thickness and the

amount of Si release should be considered to determine the total amount of dissolution. Theoretically, the amount of dissolution can be calculated according to mass balance of Si. By measuring the Si release and determining the thickness and Si content of surface layer, the total amount and depth of dissolution can be calculated using following equations:

$$M_d = NL_{Si} + (f_{Si,SL}/f_{Si,g}) * (d_{SL}/d_g) * T_{SL} * d_g \quad .....4.2$$

$$T_d = NL_{Si}/d_g + (f_{Si,SL}/f_{Si,g}) * (d_{SL}/d_g) * T_{SL} \quad .....4.3$$

where M_d is total amount of dissolution (g/m^2),

T_d is depth of dissolution (μm),

NL_{Si} is normalized release of Si (g/m^2),

$f_{Si,g}$ is the mass fraction of Si in glass,

$f_{Si,SL}$ is the mass fraction of Si in surface layer,

d_g is the density of glass (g/cm^3),

d_{SL} is the density of surface layers (g/cm^3),

T_{SL} is the thickness of surface layer (μm).

In practice, however, such a calculation is difficult and depends on the accuracy of measurements of terms on the right side of equations 4.2 and 4.3. The density of the surface layer, d_{SL}, was not measured. However, it is reasonable to use the density of palagonite (2 1 g/cm^3, see Chapter 5) for d_{SL} and this enables us to estimated both M_d and T_d. Based on the methods discussed so far, the amount (M_d) and depth (T_d) of dissolution for each of three glasses were calculated. Table 4.1 only shows the M_d and T_d of three glasses at 90°C. Also, only the last data point was taken and the data thus give the total amount of dissolution in the entire periods of

Table 4.1 Amount of glass dissolution at 90°C

		DDW	SW
ABC-118	M_d*	11.00	5.30
(360d)	T_d+	4.40	2.12
PNL 76-68	M_d	96.62	19.70
(180d)	T_d	33.30	6.79
Basaltic	M_d	15.05	2.68
(360d)	T_d	5.38	0.95

---

* In g/m^2
\+ In μm

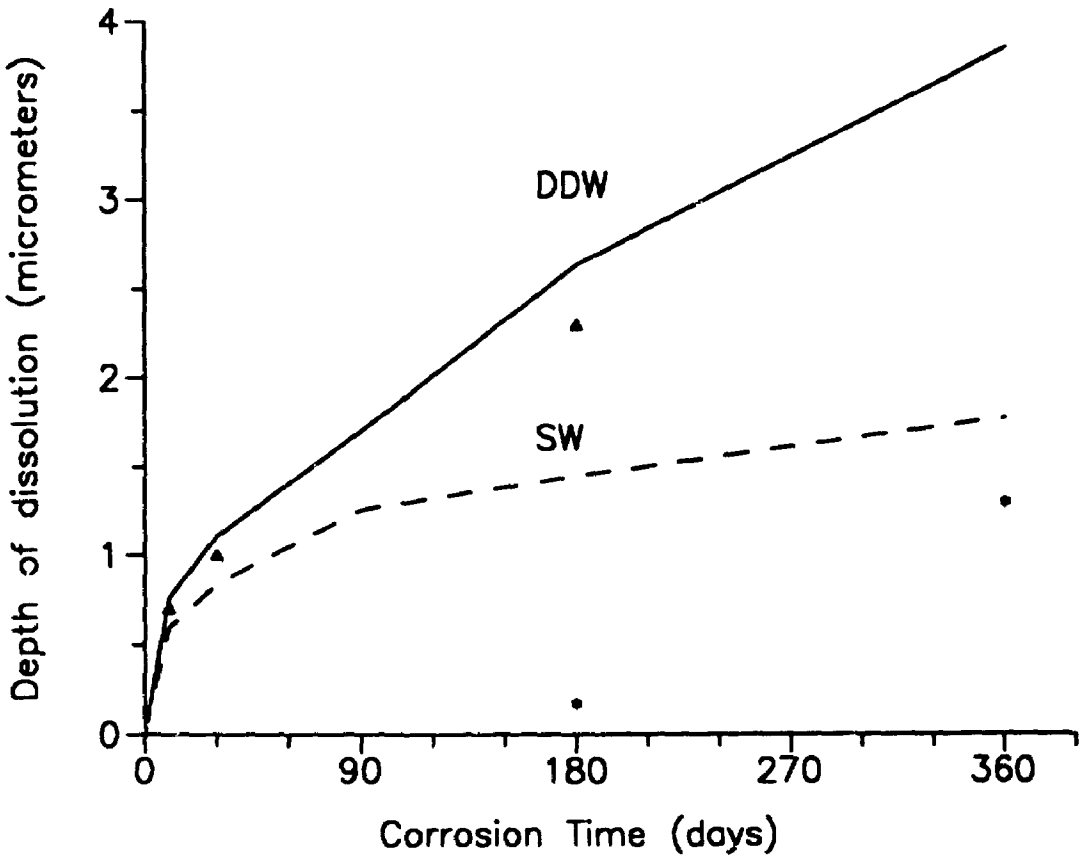

FIGURE 4.1 The depth of dissolution of ABS–118 glass in DDW and SW. Calculation was based on B release during glass corrosion. The measured thickness of surface layers is also plotted (stars: DDW; triangles: SW).

corrosion. As stated before, the data from 30°C tests are too poor to make interpretation.

Figure 4.1 shows the depths of dissolution during the corrosion of ABS-118 glass. This is translated from M_d data in Figure 3.2. The thickness of surface layers is also plotted on the Figure 4.1. It is interesting to compare the thickness of surface layers with the depth of dissolution. Even though the surface layers developed in SW are thicker than those in DDW, the depth of dissolution in SW is smaller than that in DDW. Apparently, precipitation is more effective in SW. The slopes of the two curves in Figure 4.1 are the rate of dissolution, which changes with reaction time. The kinetic implications of the changes will be discussed in section 4.5. If the portion of the curves between 180 and 360 days of is assumed to be linear, a "final rate" of dissolution for the glass in DDW and SW may be defined. This "final rate" defined as such should be a conservative value because the dissolution rate is very likely to decrease further with increasing reaction progress. Table 4.2 compares the estimated "final rate" of the three glass in both DDW and SW. The "final rate" of PNL 76-68 in DDW and SW may be not real because our longest corrosion test for the glass was 180 days; the rate of release has been shown elsewhere to decrease significantly after 180 days (Strachan, 1983).

4.2 Effects of Leachant: SW vs. DDW

The effect of leachant chemistry on corrosion of radwaste

Table 4.2 "Final rate" of glass dissolution at 90°C

		DDW	SW
ABS-118	$g/m^2.y$	6.30	1.96
	$\mu m/y$	2.52	0.78
PNL 76-68	$g/m^2.y$	152.60	28.48
	$\mu m/y$	52.62	9.82
Basaltic	$g/m^2.y$	2.18	2.14
	$\mu m/y$	0.79	0.76

glass have been subjected to many empirical studies (Apted et al., 1986; Hermansson et al., 1983; Lokken and Strachan, 1984; Strachan, 1983; Strachan et al., 1985; Westik et al., 1983). Many of these investigations evaluated the effect of ground waters and synthetic solutions on glass corrosion. The laboratory study on corrosion of basaltic glass have been studied by Furnes (1975) and more recently by Crosivier et al. (1983,1986) and Byers et al. (1987). The effect of seawater on the glass corrosion has also been investigated (Zhou and Fyfe, 1988) were the first to study effect of seawater on corrosion of simulated radwaste glasses. The control tests in DDW were conducted at the same time and under the same test conditions as those in SW for comparison purpose. Our results in DDW are comparable to those of other researches with similar experimental conditions (Lokken and Strachan, 1984; Strachan, 1983; Strachan et al., 1986; Grambow and Strachan, 1984), and therefore provide reliable reference data.

The experimental results show that the amount and "final rate" of dissolution of the two simulated waste glasses are lower in SW than in DDW (Table 4.1 and 4.2). For basaltic glass, the amount of dissolution in SW was much lower; however, the "final rate" in DDW and SW are similar. This is consistent with the fact that in natural condition, no systematic different in alteration rate was found for basaltic glass (Byers et al., 1987).

Leachant composition has been shown to influence glass corrosion primarily through pH and Si concentration (Grauer,

1985). Boron silicate glass is known to corrode faster in both acidic and alkaline solutions than in solutions of neutral pH. This pH effect may not explain the different dissolution rates in DDW and SW because pH of SW is greater than that of DDW. Experiments (Strachan et al., 1985; Pederson et al., 1983) and theoretical treatment (Grambow, 1985; 1987) have shown that rate of glass dissolution is affected by the degree of under saturation with respect to silica. The rate decreases when solution reaches saturation with respect to silica. The solubility of silica in seawater may be lower than in deionized water because solubility of silica decreases in Na, K-, Ca-, and Mg- chloride solutions, with the greatest decrease in $MgCl_2$ and $CaCl_2$ solutions (Marshall and Warakomski, 1980). As a consequence, the degree of undersaturation with respect to silica is less in SW than in DDW. This may explain the greater stability of both glasses in SW than in DDW. Similar argument was used to explain the greater stability of SRL-113 glass in salt brine (Shade et al., 1984; Strachan et al., 1985). However, as will be discussed in section 4.5, the concentration of silica in leachates is controlled by layer-silicates and not amorphous silica. It is the rapid saturation with respect to Mg-silicates that suppresses the dissolution rate of the glasses.

Zhou and Fyfe (1988) argued that the greater stability of the glasses in SW may be due to high concentration of cations such as Mg. It has been shown that the addition of many cations to solution slows the hydrolysis of silica and

2

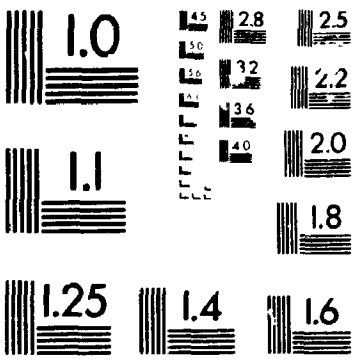

silicate glasses, even when the cations are not part of the solid (Oka et al., 1979; Iler, 1973). Most abundant cations in seawater are Na and Mg. In a leaching study of a simple $Na_2O.3SiO_2$ glass, McGrail et al. (1986) showed that the rate of Na release was depressed in saturated NaCl solutions. However, the Na release rate in the solution is in the same order of magnitude of that in DIW. Therefore high Na concentration probably has a minor effect on the rate of glass dissolution. This can be also deduced from the work of Dugger et al. (1964), which indicated that silicate non-bridging oxygens have a much high affinity for protons than for sodium ions. In contrast, Mg in SW may be more important, because Mg can be incorporated into the glass surface by the reaction (Lee and Clark, 1985):

$$\equiv Si\text{-}OH + Mg^{2+} = \equiv Si\text{-}O\text{-}Mg^{+} + H^{+} \quad \text{.....4.4}$$

It has been shown in studies of the dissolution of silicate minerals that exchange of Na^+ by H^+ (or H_3O^+) is not reversible where as the exchange of Mg^{2+} with $2H^+$ are reversible (Blum and Lasaga, 1988). A high Mg concentration in SW will shift the above reaction to the right and stabilize the glass. The reaction may also prevent a pH increase in SW which would accelerate the hydrolysis of Si-O-Si bonds. A more favourable reaction may be exchange of Na^+ by Mg^{2+}:

$$\equiv Si\text{-}O\text{-}Na + Mg^{2+} = \equiv Si\text{-}O\text{-}Mg^{+} + Na^{+} \quad \text{.....4.5}$$

Diffusion of Mg into reaction layers was shown by the SIMS depth profile in Chapter 3. The chemical durability of glass could increase with divalent oxide additions (Clark et

al., 1976; Isard and Muller, 1986). We will show in the later sections that silicate saturation and Mg diffusion are closely related and contribute to the reduction in the dissolution rate of the glasses.

4.3 Effect of Glass Composition

The three types of glasses used in the experiments show significant difference in stability. The much investigated PNL 76-68 glass has the highest dissolution rate. The amount of dissolution from PNL 76-68 was about one order magnitude higher than ABS-118 and basaltic glasses in the same period of corrosion time. On the other hand, the amount of dissolution from ABS-118 and basaltic glasses were similar (Table 4.1). The "final rate" of the two glasses in SW are also very similar.

The effect of glass composition on dissolution rate has received much attention (Paul, 1979,1981; Feng and Barkatt, 1988; Feng et al., 1988; Janzen and Plodinec, 1984). Most of the studies were extension and development of Paul's (1979) thermodynamic model. In this model, glass is regard as a mixture of oxides, ignoring how the oxides are actually incorporated into the glass structure. The silica release rate is related to the calculated free energy of hydration by: $\log K = \Delta G/RT$. The above approach is reported to be capable of predicting silica release rates for a wide range of silicate glasses to within an order of magnitude (Janzen and Plodinec, 1984). A similar approach was developed by Feng and Barkatt

(1988) and relates bond energies with durability of glass. The thermodynamic model assumes that the glass can be considered as an average assemblage of simple thermodynamically stable phases. However, as pointed out by Bunker (1987), glass is a metastable phase which is not in thermodynamic equilibrium with respect to stable oxide and silicate phases. In addition, water usually attacks those bonds which are most susceptible to hydrolysis rather than attacking thermodynamically "average" bonds at the same rate, leading to selective leaching in reaction zone. Selective leaching provides a mechanism for allowing water to penetrate the glass structure, accelerating the hydrolysis of remaining bonds. Finally, the thermodynamic calculation must be based on phases which approximate the actual structure of the glass.

Despite these limitations, predictions of the thermodynamic models are qualitatively consistent with our experimental observations. It has been shown that durability of borosilicate glass increases with the amount of SiO_2 and Al_2O_3 in the glass(Janzan and Plodinec, 1984; Feng et al., 1988). PNL 76-68 glass has lowest SiO_2 content among three types of glass and has no Al_2O_3. This may explain the high dissolution rate of the glass in the experiments. The high REE content in PNL76-68 glass apparently has no beneficial effect on glass durability.

There are remarkable similarities in corrosion behaviors and rates between ABS-118 and basaltic glasses, especially in SW. In terms of surface layer composition and morphology, Mg-

layer silicate and calcium carbonate predominated both glasses. It should be noted, however, ABS-118 glass contains about 10%wt of fission products which are not included in the simulated ABS-118 glass used in our experiments. The irradiation effects of the fission products on glass stability should be investigated.

4.4 Effects of Temperature and Other Corrosion Conditions

Temperature is one of the most important factors affecting the rate of glass dissolution. Generally speaking, the rate of glass dissolution increases with temperature and efforts were made to interpret the temperature dependence according Arrhenius equation. However, the relationship exhibits a complicated nature (Mendal et al., 1981; Grauer, 1985 for reviews). This is most probably because mechanism or rate controlling mechanism changes with temperature. The Arrhenius equation is not suitable to the processes in which the rate controlling mechanism changes with temperature. Our experimental data indicated that principal mechanisms involved in glass corrosion at 30°C are the same as those at 90°C. Both include network dissolution, leaching in reaction zone, and back precipitation. However, it is not certain that rate controlling mechanism is the same.

A few comments should be made on the corrosion behaviour of ABS-118 and basaltic glasses in oceanic mud. No weight loss was observed to either of the glasses during one year of test period. No surface layers were observed either. The reaction

zones, documented by SIMS depth profile, are about 450 Å for ABS-118 glass. The amount of dissolution cannot be estimated because changes in leachates can not be recorded. No direct comparison can be made between these tests with those in SW at 30°C, because the simulated corrosion in oceanic muds was set up at room temperature with temperature fluctuation from 18 to 26°C. Nevertheless, the preliminary results suggest corrosion reaction in oceanic muds may be slower than SW at the same temperature. This needs to be tested with controlled experiments because some experiments indicated that the presence of bentonite may accelerate glass corrosion (e.g. Christensen et al., 1984).

4.5 Mechanism and Kinetics of Glass Dissolution

Before the mechanistic implications of the experimental data are discussed, current understanding of the mechanism and kinetics of glass dissolution should be reviewed. Progress has been made in the last 15 years and various types of mechanism (ion exchange, or selective leaching, cation diffusion, matrix dissolution, back precipitation, adsorption etc.) have been recognized (Clark and Hench, 1983). However, controversy still exist over the rate controlling step in glass dissolution. Generally speaking, kinetic theories on glass dissolution can be divided into two groups: transport process (diffusion) as rate limiting step and kinetics of chemical reaction as the rate limiting step.

In the group of transport processes, diffusion of a

dissolved species through bulk glass or surface layers is assumed to control the rate of dissolution. Among the proposed processes are the diffusion of H^+ or H_3O^+, H_2O, and alkali or other soluble species through the bulk glass (Banba and Murakami, 1985; Doremus, 1975; Smete and Lomman, 1983; Smets and Tholen, 1985), and the diffusion of dissolved species through surface layers (Banba and Murakami, 1985; Grambow, 1987; Kenna and Murphy, 1980; Lanza and Parnisari, 1979).

Selective leaching of modifier cations is usually described as an ion exchange process described by reactions such as

$$\equiv Si\text{-}O\text{-}Na + H_3O^+ = \equiv Si\text{-}OH + Na^+ + H_2O \quad \ldots\ldots\ldots\ldots 4.6$$

The classical model (Doremus, 1975) assumes that leaching is an interdiffusion process controlled by the rate at which the slowest moving cation diffuses through the network structure of the bulk glass. As the rate of release decreases with increasing depth of alkali depletion in the outer glass surface, matrix dissolution will become the dominant reaction. This was described mathematically by the following equation:

$$Q = at^{1/2} + bt \quad \ldots\ldots\ldots\ldots\ldots\ldots 4.7$$

where Q is total release, t is corrosion time, and a and b are constants (Douglas and El-Shamy, 1967). This expression indicates that the parabolic term is likely to dominate at short times, but the linear term usually becomes rate controlling after a period of time determined by the ratio between the coefficients a and b. Equation 4.7 has been used to fit many experimental data. However, the dissolution rates

are usually 100 to 100,000 greater than predicted assuming that alkali diffusion is rate controlling (Bunker et al., 1983; McGrail et al., 1984). If hydronium ion diffusion is to be rate controlling, the discrepancy between actual and predicted dissolution rates could be even worse because hydronium ion diffusion must be even slower than alkali diffusion (Bunker, 1987).

Diffusion of molecular water was also considered as a rate limiting step (Smets and Lommen, 1983; Smets and Tholen, 1985). These authors suggested the glass dissolution is governed by the diffusion of water, which results in a combination of a linear rate of glass dissolution and a diffusion controlled leaching of the alkali ions. Based on size consideration, Bunker (1987) argued that most bulk glass structures probably contain voids which are the same size or smaller than water molecules. He suggested the rate of water penetration is controlled by reversible hydrolysis reactions rather than by diffusion of molecular water through bulk glass. However, the size and distribution of voids in glass have not been measured.

A more controversial issue is whether the surface layers formed during glass corrosion are protective and can act as dissolution barriers. It has been generally observed that, concurrent with surface layer formation, element release rates decrease with time. This phenomenon is observed not only in static leaching tests but also in dynamic tests, and leads to the assumption that the surface layer presents a rate limiting

diffusion barrier to transport of water or hydronium ions into the glass , and/or to transport of leached material from the glass to solution (Banba and Murakami, 1985; Barkatt et al. 1986 a,b,c,; Kenna and Murphy, 1980; Malow, 1982; Lanza and Parnisari, 1979). Efforts were made to test this assumption (Chick and Pederson, 1984; Grambow and Strachan, 1984; Coradt et al., 1985) and a negative conclusion was reached. In most cases, removal of a surface layer did not accelerate the dissolution reaction. This is particularly true for the surface layers developed in DDW. Surface layers developed in MgCl solution were found to decrease dissolution rate (Grambow and Strachan, 1984) but the authors attributed this effect to saturation rather than a diffusion barrier. The arguments in all three papers are disputable and not conclusive. However, it should be noted that in order to be a reaction barrier, the diffusion of molecular water or dissolved ions in the surface layer must be slower than the hydrolysis of silonal groups. Since the surface layer is highly porous, it may not be able to act as reaction barrier.

The rate of chemical reaction as a rate limiting step is a popular hypothesis (Bunker, 1986, 1987; Byers et al., 1987; Freude et al., 1985; Grambow, 1985, 1987; Kuhn and Peters, 1983; also Barkatt et al., 1986a,b,c at high flow rates). Emphasis has been made on network hydrolysis and silica saturation is considered as the cause for decrease in dissolution rate. Network hydrolysis reactions result in the dissolution and restructuring of the silicate network. For

alkali silicate and borosilicate glasses, Raman and solid state NMR studies (Bunker, 1986) have shown that reversible hydrolysis reaction such as those shown below occur in leached glass under most of pH conditions:

$$\equiv Si\text{-}O\text{-}Si(OH)_3 + OH^- \leftrightarrow \equiv Si\text{-}O\text{-}Si(OH)_4^- \leftrightarrow \equiv Si\text{-}O^- + Si(OH)_4 \quad .....4.8$$

In the forward direction, this reaction shows that hydroxide ions attack silicate sites which have non-bridging oxygens (NBO's) or silanols to form unstable 5-coordinate intermediates. The intermediate can decompose to break the Si-O-Si bond, resulting in network dissolution. The rate of hydrolysis is faster on sites with NBO's because the structural rearrangements required to form the 5-coordinated intermediates become easier as the site is attached to the network by few bridging oxygens. The reverse of this reaction shows that silanol group can react with each other to reform Si-O-Si bonds. In this case, the preferred reaction is between highly polymerized silicate sites and silicic acid. Since the silanols on which ion exchange reactions occur are eliminated via repolymerization, the ion exchange reactions responsible for selective alkali leaching are not reversible (Bunker, 1987).

Clearly, the hydrolysis reactions are complex, even for a simple alkali silicate glass. The rate of these reactions is not yet known. Grambow (1985, 1987) simplified the system and developed a rate equation for glass dissolution. His formulation followed the method developed by Aagaard and Helgeson (1982) for feldspar dissolution using transition

state theory. Transition state theory (Eyring, 1935) postulates that chemical equilibrium is maintained among all reactants and activated complexes during any given reaction progress. The irreversibility and the rate of the overall reaction is ascribed to the decomposition of the activated complexes, which lowers the free energy of the system and leads ultimately to a state of chemical equilibrium in the system. The rate limiting step in the reaction is affected by reaction progress. Far from equilibrium, the rate is proportional to the concentration of the activated complex in the transition state, but close to equilibrium the rate is reduced by the saturation effect.

In Grambow's formulation, silica is considered as the dominant constituent of the activated complex and the desorption of silicic acid is the only irreversible reaction considered. This reaction controls the overall dissolution rate and is controlled by the equilibria on the left side of the reaction scheme. Figure 4.2 illustrates graphically the reaction scheme of dissolution and concurrent changes in free energy of the system. The rate of dissolution can be expressed as:

$$r_m = K_+ (1-\exp(-A^*/RT)) \quad \text{.....4.9}$$

where K_+ is the rate constant for the forward reaction which depends on the glass and solution composition and on temperature. A^* is chemical affinity of the rate limiting reaction and describes the effect of saturation on the rate, and can be expressed by

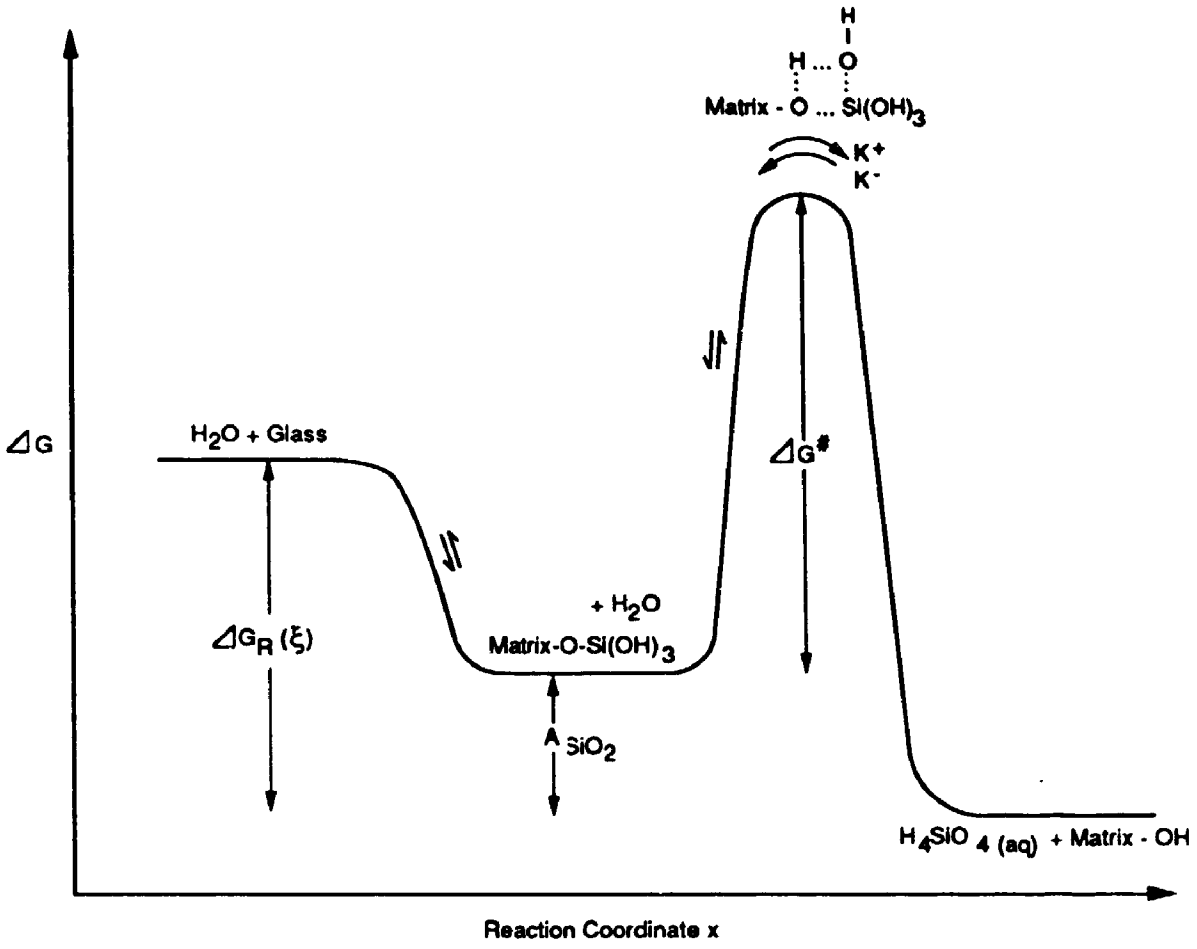

FIGURE 4.2 Reaction Scheme of glass dissolution (Grambow, 1987)

$$A^* = -2.3RT\log(IAP^*/K^*) \quad \text{.....4.10}$$

where IAP is the ion activity product and K^* is the equilibrium constants for the rate limiting reaction. In the most simple case, the rate limiting reaction is

$$SiO_2 + 2H_2O = H_4SiO_4 \quad \text{.....4.11}$$

then

$$r_m = K^* * (1-a_{H4SiO4}/K^*) \quad \text{.....4.12}$$

This equation describes the effect of silica concentration on the dissolution rate of glass in a way typical of first order reactions. Initially (far from saturation), the dissolution rate equals the forward rate constant; when the reaction approaches silica saturation, the chemical affinity decreases and reaction slows down. At saturation, the chemical affinity equals zero and the reaction stops. Grambow (1985, 1987) argued that for glass dissolution, A^* cannot become zero (no true equilibrium), since saturation only involved the reacting surface and soluble elements might still be released from the bulk glass. A final affinity of reaction and a corresponding final rate will remain under saturated conditions.

A few comments should be made on Grambow's formulation. First of all, the term "silica saturation" is not well defined. According to equation 4.11, it should refer to saturation of H_4SiO_4 with respect to amorphous silica. It should be noted that the leachates reported in the literature (Grambow and Strachan, 1985; Strachan, 1983; Strachan et al., 1986; Zhou and Fyfe, 1988) were not saturated with respect to amorphous silica. The maximum Si concentration in "silica-

saturated" region was about 100 ppm or 214 ppm as SiO_2. This value represents the maximum concentration in DDW leachants and the maxima was much lower in SW and salt brine. In DDW, the solubility of amorphous silica was reported about 321 ppm to 500 ppm at 90°C (Akabane and Kurosawa, 1958; Fournier and Rowe, 1977; Goto, 1955). Therefore, amorphous silica in the leachates was undersaturated. Crystalline SiO_2 polymorphous (e.g. quartz, cristobalite, etc.) have much lower solubility than amorphous silica and must be oversaturated in the leachates. However, these polymorphous were not found in the surface layers. We propose here that Si concentration in the leachates were regulated by silicate minerals. Which silicate phase controls Si concentration depends on the corrosion conditions (temperature, SA/V ratio, etc.) and glass and leachant compositions.

Second, by assuming that desorption of SiO_2 is the only control of overall reaction, Grambow's model fails to account the roles of many other components. Some components (Al, Zr, etc.) have been shown to affect glass stability (Paul, 1977; Feng et al., 1988).

Finally, the physical and chemical nature of the reaction zone should be considered. In Chapter 3, we have shown that the reaction zone chemistry developed in SW is significantly different from those of DDW. This difference may contribute to the greater stability of the glasses in SW over DDW.

Based on the above literature review and also on the data presented in Chapter 3, three successive stages in glass

corrosion are proposed here:

The first stage is ion exchange of alkali ions by hydronium. In SW or salt brine exchange of alkali ions is more likely by Mg^{2+} and H_3O^+. This step may be very fast compared with the overall reaction but the nature of ion exchange (H_3O^+/Na^+ vs. Mg^{2+}/Na^+) may affect the rate of subsequent reactions. Therefore the role of ion exchanges can not be ignored.

The second stage is formation of a reaction zone depleted in Na, Li, K, B, and Mo. Si may be or not depleted in the zone depending on glass composition and corrosion temperature. At high temperature Si is depleted and silica network in the reaction zone is probably rearranged. The characteristics of the reaction zone also depends on leachant composition. In DDW, this zone is enriched in Fe, Zn, Al, and other insoluble elements; in SW, this zone is enriched in Mg. The diffusion of molecular water into the glass surface and subsequent ion exchanges and hydrolysis of glass network may be responsible for the formation of reaction zones.

The third stage is slow dissolution of reaction zone material at the solid-solution interface accompanied by diffusion of ions from fresh glass boundary leading to a quasi steady-state dissolution. A surface layer may form because the build-up of dissolved components in solution leads to oversaturation with respect to certain solid phases. The accumulation of dissolved components in solution and subsequent saturation and precipitation can reduce both the

dissolution and diffusion process simply by reducing the degree of undersaturation and concentration gradients. In this respect, the saturation of silicate phases may be most important, because SiO_2 is a network former and the most abundant component in any silicate glass. However, saturation of silicate minerals does not stop the dissolution. A "final rate" of the dissolution would remain because precipitation of a surface layer will remove dissolved silica and more glass will be dissolved to maintain the saturation condition. In SW and salt brine, Mg may also diffuse into the reaction zone. This is important because Mg-silicates have low solubility and can quickly become saturated in solution. A Mg and Si enriched reaction zone is bound to dissolve very slowly in a Mg-silicate saturated or oversaturated solution.

The above model can qualitatively explain all of our experimental results at 90°C and also the results of many others (Chick and Pederson, 1984; Coradt et al., 1985; Grambow and Strachan, 1985; Strachan, 1983; Strachan et al., 1987). It is consistent with surface reaction model of Grambow (1985, 1987) but also recognizes the roles of ion exchange and diffusion, effect of glass composition, and effect of leachant composition. It suggests that the rate limiting mechanism may change with reaction progress. It should be pointed out, however, that a quantitative formulation of the model requires further study. This model also resembles Chou and Wollast's (1985) model for feldspar dissolution.

4.6 Behaviour of Major Constituents of the Glasses During Corrosion

The purpose of a mechanistic study on waste glass dissolution is to predict the long-term stability of the waste glass in repository conditions, and then to evaluate the release rate of radionuclides and their environmental hazards. The purpose may be fulfilled or supplemented by analyzing the behaviour of individual radionuclides during glass corrosion. As a starting point, we analyze the behaviour of major constituents of the glasses during corrosion, and to discuss their implications. According to their behaviour during corrosion, the major constituents of the glasses can be divided into four groups:

I. Group I includes B, Mo, Na, and Li. The oxides of these elements are very soluble and they tend to accumulate in solution. Their concentrations in the surface layers are very low or absent. A small amount of Na may be trapped in surface layers probably as interlayer cations of clay minerals. In the reaction zone, these elements are leached out in preference to Si or/and Fe. The total amount of release of these elements would increase with reaction progress. However, experimental results indicated that the rate of their release will decrease with reaction progress. The cause for the decrease is the saturation of silicate phases.

II. Group II includes Fe, Mn, Cr, Zn, Ti, Zr, REE, and U. These elements can form insoluble oxides , hydroxides, and

silicates, and tend to accumulate in surface layers. Their release to solution is insignificant and probably limited by their respective solubilities.

III. Group III elements are Si, Al, and Ca. They are partially lost to solution during glass corrosion. In the reaction zone, these elements are depleted relative to the Group II elements. The concentration of these elements in the solution are also controlled by the solubilities of their solid phases which are most likely silicates and layer silicates.

IV. Group IV represents a single element, Mg. The behaviour of this element during glass corrosion is unique. In DDW, Mg in glass is partially lost to solution just like Ca; in SW, however, Mg in SW is incorporated into the surface layer and diffuse into the reaction zone during glass corrosion.

The above systematic analysis of elemental behaviour indicates that for MCC-1 90°C type of corrosion tests, the kinetics of establishing solubility control are relatively rapid. Most glass components reach saturation within a few months to a year. If this condition is established in a waste repository, the amount of radionuclides available for release will be limited by solubility instead controlled by kinetics of glass dissolution. Considering the nature of radionuclides in radwaste glass, one may divide them into three groups (Dlouhy, 1982): fission products (e.g. Cs, Sr, Tc, Ru, Y), transuranium elements (e.g. U, Am, Pu, Cm), and activated or

induced radionuclides (e.g. radioactive isotopes of Fe, Co, Cr, Ni, and Mn). Among these, activated radionuclides are transition metals and they were shown to accumulate in surface layers and therefore maximum concentrations are most likely limited by their solubility. Transuranium elements will also reach their solubility very fast and precipitate out. This is shown by accumulation of U in surface layers and very low concentration in the leachates. The precipitates of major components (Fe-hydroxides and clay minerals) may also adsorb transuranium elements (Salter and Jacobs, 1982). Some of fission products (e.g. Cs, Sr) belong to group I or Group III elements and can be readily released. But their release would be depressed by the saturation of other components. We thus conclude that if the physicochemical conditions of MCC-1 90°C type of tests are justified under repository conditions, reaction kinetics of glass dissolution may assume much less importance, and the evolution of solid phases with reaction time and the solubilities of these solid phases are perhaps more important. Because of the difference in composition of various waste glasses, the resulting leachate chemistry can be different under the same corrosion conditions. This may lead to changes in controlling solids and the solubilities of certain elements. Although similar observations were made by Banba and co-workers in their Soxhlet-type corrosion experiments (Murakami and Banba, 1984; Banba and Murakami, 1985; Banba et al., 1986), the above conclusion is made for static MCC-1 90°C type of corrosion tests and may be not hold

for dynamic corrosion tests. A more general conclusion by Mendal et al. (1984) remains to be testified (Freude et al., 1985).

CHAPTER 5 - VOLCANIC GLASS AS NATURAL ANALOGUES OF RADWASTE GLASS

5.1 Introduction

In the previous chapter, the corrosion mechanisms and rates between basaltic glass and simulated waste glasses under laboratory conditions were shown to be similar. This chapter will analyze the long term corrosion mechanism and rate of dissolution of volcanic glasses in submarine environments. One of the most critical aspects of the evaluation of radioactive waste forms is the extrapolation of their material properties (as determined in short term experiments) over long periods of time. Such extrapolation over geological time has to be verified or confirmed by natural analogues of similar age. With respect to the long-term stability of radwaste glasses, natural glasses are suitable for analogues because they are structurally similar to nuclear waste glasses and have existed in natural environments for millions of years. Moreover, in certain cases, the alteration history of volcanic glass can be traced.

Natural glasses that have been considered as analogous to nuclear waste glasses are: a) tektites (Barkatt et al., 1984); b) rhyolitic glasses (Malow and Ewing, 1981; Dickin, 1981); and c) basaltic glasses (Allen, 1982; Malow et al.,1984; Lutze et al.,1985, 1987; Grambow et al.,1986; Byers et al.,1987; Crovisier et al., 1983, 1986, 1989). Basaltic

glasses have silica contents similar to borosilicate waste glasses and thus have received most attention.

Two cases will be considered here. In the first case, palagonitization of glass rinds of pillow lava is studied, and its rate is estimated. Discussion of such has been made in literature (e.g. Byers et al., 1987). Our emphasis will be on the nature of palagonite, mechanism of palagonitization and the implications to long-term stability of nuclear waste glass. In the second case, the alteration of glass shards in pelagic clays are studied. Since pelagic clays are considered as the best candidate host rocks for sub-seabed disposal of nuclear wastes (Hollister et al., 1981), the long term stability of volcanic glass in pelagic clays may represent a closer analogue to radwaste glasses disposed in sub-seabed environments. To date, however, no analogue studies have made use of the volcanic glass in deep sea sediments.

5.2 Alteration of Glass Rinds of Pillow Lava from Leg 37, DSDP

5.2.1 Background of Leg 37, DSDP

The glass rinds used in this study are from the Mid-Atlantic Ridge and were retrieved during Leg 37 of the Deep-Sea Drilling Project (DSDP). The drilling sites of DSDP leg 37 are located in the FAMOUS area, 300 kms south of the Azores. The FAMOUS area is one of intense fracturing, both parallel and transverse to the spreading axis, with major fracture zones causing numerous offsets in the median valley. The rift valley is about 31 kms wide with the outer edges

rising to about 1500 meters above the inner floor. The outer edges of the rift valley are 1.3 and 1.7 m.y. in age for the eastern and western side, respectively. Recent volcanism occurs in the central part of the rift valley and along the foot of the eastern fault scarps. The major rock types occurring in the area are olivine basalts, picrites, and plagioclase phyric basalts, all of tholeiitic composition (Aumento, Melson, et al., 1977).

Four Leg 37 drilling sites (Sites 332, 333, 334, 335) were made within the crest mountains and high fractured plateau, west of the median valley, along flow line parallel to the direction of spreading. Because most of samples used in this study are from Site 335, a short introduction to this site is presented here.

Site 335 is located on a sea-floor spreading flow line extending from the median rift of the Mid-Atlantic Ridge through Sites 332, 333, 334. Water depth here is 3,198 m. Acoustic basement underlines a 454-m thick sequence of foram-bearing nannofossil ooze. The oldest cored sediment is 13 m.y.. Acoustic basement consists of a very uniform sequence of pillow basalts with numerous glass rinds and intercalations of nannofossil chalk. The basalts are aphyric to sparsely phyric with 1-5 modal percent of plagioclase and olivine phenocrystals. Sparse crystals of green clinopyroxene are present in a few specimens (Aumento, Melson, et al., 1977).

5.2.2 Experimental Methods

The samples were taken from the glass rinds of the pillow lava. Table 5.1 shows the positions at which the samples were taken. Bulk samples were used to prepare thin sections for optical microscope and electron microprobe (EMP) analyses. Slightly crushed bulk samples were mounted on aluminum stubs and coated with carbon for scanning electron microscopy (SEM) study. In order to characterize the nature of palagonite, glass and associated palagonite were mechanically separated. To ensure the purity, palagonite was checked grain by grain using an optical microscope. The palagonite separates were then ultrasonically cleaned in an acetone bath and ground into powder. Suspensions of the powders were made, and deposited onto glass slides for X-ray diffraction (XRD) or deposited onto 3 mm holey carbon grids for transmission electron microscopy (TEM) analysis. Ultramicron thin sections with thickness of about 600 Å were also prepared for high resolution scanning and transmission electron microscopy (STEM) analysis. The ultramicrotomy followed procedures described by Lee et al.(1975).

Preliminary XRD analyses were carried out with a Rigaku X-ray diffractometer system. A low-angle X-ray powder diffraction study was further performed to selected samples according to the method described by van der Gaast et al.(1986). The samples were equilibrated in a humidity generator at 100, 50, and 0% relative humidity(RH) which was maintained during the XRD measurements. The XRD data were stored on a floppy disc and corrected for the Lorentz

Table 5.1 Sampling position at site 335, DSDP

No.	Core	Section
335-1	6-2	134-136cm
335-2	6-6	22-24cm
335-3	7-2	70-72cm
335-4	7-2	141-143cm
335-5	7-3	29-31cm
335-6	9-3	14-17cm
335-7	9-5	46-48cm
335-8	10-2	37-39cm
335-9	12-1	36-38cm
335-10	14-4	63-65cm

polarization factor and irradiated sample volume. To avoid errors in interpretation, the patterns of samples held at 100, 50, and 0% RH were plotted at comparable intensities, using MoS_2 (reflection at 6.09 Å) as an internal standard.

SEM study was done with an ISI DS-130 research instrument equipped with an EDX detector, operated at an accelerating voltage of 20-25 KV. Structural characteristics of palagonite were initially observed using a JEOL JEM 100C TEM, with an accelerating voltage of 100 KV. High resolution TEM were then carried out using a Phillips 400 STEM system equipped with EDX detector, operated at 100 KV. The chemical compositions of glass and palagonite were analyzed with a JEOL 8600 Superprober,and the size of the electron beam was defocused to 15-20μm to prevent sodium loss during probing.

5.2.3 Petrography

The glass is primarily dark brown to black sideromelane, with yellowish-orange palagonite rinds on surfaces and along fractures. Spherulites occur at the inner margins of the glass rinds, becoming larger and more abundant inward until they coalesce into a variolitic texture.

Palagonitization of Site 335 glass was usually initiated on glass surfaces, along fractures, and around vesicles in the glass (Figure 5.1). Petrographic evidence clearly suggests that alteration of basaltic glass is controlled by water flow through the basalt. Thickness of palagonite can vary several orders of magnitude depending on accessibility to water. In

FIGURE 5.1 Optical micrographs of palagonite from Site 335. A. Palagonitization along fractures; B. The dentritic zone; C. Palagonitization along glass surface; D. Palagonitization around a vesicle. **G**: glass; **P**: palagonite; **GP**: gel-palagonite; **FP**: fibrous-palagonite; **C**: clay; **CC**: calcite; **Z**: zeolite.

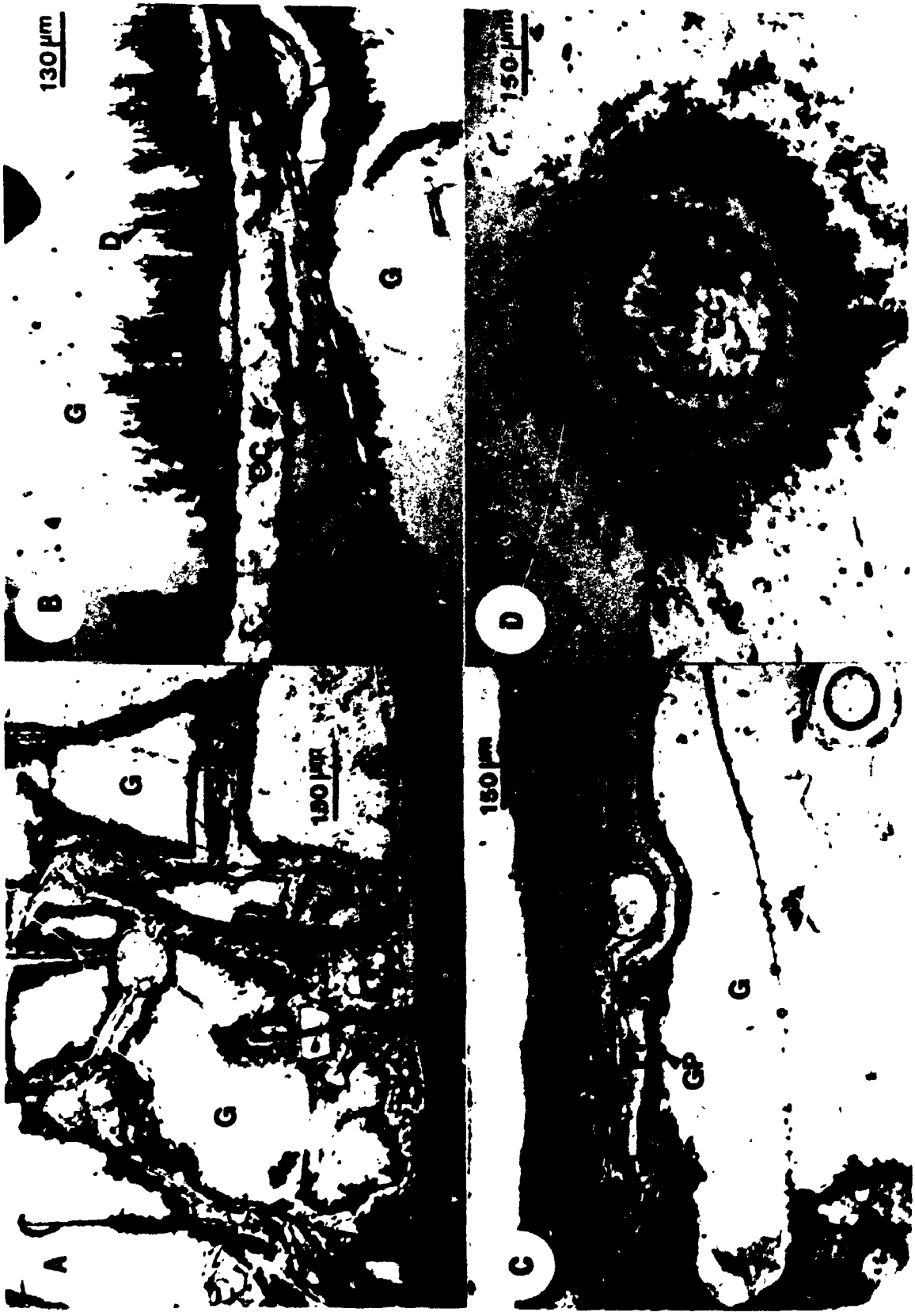
A
B
C
D
G
GP
130 µm
150 µm
150 µm
150 µm

general, palagonite is most developed on the pillow surfaces and on grain edges of glass, and less developed along fractures. Palagonitization in vesicles is variable. Olivine and plagioclase phenocrystals initially contained in fresh glass have usually remained unaltered during the palagonitization processes.

An ideal and complete cross-section of the glass-palagonite interface contains, from centre outward, a glass core, a dark zone of dendritic form, a dark brown palagonite zone, and a laminated orange or yellow coloured palagonite zone. Authigenic minerals, including smectite clays, phillipsite, calcite, and Fe and Mn oxide minerals, fill nearby fractures (Figure 5.2a). In most cases, a zone of dendritic form develops first along interfaces between glass and solution. This zone represents the alteration front and is usually located between glass and palagonite. Under polarized light, it is completely dark. The dendritic branches are perpendicular to the alteration front and grow into the glass (Figure 5.1b). This zone is not adequately addressed in the literature, probably because it occupies only a very small space (usually less than 30μm in thickness). It was termed "mist zone" by Morgenstein and Riley (1974) and was included in "immobile product layer" by Staudigel and Hart (1983). These authors suggested that the dendrite zone is riddled with microchannels or microcracks which permit water to move into glass. Our SEM analysis indicates that it is a zone populated with etch pits, and the latter are often empty (Figure 5.2b).

FIGURE 5.2 Optical and SEM micrographs of the cross section from glass core to palagonite. A. A typical cross section from glass core to palagonite; B. Dissolution pits along reaction front. **G**: glass; **P**: palagonite; **GP**: gel-palagonite; **FP**: fibrous-palagonite; **EP**: etch pits; **Z**: zeolite. The numbers marked in photo A represent positions at which EMP analysis were done (see Table 5.4).


130 µm
A
G
GP
P
P

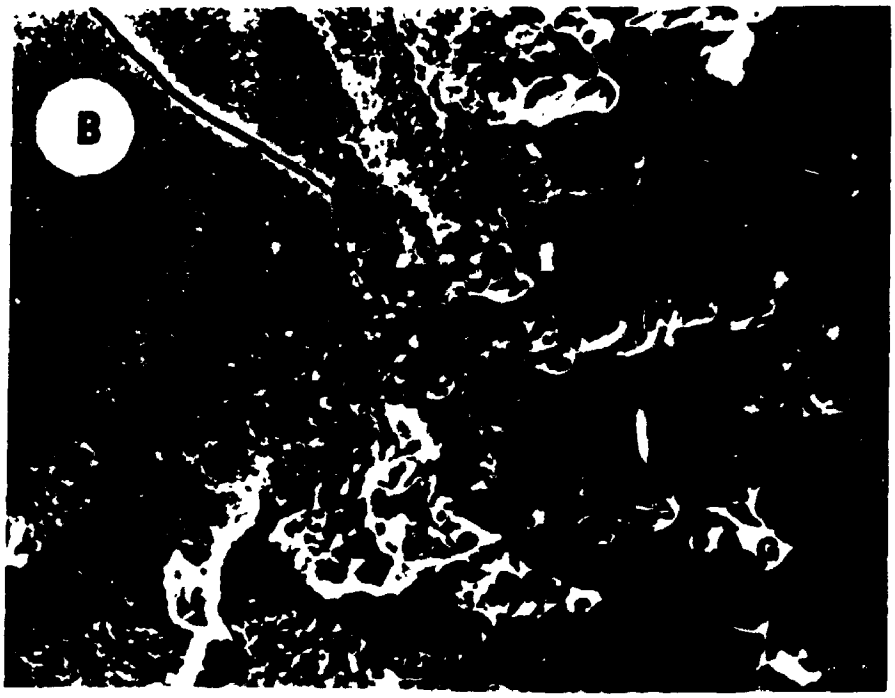
B

Using SEM/EDX, no alteration can be detected on glass in the areas between etch pits. The composition of the glass is not significantly different from glass in the cores. This has important bearings on mechanism of glass alteration (see discussion in section 5.2.7). Although this alteration front has distinct optical and physical properties, it does not constitute a separate mineralogic unit. It is a physical mixture of glass and etch pits. This zone will not be discussed further except in connection with the mechanism of glass alteration.

Palagonite next to the alteration front is dark brown in colour, anslucent, and has no lamination. This zone is usually less than 0.5 mm thick. Farther away from the glass centre is an orange or yellow coloured, finely laminated, transparent, birefrigent, fibrous structured palagonite. Both dark brown and orange coloured palagonites may contain unaltered phenocrysts of plagioclase, pyroxene and olivine. These observations are consistent with those of Andrews (1978). The dark brown palagonite may correspond to gel palagonite, and orange coloured palagonite to the fibrous palagonite of Peacock (1926). In following discussion, we will use "gel-palagonite" and "fibrous-palagonite" instead of the terms dark brown palagonite and orange coloured palagonite. Fibrous palagonite is replaced in situ by a greenish, well-crystallized clay phase, which is extremely Mg-rich. The small amount of this phase may prevent it from being detected by XRD. It is significant in terms of the geochemical budget for

Table 5.2 Composition of selected basaltic glass and palagonite from Site 335

Oxide	335-2		335-3		335-5		335-6		335-7	
	G	GP	G	GP	G	FP	G	GP	G	FP
SiO2	50.49	38.62	49.63	36.74	49.86	43.65	49.64	47.28	49.47	43.87
TiO2	1.26	2.28	1.26	4.42	1.24	1.88	1.25	1.93	0.92	2.45
Al2O3	15.36	12.99	15.24	11.35	14.98	13.26	15.45	12.77	15.28	13.83
Cr2O3	0.03	0.10	0.00	0.00	0.26	0.11	0.00	0.00	0.33	0.15
FeO(T)	9.60	18.58	9.78	21.32	9.11	15.85	10.15	16.31	9.34	14.93
MnO	0.27	0.14	0.23	0.10	0.20	0.00	0.37	0.14	0.19	0.02
MgO	8.03	3.01	8.05	1.83	7.96	4.31	8.02	4.37	8.10	4.78
CaO	11.73	2.13	12.41	2.25	11.81	1.15	12.35	1.69	12.04	1.48
Na2O	2.36	1.53	2.60	1.47	2.70	0.73	2.69	1.22	2.49	0.77
K2O	0.17	2.32	0.18	2.13	0.16	4.03	0.19	3.61	0.27	3.39
P2O5	0.16	0.19	0.45	0.02	0.36	0.03	0.39	0.08	0.10	0.26
Total	99.46	81.89	99.82	81.62	98.64	85.01	100.52	89.40	98.53	86.01

G: glass, average of three to five analysis; GP: gel-palagonite; FP: fibrous-palagonite.

elements like Mg. Table 5.2 shows chemical compositions of selected palagonites and their associated glasses from Site 335. As will be discussed in Section 5.2.5, the composition of palagonite is variable.

Beyond the palagonite are zeolite and clay veins. The zeolite is mainly composed of K-rich phillipsite, in radiating or prismatic crystals. Clays in the veins are usually Fe-rich, with moderate amounts of Ti. The presence of this type of clay in fractures may indicate that it is not appropriate to assume that Ti or Fe is immobile during palagonitization.

5.2.4 Structure and Mineralogy of Palagonite

The nature of palagonite is not well defined. Palagonite has been shown to be a material of variable composition. Honnorez (1981) considered palagonite to be a mixture, in variable proportions, of altered, hydrated, and oxidized glass with authigenic minerals such as clay, zeolites, and chlorites. However, distinction should be made between mineralogy of palagonite and the minerals associated with palagonite. Confusion may arise when one does not make this distinction (e.g. Ramanaidou and Noack, 1987). It has been well documented that authigenic minerals such as zeolites, carbonate, clay minerals, and Fe- and Mn- oxides are closely associated with palagonite. X-ray diffraction of palagonite itself, however, shows only a poorly resolved layer silicate structure (Andrews, 1978; Bonatti, 1965; Hay and Iijima,

1968a, 1968b; Singer, 1974; Stokes, 1971). Eggleton and Keller (1982) noted the similarity of average palagonite to smectite when recalculated to a cation charge of +22, and concluded that palagonite is composed of a dioctahedral smectite with significant Mg in the octahedral sheet. Direct evidence regarding the mineralogic composition of palagonite is generally lacking.

The XRD pattern of the parent glass from Site 335 shows a hump from 2θ of 16°-39° with peak position at 27.5° (Figure 5.3a). The hump is common for glass although its peak position might shift depending on the composition of the glass. The glass shows a broad hump at about 12 Å on low angle XRD (Figure 5.3b). Changing relative humidity shows no shift or increase in intensity at low angles. The glass shows smooth surface under TEM and its electron diffraction pattern further confirms its amorphous nature. Therefore, clay minerals or clay mineral precursor structure are not present in the parent glass.

XRD study of Site 335 palagonite shows two strong peaks at 4.5 Å and 2.6 Å and a moderate peak at 1.52 Å (Figure 5.4a). The basal reflection of palagonite is weak and variable from 12-15 Å and becomes even weaker after treatment with ethylene glycol. By low angle XRD methods, a shifting peak is seen with changing humidity (Figure 5.4b). The peak is at 16.2 Å at 100% RH, 15.8 Å at 50% RH, and 12.9 Å at 0% RH. This kind of shifting is normal for phyllosilicate minerals although the scale of shifting is smaller than most of the smectite

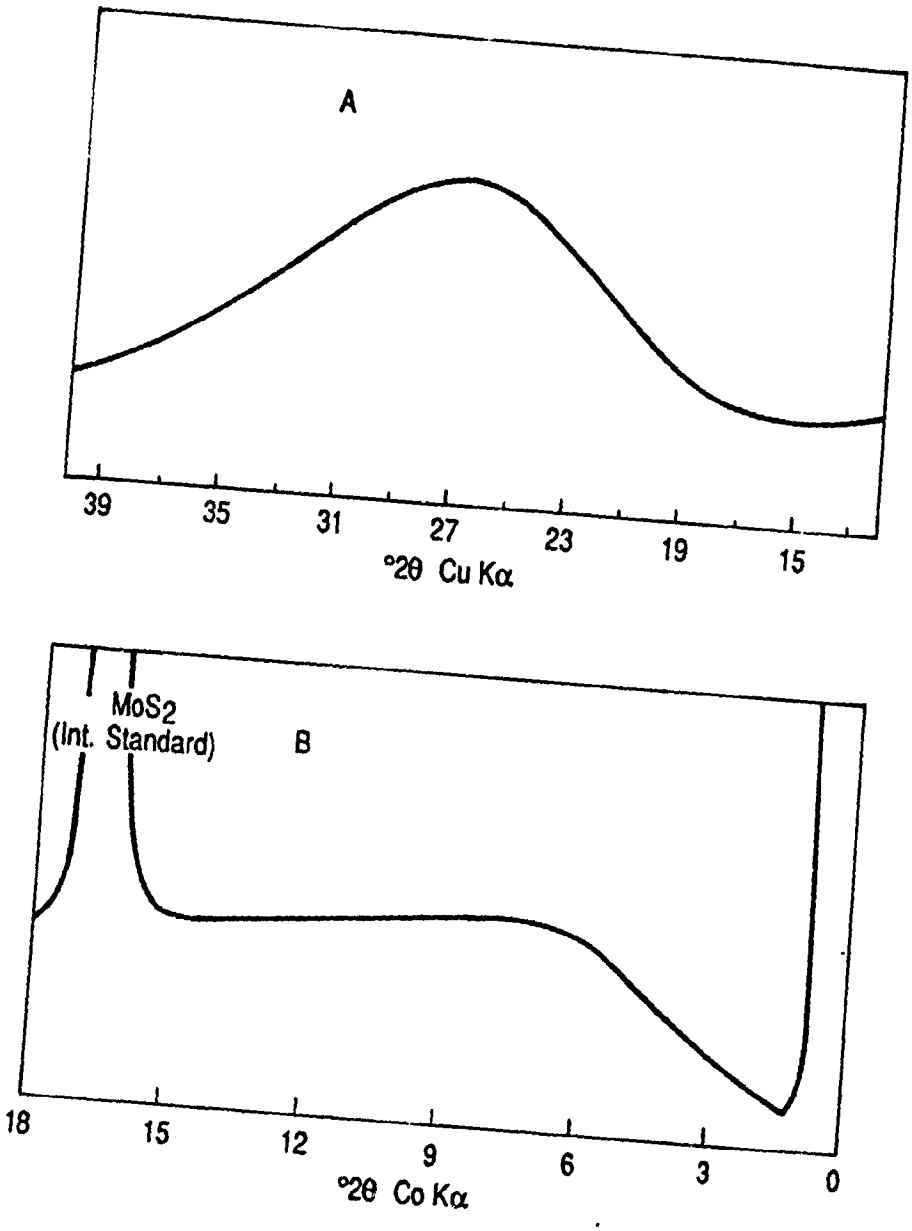

FIGURE 5.3 X-ray diffractograms of glass
A. Normal XRD; B. Low-angle XRD

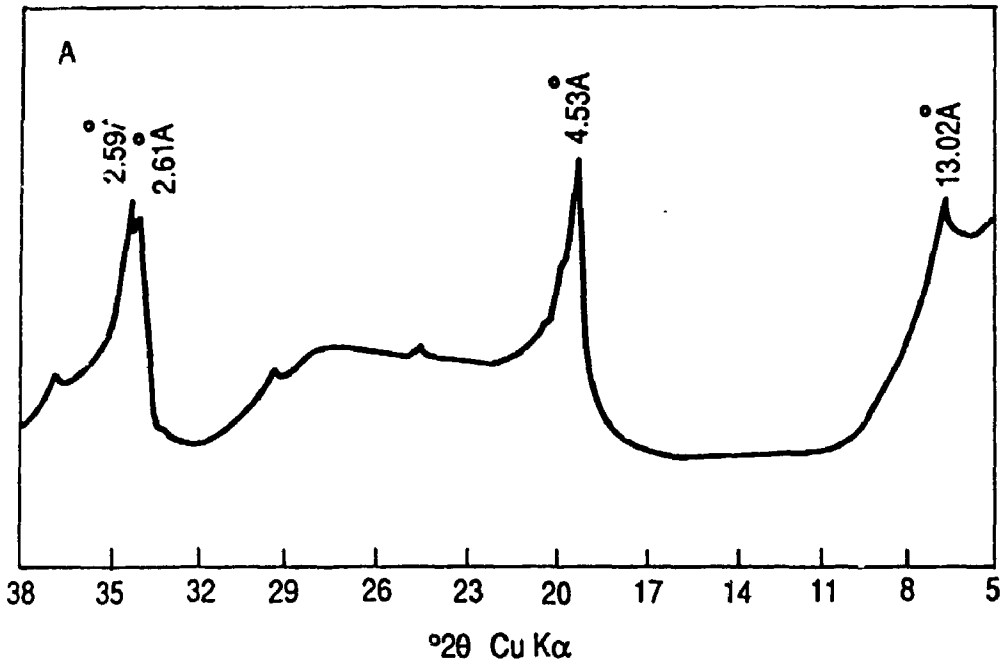

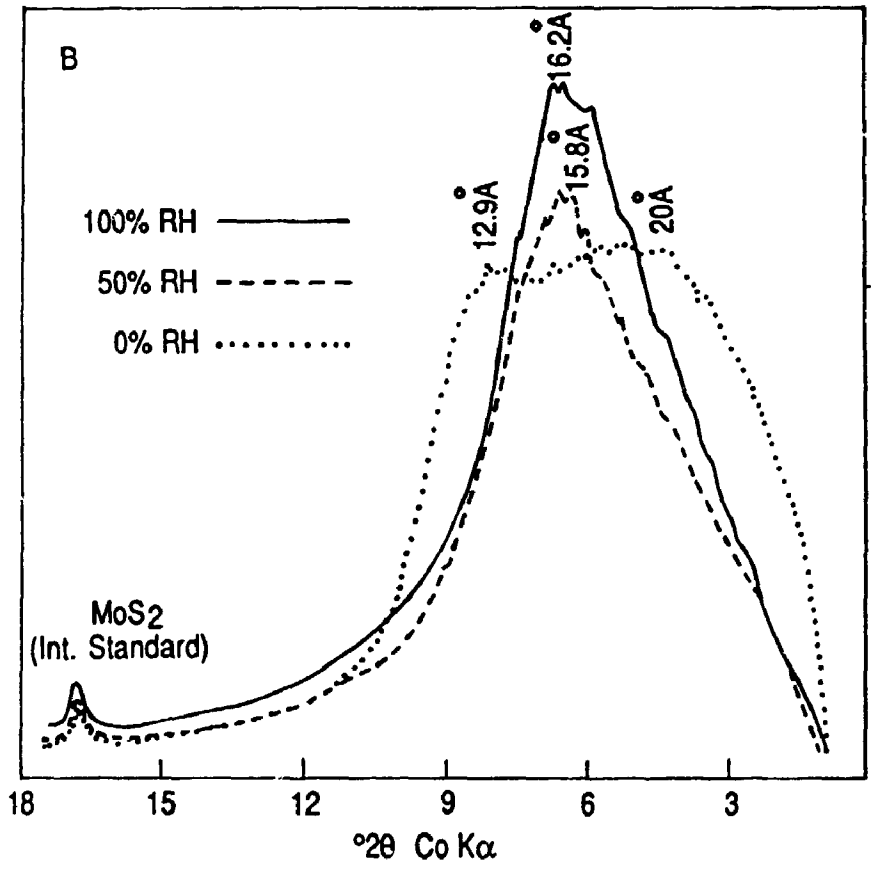

FIGURE 5.4 X-ray diffractograms of palagonite
A. Normal XRD; B. Low-angle XRD

minerals (van der Gaast et al., 1986). In addition to the shifting peak, there is a low angle hump at 20 Å which can best be seen at 0% RH.

TEM study indicates that most of the palagonite is composed of fibrous to lathe or strongly folded layer particles similar to smectite minerals (Figure 5.5a). Lattice images (Figure 5.5b) of the palagonite particles show a d-spacing of 10 - 13 Å which corresponds to the X-ray diffraction of 12.9Å at 0% RH. These particles usually have a well organized crystallinity along the a- and b- axes. This is indicated by electron diffraction patterns which show strong spots at 4.5 and 2.6 Å. Presumably, these are 011 and 020 diffraction of 2:1 clay minerals. Along c-axis, stacked layers are usually less than 10. High crystallinity along a- and b- axis of palagonite was also observed by Singer (1974).

The precursors of smectite-like particles are clusters of small, spheroidal particles, a few hundred angstroms in diameter (Figure 5.6a). They are very poor in crystallinity and similar to the "protocrystallite" described by Banfield and Eggleton (1988). Figure 5.6b suggests a transitional relationship from these protocrystallite particles to smectite-like particles. These protocrystallites are less abundant than smectite-like particles, and the former may represent materials in gel-palagonite and the latter may represent those in fibrous palagonite.

The structural characteristics of smectite-like minerals described above are similar to those of stevensite. Table 5.3

Table 5.3 X-ray diffraction data of palagonite and stevensite

Stevensite[a]		Palagonite			
Å	I	Å	I	Å	I
24	20?	20	w	–	–
12.4	100	13.02	s	12.80	w
5.0	20	4.87	w	–	–
4.54	100	4.53	vs	4.53	vs
3.50	50	3.60	w	3.49	s
2.62	90	2.60	vs	2.60	vs
2.28	20	–	–	2.28	w
1.725	40	–	–	1.75	s
1.520	90	1.52	s	1.52	s

[a]ASTM card # 7-357

FIGURE 5.5 TEM micrograph and lattice image of palagonite. A. Micrograph showing smectite morphology; B. Lattice image showing 10 Å structure.

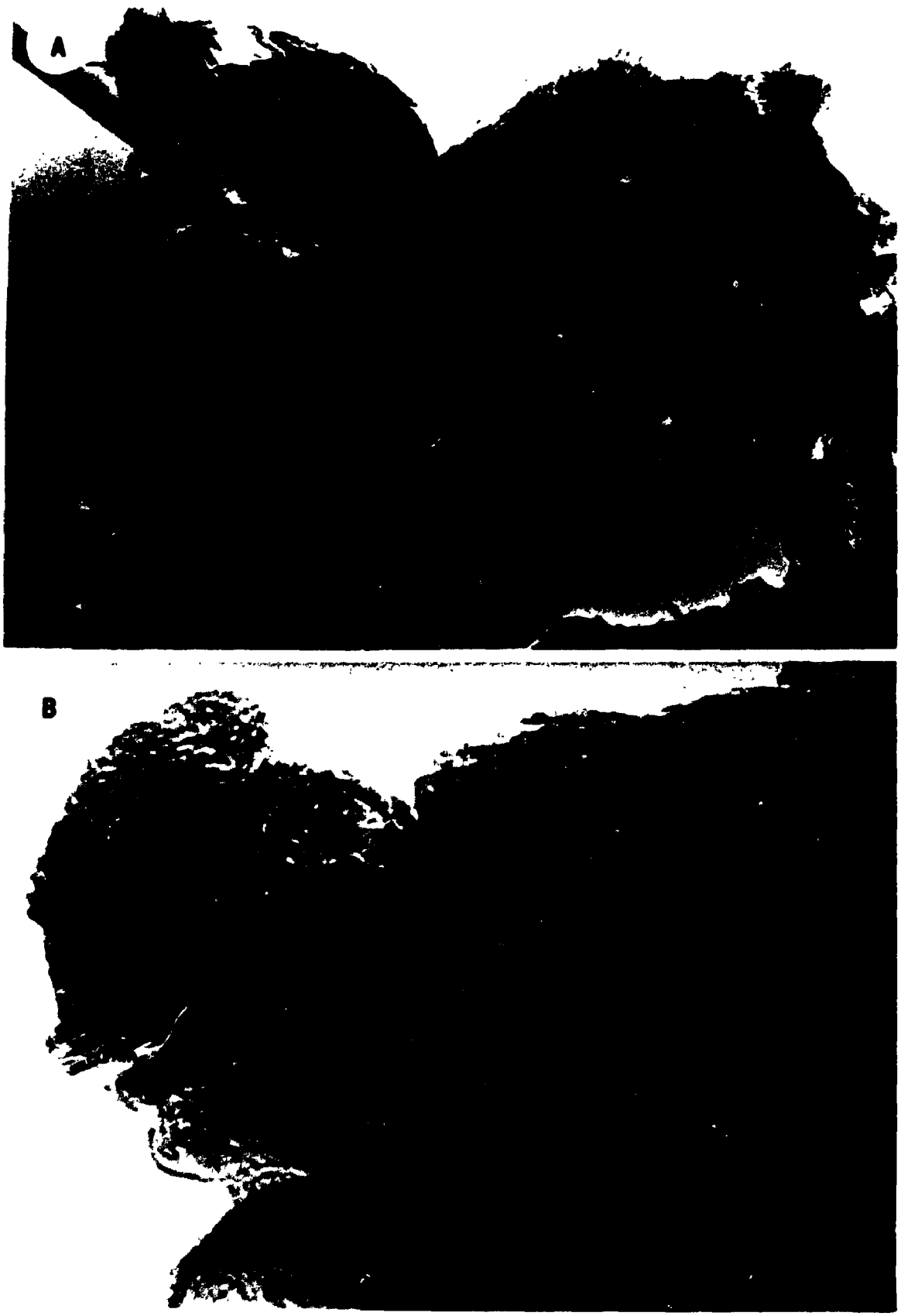
A
B

FIGURE 5.6 TEM micrograph of the spheroidal "protocrystallite" and its transition to stevensitic smectite. A. "Protocrystallite"; B. Transition stage between the "protocrystallite" and stevensitic smectite.

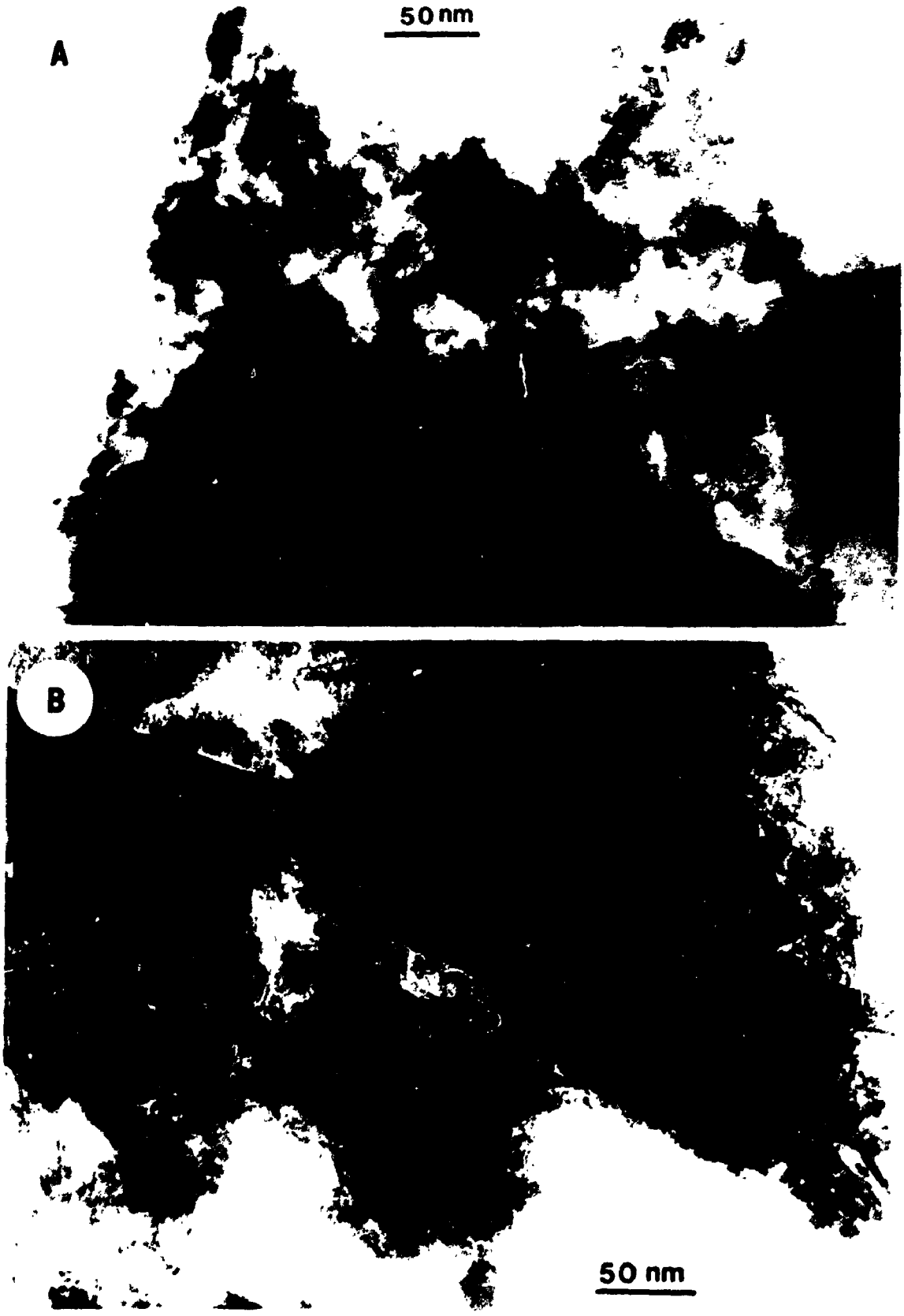
50 nm
A
B
50 nm

compares the XRD data of palagonite and those of stevensite. Stevensite was established as a member of smectite group by Faust and Murata (1953). Brindley (1955) confirmed this result and, at the same time, suggested the mixed-layer characteristics of stevensite. He suggested that the mixed-layer quality is responsible for low cation-exchange capacity and small swelling ability of stevensite compared with other trioctohedral smectite minerals. This is compatible with the fact that palagonite shows smaller shift in (001) peak than most of smectite minerals with changing RH. Despite the similarity in structural aspects, palagonite is significantly different from stevensite in chemical composition. The structural formula of stevensite as suggested by Faust and Murata (1953) is:

$$[Mg_{2.88}Mn_{.02}Fe_{.02}^{3+}]Si_4O_{10}[OH]_2$$

which differs from saponite in lacking an essential amount of aluminum. Stevensite, found in experimental alteration of basaltic glass (Trichet 1969, 1971), is also Mg-rich. The palagonite from Site 335 is rich in Fe and Al, and has a Mg/Si ratio much less than that in stevensite. The discrepancy is due to, at least partly, the composite nature of palagonite. STEM analysis indicates that the protocrystallites are richer in Al, Fe, and Ti, and the smectite-like minerals are less abundant in these elements. Also, because stevensite is considered as a talc-saponite interlayered mineral and if the interlayered saponite in stevensite is Fe-rich, the composition of stevensite can greatly deviate from those

proposed by Faust and Murata (1953).

5.2.5 Chemical Changes During Palagonitization

The chemical changes resulting from palagonitization have been the subject of many studies in the past (e.g. Hay and Iijima 1968, a;b; Furnes, 1978; 1980; Honnorez, 1978; Furnes and El-Anbaawy, 1980; Andrews, 1978; Ailin-Pyzik & Sommer, 1981; Staudigel and Hart, 1983; Eggleton & Keller, 1982). However, controversy still remains over the directions and magnitude of chemical changes. One of the issues is whether such chemical changes are isovolumetric or Ti- or Fe-constant.

To make the best possible estimate of the chemical changes involved in any metasomatic processes, volume changes associated with alteration, or the absolute variation of one chemical constituent must be known (Gresens, 1967). The most usual practice is to compare the chemical analysis of unaltered and altered material assuming that either volume or one of the less mobile components does not change during the course of alteration. Based on petrographic observations, Hay & Iijima (1968a,b) and Furnes (1978, 1980) concluded that palagonitization is an isovolumetric process and calculated the chemical changes on an isovolumetric basis. However, Andrews (1978) and Eggleton and Keller (1982) pointed out the problems associated with this method and made their calculation based on a Ti-constant method. The latter assumption requires that authigenic minerals associated with palagonite are Ti (or Fe) free or, at least Ti (or Fe) poor,

and that no or little Ti (or Fe) is dissolved and carried away in solution during the alteration. Such conditions can usually be met only in the early stage of palagonitization (see following discussion).

Relative losses and gains of eight major elements during submarine palagonitization have been compared at different degrees of Ti accumulation (Staudigel & Hart, 1983). This unique treatment reveals the interrelationship between major elements during submarine alteration of glass. It was suggested by those authors that Ti accumulation may be used as maturity indicator for palagonites. However, this generalization must be treated with caution. As discussed previously, a typical cross section as in Figure 5.2a includes, from glass core outward, dark dendrites, gel palagonite, and fibrous palagonite. A line probe analysis through this cross section is shown in Table 5.4, and Ti & Fe changes are plotted in Figure 5.7. Petrography indicates that dark brown gel- palagonite, being closer to glass, is certainly later (or less mature) than the orange coloured fibrous palagonite. Ti and Fe contents, on the other hand, increase from glass to gel-palagonite and then decrease from gel-palagonite to fibrous-palagonite. Similar trends can be identified from analytical data of Baragar et al.(1977) from DSDP Leg 37. Therefore, Ti or Fe accumulation is not a good indicator for "maturity" of palagonite.

To explain the compositional variations shown in Figure 5.7, a multi-step process of palagonite formation is required.

Table 5.4 Line probe analysis along a palagonite-glass cross section

	Glass	GP1	GP2	GP3	FP1	FP2	FP3	FP4	FP5
SiO2	49.86	39.24	35.97	41.10	44.91	43.65	43.75	43.58	44.25
TiO2	1.24	2.40	2.87	2.41	1.47	1.88	1.97	1.88	2.03
Al2O3	14.98	12.22	11.10	11.74	12.27	13.26	12.65	12.39	12.67
Cr2O3	0.26	0.18	0.18	0.11	0.14	0.11	0.20	0.36	0.00
FeO	9.11	20.08	19.81	18.76	14.57	15.85	16.23	15.14	16.17
MnO	0.20	0.00	0.10	0.00	0.06	0.00	0.00	0.00	0.12
MgO	7.96	2.10	1.55	3.03	4.32	4.31	4.83	4.86	4.69
CaO	11.81	2.23	1.78	1.93	1.51	1.15	1.19	1.21	1.18
Na2O	2.70	2.18	1.84	1.64	1.19	0.73	0.74	0.72	0.53
K2O	0.16	2.32	2.02	2.75	3.54	4.03	4.37	4.10	4.33
P2O5	0.36	0.11	0.00	0.08	0.21	0.03	0.27	0.03	0.45
Cl	0.01	0.09	0.09	0.04	0.07	0.08	0.09	0.08	0.03
Total	98.65	83.15	77.31	83.60	84.25	85.09	86.25	84.35	86.44

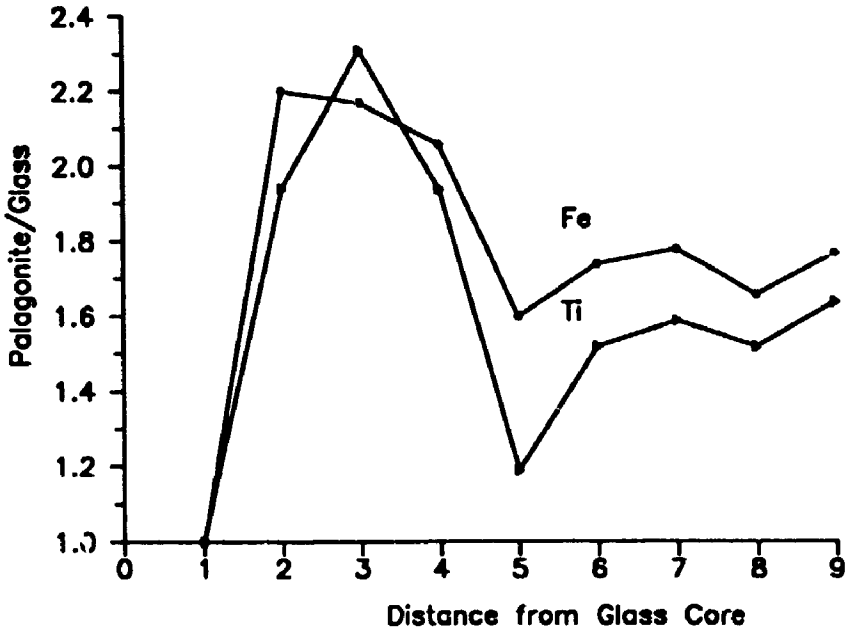

FIGURE 5.7 Variations in Fe and Ti contents across a glass–palagonite boundary. The numbers along X–axis correspond to the positions marked in Figure 5.2a. The cross–section is about 150 micrometres.

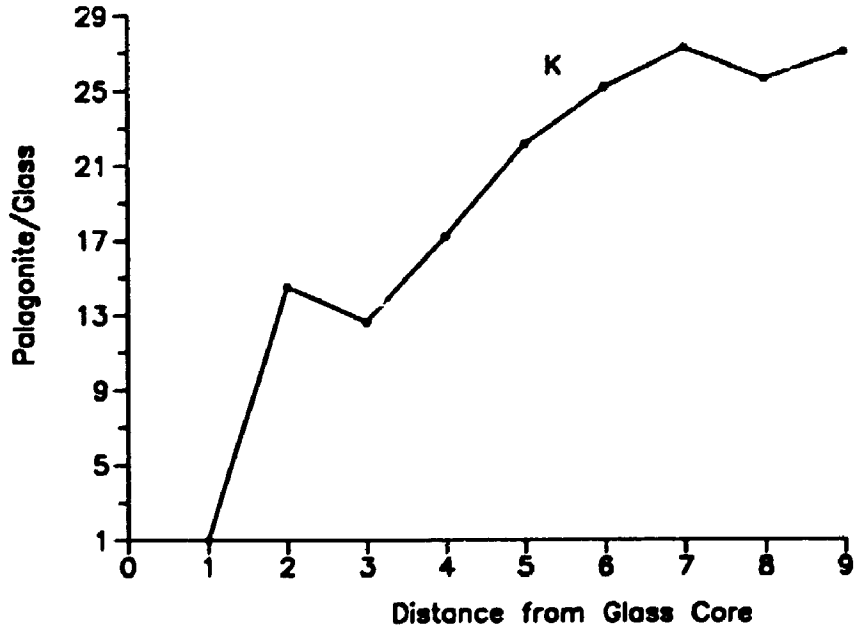

FIGURE 5.8 Variations in K contents across a glass–palagonite boundary.

In the early step, basaltic glass is dissolved and gel palagonite formed. Authigenic minerals formed during this stage are mainly phillipsite which is Ti and Fe poor. Therefore Ti and Fe may not be mobile during this stage but tend to accumulate as a result of removing other elements. The physicochemical condition required for this is an alkaline solution, in which Si and Al may be mobile while Ti and Fe are not. It is possible to produce localized alkaline solution during glass alteration due to ion exchange between H+ and alkalis in basaltic glass. In the later step, gel palagonite is converted in situ to fibrous palagonite. Small amounts of Ti and Fe are locally remobilized. Ti and Fe lost from palagonite probably move to fractures adjacent to it and are incorporated into clay minerals or oxides. Local mobility of Ti during low temperature alteration was also noticed by Robinson et al.(1977) in site 332, where leucoxene was found in vesicles of a few basalts. However, it is not clear as to why Fe and Ti appear to be mobile in this stage.

It seems that the first step in palagonitization, glass to gel palagonite, is Ti and Fe constant but not volume constant. A large accumulation of Ti and Fe must results from loss of other elements. Such loss can result in a volume reduction. Should volume remain constant, density change during palagonitization (2.75 g/cm^3 for glass and 2.10 g/cm^3 for palagonite) could only result in a 30 percent increase in Ti and Fe content. An accumulation factor greater than 1.3 may indicate the volume reduction involved. The second step, gel

palagonite to fibrous palagonite, may be isovolumetric because of in situ replacement. However, as pointed out earlier, Ti and Fe may be mobile during this process. The two steps of palagonitization discussed here should be considered part of a continuum during which palagonite changes structure and chemical composition as alteration proceeds.

Mean compositions of glass, gel-palagonite, and fibrous-palagonite were used to calculate elemental mobility during palagonitization (Table 5.5). Elemental mobility during the first step of palagonitization, assuming constant Ti, is shown as L1 (see Appendix 4 for calculation methods). SiO_2, Al_2O_3, MgO, CaO, and Na_2O all suffered more than sixty percent weight loss. K_2O was enriched over six hundred percent, while FeO appears to be constant. This process is accompanied by about sixty percent total weight loss.

Elemental mobility during the second step of palagonitization is shown as L2 in Table 5.5, based on an assumption of constant volume. CaO and Na_2O continue to be lost and K_2O continues to increase during isovolumetric conversion of gel-palagonite to fibrous palagonite. However, SiO_2, Al_2O_3, and MgO are taken back from solution; in contrast, FeO(total) and TiO_2 are lost in this process. The overall elemental gain or loss is the resultant effect of steps 1 and 2, and is shown as L and X% in Table 5.5. There is a significant difference between these data and previous calculations (Andrews 1978, Eggleton and Keller 1982, Furnes 1978,1980). In previous calculations, Fe and Ti were either

Table 5.5 Elemental mobility during palagonitization of basaltic glass

	G	GP	FP	L1	X1%	L2	X2%	L	X%
SiO2	49.86	38.77	44.03	-31.08	-62.34	5.26	13.57	-28.53	-57.23
TiO2	1.24	2.56	1.85	0.00	0.00	-0.71	-27.73	-0.34	-27.73
Al2O3	14.98	11.69	12.65	-9.32	-62.20	0.96	8.21	-8.85	-59.10
Cr2O3	0.26	0.16	0.16	-0.18	-70.19	0.00	0.00	-0.18	-70.19
FeO	9.11	19.55	15.59	0.36	3.95	-3.96	-20.26	-1.56	-17.11
MnO	0.20	0.03	0.04	-0.19	-92.73	0.01	33.33	-0.18	-90.31
MgO	7.96	2.23	4.60	-6.88	-86.43	2.37	106.28	-5.73	-72.01
CaO	11.81	1.98	1.25	-10.85	-91.88	-0.73	-36.87	-11.20	-94.87
Na2O	2.70	1.89	0.78	-1.78	-66.09	-1.11	-58.73	-2.32	-86.01
K2O	0.16	2.36	4.07	0.98	614.45	1.71	72.46	1.81	1132.13
P2O5	0.36	0.06	0.20	-0.33	-91.93	0.14	233.33	-0.26	-73.09
Cl	0.01	0.07	0.07	0.02	239.06	0.00	0.00	0.02	239.06
Total	98.56	81.35	85.28	-59.16		3.93			

assumed to be constant or to have increased. This is not compatible with the fact that clay veins next to palagonite contain significant amount of Fe and Ti. Our calculation indicates that about 27 percent of Ti and 17 percent of Fe in glass can be mobilized during the process of palagonite formation. The magnititude of Ti and Fe mobilization may vary depending on local physicochemical conditions but our calculation explains the source of Fe and Ti in clay minerals.

A distinction should be made between the two steps of palagonitization discussed here and the three stages of palagonitization suggested by Honnorez (1978, 1981). The discussion in this paper refers mainly to the "initial" stage of palagonitization according to Honnorez's classification.

For submarine alteration of basaltic glass, the enrichment of K may be used as a maturity index of palagonite. It has been well documented that K is enriched in palagonites relative to their parent glasses during submarine alteration. Figure 5.8 shows that K concentration increases from glass core, to gel-, to fibrous palagonites. This indicates that K is taken up from seawater not only during the formation of gel-palagonite but also during the in situ conversion of gel-palagonite to fibrous-palagonite. K enrichment as a maturity index of palagonite can be justified by the mineralogical changes during palagonitization. Smectite minerals formed during the course of palagonitization are K-rich. Palagonite may eventually be replaced by K-rich phillipsite and smectite (Honnorez, 1978;1981).

5.2.6 Temperature of Palagonitization

There have been many discussions concerning the temperature of palagonitization(Peacock, 1926; Fuller, 1932; Wentworth, 1938; Nayudu, 1964; Bottani, 1965, 1967; Moore, 1966; Hay and Iijima, 1968a, 1968b; Honnerez, 1972; Furnes, 1974, 1975, 1978). Fuller(1932), Nayudu(1964), Bottani(1965,1967) and many others believed that palagonite forms at high temperature during and shortly after eruption of hot lava into the sea. However subsequent field and experimental observations have clearly demonstrated that palagonite can form at low temperature as a post-eruptive process. Moore(1966) has observed a progressive thickening of palagonite in successively older submarine lavas near Hawaii. Furnes(1975) conducted an experimental investigation of the relationship between palagonitization rates and temperature. This work put an end to the discussion about the possibility of palagonitization at low temperature. It has been suggested that most palagonitization occurs during low temperature weathering and diagenesis (Fisher and Schmincke 1984). Nevertheless, it is still true that the rate of palagonitization increases with temperature(Furnes 1975, Jakobsson and Moore, 1986).

Downhole heat flow measurement indicates that present temperature at Site 335 is lower than 10°C (Hyndman et al.,1977). It is not clear that if this represent the dominant temperature at the site in 13 m.y.'s history. However, oxygen

isotopic study indicates that the basalts were altered by very cold seawater (Muehlenbachs, 1977). Muehlenbachs and Clayton(1972) demonstrated that basalt weathered by cold seawater leads to O-18 enrichment whereas hydrothermal alteration of basalts leads to O-18 depletion of the basalts. All of the analyzed basalts from leg 37 have been enriched in O-18 due to weathering by cold water. Therefore palagonitization at Site 335 most probably took place at low temperature.

5.2.7 Mechanism and Kinetics of alteration of Basaltic glass

The mechanism by which palagonite forms has been proposed as a hydration process (Peacock, 1926), solid-state diffusion/hydration (Moore, 1966), and solution-precipitation (Hay & Iijima, 1968b). The solution-precipitation mechanism is based on the physical characteristics of altered samples (sharp glass/palagonite contact and an etched glass surface) as well as the chemical changes which result from palagonitization (Byers et al. 1987). Figure 5.2b provides new evidence for this mechanism. Presence of empty etch pits along the glass/palagonite boundary indicates that fresh glass is dissolved, and the material mobilized and deposited over very short distances. It should be noted that etch pits were not found in the experimental studies. This may reflect the possibility that specimens used in experiments may be more homogeneous than their natural counterparts. Nevertheless, as discussed in Chapters 3 and 4, surface dissolution

predominates the glass corrosion process, which is compatible with natural alteration. It is interesting to note, however, that palagonite itself is not thermodynamically stable and changes its chemistry and structure over the course of alteration (see section 5.2.5 and Staudigel and Hart, 1983). Palagonite appears to be in disequilibrium with the solution from which it precipitates. This is possibly explained if the removal of material from the glass is not by dissolution but by mechanical removal of 100-8000 Å size globules. Such globules deposited from solution are not necessary in equilibrium with the solution. This mechanism was suggested by Honnorez (1972) and demonstrated by Trichet (1969, 1972). Staudigel and Hart (1983), however, questioned this idea and pointed out that Trichet's experimental observations can be equally well explained by dissolution.

Eggleton and Keller (1982), using high resolution transmission electron microscopy, noted that palagonite forming from basaltic glass by hydration consists of spherical structures with diameters ranging from 200 to 600 Å. Exfoliation of 10 Å 2:1 clay layers allows the development of thin (30-60 Å) crystals of dioctahedral smectite with significant Mg in the octahedral site, which ultimately forms a tangled network of sub-micron - size bent flakes. Both Trichet (1969,1972) and Eggleton and Keller (1982) showed that a spherical phase is formed first during glass alteration, and this spherical phase is not stable and tends to transform to smectite. While Eggleton and Keller considered the spherical

particles as a hydration product of basaltic glass, Trichet suggested that they were formed by deposition of physically removed globules from the glass.

As shown in section 5.2.4, palagonitization of DSDP Site 335 glass is initiated by the formation of clusters of small spheroidal particles. Morphologically, they are different from those described by Trichet (1969,1972). These spheroidal particles were not found in the parent glass. It is unlikely that they were formed by deposition of physically removed globules from the glass. We suggest that protocrystallites in palagonite were formed by precipitation from solution at the very beginning of palagonitization. The protocrystallites are meta-stable, and change their structure and chemistry and are replaced in situ by stevensitic smectites with changes in physicochemical conditions. The dissolution of glass is apparently controlled by surface reactions whose rate is influenced by composition of interstitial water.

The rate of palagonitization may be estimated using the thickness of the palagonite and the age of the glass. Two things should be noted:

1) The thickness of the palagonite is not equal to but smaller than the thickness of the glass dissolved, because palagonitization is not isovolumetric. In the literature, rate of glass alteration has been estimated based on isovolumetric conversion (e.g. Grambow et al., 1986; Byers et al., 1987). This leads to underestimation of the rate of glass alteration; and

2) Reaction time of glass with water is not necessarily equal to the age of the glass. Formation of authigenic minerals may seal fractures by which water invades and then protects glass from further attack by water. The age of glass represents the maximum alteration time.

A somewhat conservative approach is to count the thickness of authigenic minerals. This will at least account for the volume loss during palagonitization. Table 5.6 shows measured thickness of palagonites and authigenic minerals in Site 335. It is understood that the samples used are limited and may be not representative in terms of distribution of palagonite and associated authigenic minerals. From these samples, palagonite is usually less than 3 mm, and authigenic mineral veins less than 7 mm in thickness. Thus the rate of glass alteration is about 1.0 μm per thousand years.

5.2.8 Summary

Palagonitization of basaltic glass of DSDP Site 335 is initiated on glass surfaces, along fractures, and around vesicles in glass. The alteration front is populated with empty etch pits. A typical cross section from glass to palagonite contains a fresh glass core, an alteration front, gel-palagonite, and fibrous-palagonite. Authigenic minerals include smectite clays, phillipsite, calcite, and Fe and Mn oxides, and fill the fractures. Phillipsite, which is formed in the early stage of alteration, contain little Fe and Ti. Authigenic clays, however, contain moderate amounts of Fe and

Ti. Gel-palagonite is dark brown in colour, translucent, and isotropic, whereas fibrous-palagonite is orange or yellow coloured, transparent, birefringent, and fibrous. Palagonite is a composite material but is composed largely of stevensitic smectite. The latter shows well organized crystallinity along a- and b- axes, but poor crystallinity along c-axis. Fe and Ti contents increase from glass to gel-palagonite, then decrease from gel-palagonite to fibrous-palagonite. K is constantly enriched during the course of palagonitization.

Palagonitization is divided into a Ti-constant step and a volume constant step. In the first step, glass dissolves and gel-palagonite of protocrystalline nature is formed. This step is accompanied by large volume reduction and over sixty percent loss of Si_2O, Al_2O_3, MgO, CaO, and Na_2O, Ti and Fe are immobile and relatively enriched by this process. In the second step, gel-palagonite is replaced in situ by fibrous palagonite. CaO and Na_2O continued to be lost and K_2O continues to increase during this process. However, SiO_2, Al_2O_3, MgO are taken back from solution. TiO_2 and FeO(T) are locally mobilized to nearby fractures and incorporated into clay minerals and oxides. K-enrichment is proposed as a maturity index for palagonite.

Palagonite is considered as an alteration product formed by precipitation from solution. Because volume reduction is very likely accompanied with palagonitization, direct use of thickness of palagonite will underestimate the rate of glass alteration. A more conservative method is used and indicates

that the dissolution rate of basaltic glass at Site 335 is about 1.0 μm/thousand of years. The relevance of these findings to analogues for nuclear waste disposal will be discussed in Section 5.4.

5.3 Alteration of Volcanic Glasses in Deep Sea Sediments

5.3.1 Introduction

Since deep-sea sediments are considered as host rock for subseabed disposal of nuclear wastes (Hollister et al.,1981), glasses in such environments appeared to the author as a closer analogue than the glassy rims of pillow lavas in the sea-floor. Five DSDP cores (Sites 436, 449, 450, 473, and 543) were thus selected to study the effects of interstial water chemistry and host rock mineralogy on glass dissolution. Unfortunately, the glass contents in three cores (Sites 449, 473, and 543) are much lower than that reported in the DSDP Initial Reports and not adequate for detailed study. Samples from Site 436 contain mainly rhyolitic glass and the data on interstitial water at this site is incomplete. Thus Site 436 was also dropped for further study. Samples from Site 450 contain sufficient amounts of glass of composition ranging from rhyolitic to basaltic. The alteration of the glasses from this core will be discussed here.

Site 450 is located on the eastern side of the Parece Vela Basin, Philippine Plate (Langseth et al., 1980). Water depth is 4707 m and drilling penetrated to a depth of 340 m sub-bottc . The upper 333.0 m comprise a sedimentary section

consisting of pelagic clays, vitric tuffs, and fine vitric tuffs. The basal 7.0 m is intrusive mafic rock. The sedimentary section is Pleistocene to middle Miocene (? - 15 m.y.) and is conveniently divided into two units from the top downward: Sub-unit 1a is 26.5 m of dark brown pelagic clay with minor disseminated volcanic glass. Sub-unit 1b is 57.0 m of middle to upper Miocene dark yellowish brown, dark greyish brown, and dark grey ash-rich pelagic clay with minor dark to very dark ash beds. Dominating the sedimentary column, sub-unit 2a is 241.0 m of middle Miocene dark grey, fine vitric tuffs, in some places nannofossil-bearing, and paler, with minor grey and black vitric tuffs and tuffaceous volcaniclastic conglomerates. Sub-unit 2b is 8.5 m of the same fine vitric tuff as Sub-unit 2a, except that hydrothermal alteration has increased the zeolite content and discoloured the sub-unit reddish brown. Sub-unit 2c is 1 cm of pale yellowish white, fine vitric tuff forming a baked contact with the underlying intrusive plagioclase-clinopyroxene-olivine-phyric intrusive pillow basalt.

5.3.2 Sampling and Analytical Methods

Samples were collected from the youngest to the oldest units ranging in age from <1 to 15 m.y.. Figure 5.9 shows sampling positions relative to the stratigraphy of the core. Each sample was 10 cc as received. A subsample was taken from each sample and grounded in quartz mortar with water. Random oriented slides were then prepared for whole rock XRD

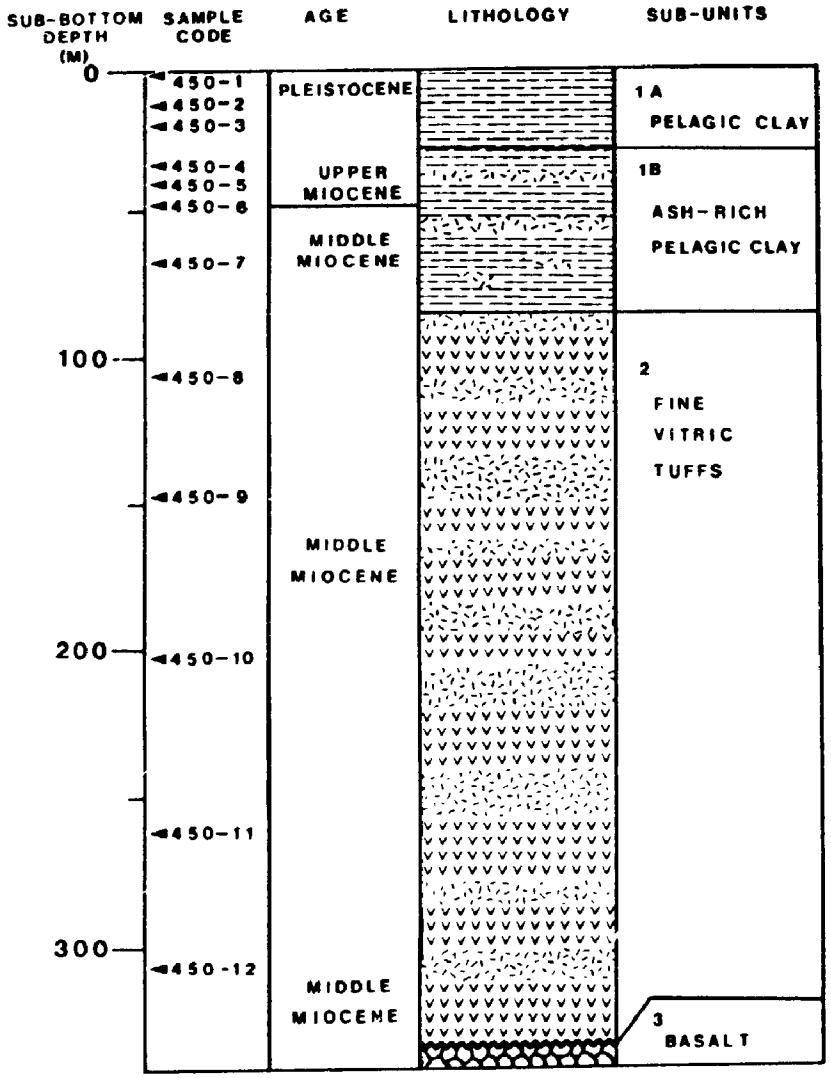

FIGURE 5.9 Lithology, age, and sampling positions at Site 450, modified from Kroenke et al. (1981).

analysis.

A second subsample was used to study the clay mineralogy and glass alteration. The subsamples were washed with distilled water to remove salt. This will prevent flocculation of the clays. The samples were then wet sieved through 5μm filter paper. The fraction larger than 5μm was air dried, then directly mounted onto aluminum stabs for SEM analysis, or/and buried in epoxy and polished for optical microscopy and electron microprobe study of glasses. The fraction less than 5μm was used to concentrate the clay fraction. Carbonate minerals were removed to improve suspension. The < 2μm fraction of each sample was separated by settling through a distilled water column. The clay suspension was used to make basal oriented slides. The slides were X-rayed after air drying and again after treatment with ethylene glycol.

5.3.3 Results

Glass contents in samples of Unit 1 pelagic clay and ash-rich pelagic clay are usually less than 20 percent. In Unit 2, fine vitric tuffs contain more than 30 percent of glassy material. Clay minerals, feldspars, quartz, cristobalite, and carbonate minerals are abundant in the sediments. The glasses are colourless to light brown to dark brown in colour, and are a few tens to a few hundred micro-metres in size. Morphologically, they can be divided into two groups: block shaped and pumice. Block shaped glass has planar or curviplanar surfaces, angular with sharp edges and sometimes

Table 5.6 Chemical compisition of selected glasses from Site 450, DSDP

Oxide	450-4	470-7	450-9	450-10	450-12
SiO2	65.73	72.78	55.17	62.71	54.84
TiO2	0.56	0.21	0.90	0.88	1.08
Al2O3	14.46	11.86	14.15	13.63	13.11
FeO(T)	6.01	1.54	11.22	5.03	12.75
MnO	0.00	0.00	0.00	0.00	0.00
MgO	1.23	0.30	2.88	1.38	3.22
CaO	3.77	1.62	6.86	3.86	7.50
Na2O	2.87	1.85	2.10	2.42	2.81
K2O	2.29	2.22	1.38	2.02	1.05
Total	97.02	92.38	94.66	91.93	91.36

conchoidal fractures. Pumices are highly vesicular with thin vesicle walls. The vesicles are usually elongated and parallel. In most cases, the pumices are colourless and silica rich. Table 5.6 shows the chemical composition of glasses from Site 450. The silica contents of these glasses range from 76 to 45 wt percent. Good correlation exists between the colour and silica contents of the glasses. That is, silica tends to decrease from colourless to light to dark brown colour.

In thin sections, no alteration layers were seen in the glass. The glasses usually have a very clear surface. This is interesting because, palagonite, as alteration product of basaltic glass, is often closely associated with basaltic glass. Most of sampled basaltic glass is more than 10 m.y. old and then extensive alteration could have taken place. SEM observation of the glasses confirmed that alteration layers are almost absent. Original features of explosive eruptions are well preserved. These include smooth block and curviplanar surfaces, angular and sharp edges, conchoidal fractures, round vesicles with smooth walls (Figure 5.10 a,b,c). In a few cases, alteration features can be seen but the alteration layers are not clear (Figure 5.10 e).

Clay minerals present in the sediments include smectite, chlorite, illite, and kaolinite. Among these phases smectite is most abundant. Chlorite content is variable. Illite and kaolinite are usually minor components. Balshaw (1981) reported the clay mineralogy of the up-portion of the core (0 - 40.0 metres) and concluded that smectite makes up more than

FIGURE 5.10 Selected SEM micrographs of the volcanic glass from DSDP Site 450. A. A glass shard in 450-4; B. A general view of glassy material in 450-7; C. A fresh sideromelane in 450-10; D. A glass shard in 450-11 showing some alteration. Note the difference between the (irregular) etch pits and the (round) vesicles of the glass shard shown in photo C.

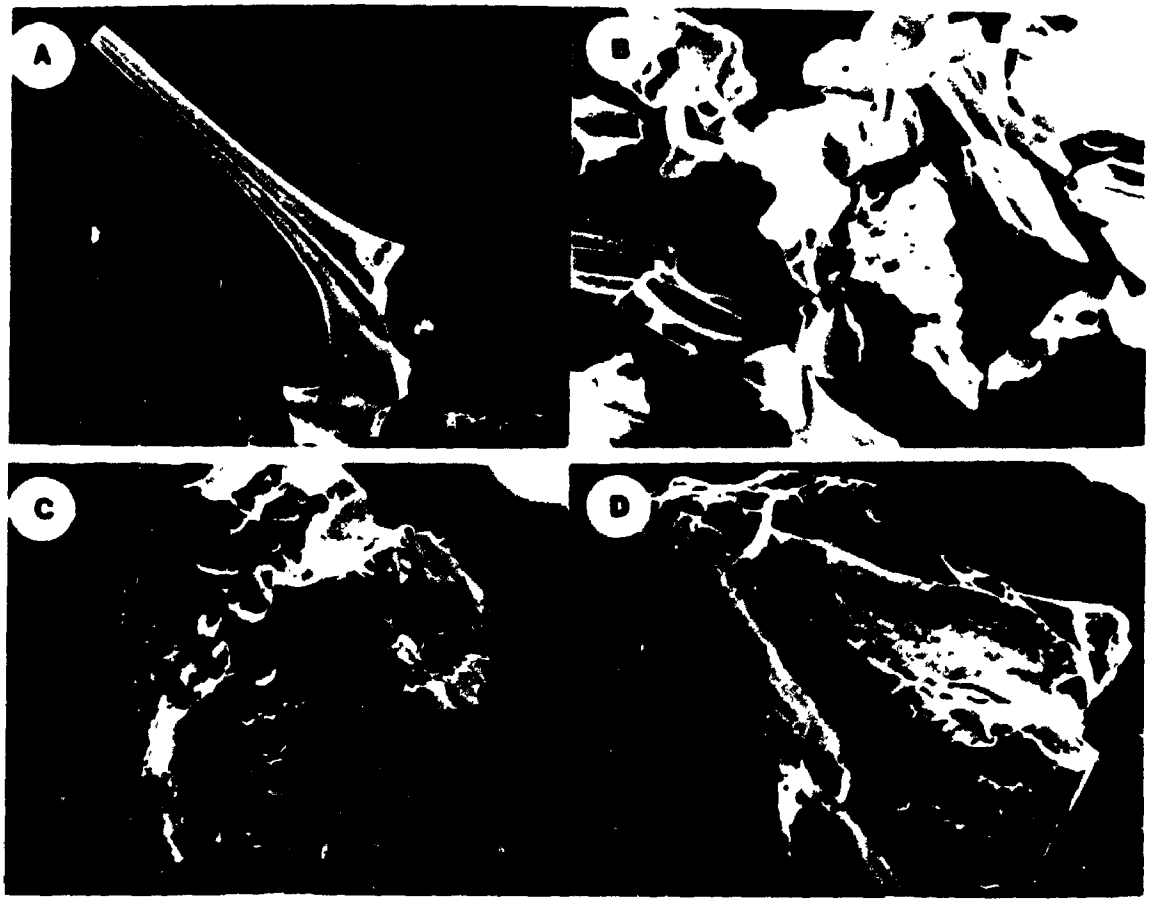
A
B
C
D

85 percent of the total clay.

5.3.4 Discussion

The absence of surface alteration layers could have resulted from one or more of following causes:

a) Dissolution is congruent and all components of glass dissolve at the same rate and no precipitation occurs at the immediate surroundings of the glass;

b) Surface layers were present but destroyed during sample preparation;

c) There is preference in glass dissolution, e.g. dissolution occurs for some of the glass and leave others unaltered; and

d) No alteration has taken place since the glasses deposited.

The last cause seems not likely considering the age of the sediments at the site. Causes b) is related to the analytical methods employed. Considering the extensive washing and fragile nature of surface layers, the alteration features could be destroyed. On the other hand, well preserved explosive textures in glasses (Figure 5.15 a, b, c) indicate that at least some of the glasses are fresh. Should dissolution have occurred to these glasses and surface layers were destroyed during sample preparation, these original textures are not likely to be preserved in the residue glasses. Preference in glass dissolution is common. For example, high silica glass is known to dissolve slower than

low-silica glass. This was actually noticed during the observation of the glasses at the site. The glasses that show any sign of dissolution are usually the coloured ones but rhyolitic glass seems fresher.

Among the glasses of Site 450, a great portion is siliceous in composition. The alteration of silicic (SiO_2 >65 wt%) glass differs from that of basaltic glass in many ways (Fisher and Schmincke, 1984). Simply put, the alteration of sideromelane involves the formation of the intermediate but chemically different product palagonite which is eventually transferred into thermodynamically stable phases, chiefly smectite. In contrast, alteration of silicic glass appears to involve an initial stage of diffusion-controlled hydration and alkali ion exchange but minor overall chemical changes. This is commonly followed by a stage of glass matrix destruction and precipitation of secondary phases in the pore space created by the dissolution of the glass. The spatial relationship between the secondary phases and parent glass is not as clear as that of between palagonite and sideromelane. The reasons for these differences are poorly understood. Differences in the glass structure are probably important, the stronger resistance of silicic glasses during the initial stages of alteration being due to much higher content of the network-forming elements Si and Al.

The clay mineralogy may be used to estimate the degree of alteration of associated glass. Balshaw (1981) analyzed the origins of clay components of pelagic sediments in the South

Philippine Sea, and concluded that alteration of glass in the sediments is a most important contributor of smectite of the sediments. Hein and Scholl (1978) considered the smectite layers in late Cenozoic volcanic sediments in the South Bering Sea were formed by alteration of volcanic ash. Considering the fact that smectite contents of the Site 450 sediments are usually more than 90 percent of total clay, one must conclude that glass alteration is involved.

The difficulties in establishing the nature and process of glass alteration at this site make it virtually impossible to quantify the rate of glass dissolution in the pelagic sediments. A conservative method is to assume that all of authigenic clay minerals in Unit 2 are derived from alteration of glasses in the sediments. Taking the data on the size distribution and glass contents in the DSDP Initial Report Volume 59 and assuming the geometry of the glass is a plate with dimension of 100*100*10 μm^3, the reduction in thickness of the plate is 9.8 μm (Table 5.7). Because two reaction faces are involved, reduction in thickness from one face is 4.9μm. Taking the minimum age of 10 m.y., the rate of glass dissolution is 0.49μm/m.y.. This is three orders of magnitude smaller than the rate for Site 335 glass from pillow lavas. The difference in glass composition may be a most important factor. Other factors which may be responsible for the slow rate of dissolution: 1) The fluid convection in the sediments are expected to be much smaller than that of in basalts. The soft sediments have no fractures along which water may moves

Table 5.7 Model contents of glass and clays in Unit 2 of Site 335 and estimate of reduction in thickness of glass

Model content (volume)	Number of samples used (n)	Mean values ($\bar{x}$)	Standard deviation (σ)
clay	85	37.37	26.49
glass	85	38.17	24.29

Geometry of glass (assuming as a plate):

Before dissolution: a x a x (b + b')

After dissolution: a x a x b

Volume relation:

$$a^2(b + b') = a^2b + V_c \quad \text{.....(1)}$$

$$V_c = 37.37/38.17 \times a^2 = 0.98a^2b \quad \text{.....(2)}$$

there V_c is volume of clay in the sediments.

Reduction in thickness of the glass plate:

From equation (1), one get

$$b' = V_c/a^2 \quad \text{.....(3)}$$

use eatimated values, a = 100μm, b = 10μm, and combine equation (2) with equation (3), one get b' = 9.8 and b'/2 = 4.9 μm.

therefore the interstitial water is stagnant; and 2) The interstitial water is buffered by sediments and the water may be less reactive than the fluid in fractures of pillow lava.

5.4 Implications of the Natural Analogues

The case studies presented in previous sections provide information on long-term stability of volcanic glasses in submarine environments. A remaining question is how this information can be used to verify the long-term stability of nuclear waste glasses in similar conditions. As pointed out by Ewing and Jercinovic (1987) and Lutze et al.(1987), one must carefully define the question when one considers the possibility of using natural glasses as analogues for nuclear waste glass. The phrase "natural analogue" conveys the sense that in natural systems (usually of great age) there are situations or materials that are analogous to the conditions or materials of interest (Ewing and Jercinovic, 1987). In the broadest sense, an analogy refers to a similarity between things otherwise unlike, that is a partial resemblance. This view of "analogy" immediately limits what one may expect from this approach. Proof or verification of a hypothesis, e.g. the long-term durability of borosilicate glass can only be approached (never arrived at), and then only to the extent that details of one system correlate with the details of another system (Lutze et al.,1987).

In Chapter 3, we have already demonstrated that basaltic glass behaves similarly to simulated radwaste glasses during

laboratory corrosion tests. Characterization of palagonite (Section 5.2) indicates that the process and products of naturally altered basaltic glass are analogous to those produced in laboratory tests. Both palagonite and surface layers are alteration product from thermodynamically unstable glass, and form by precipitation in the vicinity of the glass. Palagonitization is controlled by the surface area exposed to solution. As in laboratory tests, surface area would be a major factor in long-term alteration of nuclear waste glasses. Palagonite, like surface layers formed in laboratory study, is too porous to act as a physical barrier to protect fresh glass. Surface dissolution may be a rate-limiting mechanism which would be suppressed by saturation of silicate phases.

The above comparison indicates that similar mechanisms control the glass corrosion or alteration in natural and laboratory conditions. The dissolution rates in the two conditions can not be compared directly because the corrosion temperature in the laboratory was different from that in the field condition. The rate of dissolution of basaltic glass in SW at 90°C was found to be 0.76 μm/y. If we assume the rate of glass dissolution would be double for every 10 - 12°C increase in temperature (Adams, 1984; Jakobson and Moore, 1986), the rate at 10°C would be about 2 μm/ky. This is in remarkably agreement to the dissolution rate of basaltic glass at Site 335 (1 μm/ky) and other locations (Moore, 1966; Grambow et al., 1985).

The chemical compositions of palagonite vary depending

on physicochemical conditions at which it forms. This indicates the formation of secondary products is governed by thermodynamics. In addition, although the conversion from glass to palagonite is accompanied by loss of many glass constituents, the precipitation of crystalline phases (phillipsite, smectite, Mn and Fe-oxides) in vicinity of palagonite may account for most of these losses. The actual release of the glass components is most likely controlled by t solubility of the stable phases of the components. This is again consistent with laboratory observations.

In conclusion, palagonite and palagonitization can be used as natural analogues of alteration of waste glasses in repository conditions. Because the temperature in a high level waste repository can be 100°C or higher, the palagonitization process of basaltic glass at elevated temperature would provide better analogues. Such conditions can be found in areas of active volcanism (Jakobson and Moore, 1986).

CHAPTER 6 - SUMMARY AND CONCLUSION

Glass corrosion in MCC-1 tests at 90°C was characterized by the dissolution of glass and formation of surface layers. Dissolution was uniform over the entire glass surface exposed to solution. Surface layer composition depends on both glass and leachant compositions. In DDW, the surface layers were enriched in insoluble elements such as Fe, Al, Zn, REE; surface layers developed in SW were enriched in Mg and Cl, but also Fe, Al, Zn, etc.. The surface layers formed in both leachants were very poor in crystallinity. In SW, a Mg enriched layer silicate(s) was the dominant component in surface layers of all the three glasses. A reaction zone was found between surface layer and unaltered glass. This was usually less than 1000 Å and depleted in soluble elements such as B, Na, and Mo. For PNL 76-68 glass, Si was also depleted in this zone. When SW was used as leachant, Mg was found to diffuse through the reaction zone.

All three glasses studied showed greater stability in SW than in DDW. In DDW, the amount of dissolution was 4.40 and 5.38 μm in 360 days for ABS-118 and basaltic glasses respectively, and was 33.30 μm in 180 days for PNL 76-68 glass. The amount of dissolution in SW during the same period was about three times smaller for all the glasses.

Among the three types of glass, PNL 76-68 was least stable in both DDW and SW. ABS-118 glass and basaltic glass

showed comparable dissolution rates. The rate of glass dissolution decreases with reaction time (progress). The " final rate" of dissolution of ABS-118 and basaltic glasses in SW is about 0.76 μm/y; that of PNL 76-68 glass is about one order magnitude greater. The " final rate" of basaltic glass in DDW is close to that in SW. However, that of ABS-118 glass in DDW is more than three times greater than the final rate in SW.

Glass corrosion proceeded much slower at 30°C than 90°C. Because of limitations of the experimental and analytical methods, no systematic information can be retrieved from corrosion tests. However, material characterization on corroded glass suggested similar corrosion mechanisms to those at 90°C. The glass specimen corroded in oceanic muds exhibit even less change. No surface layer was detected. A reaction zone of 300 Å was found on ABS-118 glass after one year.

The glass corrosion was considered including three successive stages: (1) ion-exchanges between alkali in glass and H_3O^+ (and/or Mg^{2+}) in leachant; (2) formation of a reaction zone which was depleted in B, Na, Li, Mo, and Si; and (3) slow dissolution of the reaction zone at solid/solution interface accompanied by diffusion of ions from the fresh glass boundary, and subsequent precipitation of hydroxides and silicates. The dissolution reaction slows down when silicate phases attain saturation. Mg diffusion through the reaction zone and rapid saturation of Mg-layer silicate contribute to the enhanced stability of the glasses in SW.

Most of glass components and perhaps most of radionuclides in waste glass would be saturated and precipitate in a few months to one year under MCC-1 90°C corrosion conditions. Therefore, the release of these radionuclides would be limited by their solubility not by reaction kinetics. The saturation of silicate minerals would also slow down the corrosion process. Therefore, if the corrosion conditions of MCC-1 90°C tests can be justified in the waste repository, the evolution and solubility of the precipitates over reaction progress assume more importance than reaction kinetics.

Palagonitization of basaltic glass from DSDP Site 335 bears remarkable similarities to the corrosion processes in the laboratory conditions. Palagonitization is divided into a Ti- constant and a volume constant step. In the first step, glass dissolves and gel-palagonite of protocrystalline nature is formed. This step is accompanied by a large volume reduction. In the second step, gel-palagonite is replaced in situ by fibrous-palagonite. These processes were found to be analogous to the surface layer formation during corrosion of natural and simulated waste glasses. The changes in composition of palagonite with physicochemical conditions was assumed to reflect the thermodynamic control on its formation. This argument, together with the authigenic minerals precipitated at vicinity of palagonite, suggested that the release of major constituents will be controlled by solubilities of phases formed from the elements involved.

The dissolution rate of basaltic glass at Site 335 was found to be 1 μm/ky. Glass shards in pelagic clays have much slower dissolution rate. The explosive textures of the glass shards are well preserved and suggested that little alteration has taken place. After temperature correction, the laboratory determined dissolution rate was found in same order as those of basaltic glass from Site 335. At 90°C, the glasses studied would dissolve at a rate of a few to a few tens of micrometers per year. The basaltic and simulated ABS-118 glasses would have a dissolution rate of a few micrometers per thousand years at 10°C. The rate for PNL 76-68 glass should be an order of magnitude greater.

Appendix 1 Matrix of Corrosion Tests

Table A1.1 MCC-1 tests at 90°C

Time (days)	ABS-118 DDW	ABS-118 SW	PNL 76-68 DDW	PNL 76-68 SW	Basalt DDW	Basalt SW
10	A1	A6	P1[a]	P5[a]	B1	B6
30	A2	A7	P2[b]	P6[b]	B2	B7
90	A3	A8	P3	P7	B3	B8
180	A4	A9	P4	P8	B4	B9
360	A5	A10	_	_	B5	B10

[a]Duplicates, [b]Triplicates

Table A1.2 MCC-1 teasts at 90°C

Time (days)	ABS-118		Basalt	
	DDW	SW	DDW	SW
10	A11	A16	B11	B16
30	A12	A17	B12	B17
90	A13	A18	B13	B18
180	A14	A19	B14	B19
360	A15	A20	B15	B20

Table A1.3 Corrosion tests in oceanic muds at room temperature

Sample code	Leachate	Glass	Times(months)
A21	pore water	ABS-118	12
A22	pore water	ABS-118	12
A23	pore water	ABS-118	12
B21	pore water	BG	12
B22	pore water	BG	12
B23	pore water	BG	12

Appendix 2 Analytical Methods and Instruments

Solution Analysis:

Si and B: Dissolved Si and B in the leachates were analyzed using molybdate blue method and curcumin method respectively (Grassholf et al., 1983). A technicon auto analyzer (located in Department of Land Resources, University of Guelph) was used to analyze Si and a Shimadzu UV-250 Photospectrometer (located in Department of Plant Science, University of Western Ontario) was used to analyze B. The detection limits were 0.2 mg/l for Si and 0.1 mg/l for B.

Fe and Zn: The concentration of Fe and Zn in the leachates were determined by atomic adsorption method. A Perkin-Elmer 5000 mechine (located in Department of Geology) was used. Fe was measured at wavelength of 248.3 nm with lamp current of 12 mA; Zn was measured at wavelength of 213.9 nm with lamp current of 10 mA. The detection limits were 0.1 mg/l for Fe and 0.05 mg/l fcr Zn.

U: Uranium in the leachates was determined by analytical neutron activation method and performed by Nuclear Activation Services Limited at Hamilton, Ontario. The detection limit was 0.01 mg/l.

Solid Analysis:

X-ray Diffraction: A Rigaku x-ray diffractometer (located in Department of Geology) was used.

Low Angle XRD: The analysis was performed by Dr. S.J. van der Gaast of Netherlands Institute for Sea Research. The details of the method was described by van der Gaast et al.(1986).

Scanning Electron Microscopy (SEM): An ISI DS-130 research instrument equipped with an EDX detector was used. The machine was operated at an accelerating voltage of 15-25 KV. The analysis was done in the Surface Science Western of the University of Western Ontario.

Transmission Electron Microscopy (TEM): A JEOL JEM 100C TEM (located in Department of Anatomy, University of Western Ontario) and a Phillips 400 STEM (located in Department of Microbiology, University of Guelph) with a EDX detector were used, both operated at an accelerating voltage of 100 KV.

Electron Microprobe (EMP): A JEOL 8600 Superprobe (located in Department of Geology) was used and operated at an accelerating voltage of 15KV.

Secondary Ion Mass Spectrometry (SIMS): A CAMECA ims 3f secondary ion microscope (located in the Surface Science Western, University of Western Ontario) was used. The Prime beam current was 200 nA. The method of specimen isolation (SI) was employed to avoid sample coating which could complicate the depth profiles.

Inductively Coupled Argon Plasma (ICP): The ICP analysis was performed by Barringer Magenta Limited.

Appendix 3 Experimental Results

Table A3.1 MCC-1 test results of ABS-118 glass at 90°C

Sample code	Leachant	Time (day)	Normalized weight loss ($g.m^{-2}$)	pH	Conc. in Leachates (mg/l) Si	B	Zn
A1	DDW	10	0.4	5.85	2.5	0.9	0.42
A2	DDW	30	4.0	6.37	3.1	1.3	0.48
A3	DDW	90	5.1	6.98	4.8	2.0	0.51
A4	DDW	180	8.4	8.30	16.1	3.1	0.63
A5	DDW	360	13.2	8.35	23.7	4.4	0.52
A6	SW	10	1.2	8.34	1.6	5.4	0.00
A7	SW	30	1.2	8.52	2.6	5.7	0.14
A8	SW	90	-0.4	8.30	3.7	6.2	0.18
A9	SW	180	-1.6	8.25	5.4	6.4	0.13
A10	SW	360	-2.0	8.25	2.8	6.8	0.12

Table A3.2 MCC-1 test results of PNL 76-68 glass at 90°C

Sample code	Leachant	Time (day)	Nomalized weight loss ($g.m^{-2}$)	pH	Conc. in Leachates (mg/l) Si	B	Zn
P1	DDW	10	3.6	9.26	15.6[a]	4.1[a]	0.06
P2	DDW	30	8.4	9.30	26.0[b] (4.37)	7.3[b] (0.16)	0.34 (0.30)
P3	DDW	90	19.0	9.10	54.2	17.2	0.40
P4	DDW	180	26.0	9.27	62.2	28.5	0.60
P5	SW	10	1.2	8.29	4.9[a]	6.7[a]	0.20
P6	SW	30	2.0	8.60	2.0[b] (0.25)	7.9[b] (0.66)	0.26 (0.08)
P7	SW	90	-2.4	8.58	5.7	8.4	0.35
P8	SW	180	2.0	8.10	29.0	13.7	0.70

[a]Average of the duplicates;
[b]Mean value and standard deviation of the triplicates.

Table A3.3 MCC-1 test results of basaltic glass at 90°C

Sample code	Leachant	Time (day)	Normalized weight loss ($g.m^{-2}$)	pH	Concentration in Leachates (mg/l) Si	Fe	U
B1	DDW	10	3.2	8.48	7.9	0.00	0.11
B2	DDW	30	4.8	8.55	14.5	0.12	0.04
B3	DDW	90	5.6	8.41	18.0	0.28	<0.04
B4	DDW	180	3.2	8.97	21.8	0.62	0.05
B5	DDW	360	8.8	7.85	22.5	0.65	<0.04
B6	SW	10	-3.2	8.44	1.3	0.00	<0.04
B7	SW	30	0.8	8.55	2.1	0.12	<0.04
B8	SW	90	-0.4	8.16	1.5	0.19	<0.04
B9	SW	180	-0.4	8.50	0.7	0.04	0.06
B10	SW	360	-2.4	8.95	0.9	0.08	0.04

Table A3.4 MCC-1 test results of ABS-118 glass at 30°C

Sample code	Leachant	Time (day)	Normalized weight loss ($g.m^{-2}$)	pH	Concentration in Leachates (mg/l) Si	B	Zn	Fe
A11	DDW	10	0.4	5.28	0.0	0.3	0.05	0.00
A12	DDW	30	3.2	5.80	0.0	0.6	0.05	0.00
A13	DDW	90	1.6	4.51	0.2	0.9	0.05	0.00
A14	DDW	180	3.2	5.20	0.1	0.5	0.07	0.05
A15	DDW	360	-1.6	4.50	0.3	0.2	0.28	0.03
A16	SW	10	0.8	7.91	0.5	5.1	0.00	0.00
A17	SW	30	2.4	7.93	0.5	5.0	0.08	0.00
A18	SW	90	0.8	7.60	0.9	5.2	0.11	0.00
A19	SW	180	-1.2	7.82	0.9	5.17	0.07	0.00
A20	SW	360	-1.2	8.20	2.5	6.12	0.22	0.07

Table A3.5 MCC-1 test results of basaltic glass at 30°C

Sample code	Leachant	Time (day)	Normalized weight loss ($g.m^{-2}$)	pH	Conc. in Leachates (mg/l) Si	Fe
B11	DDW	10	-4.8	5.60	0.0	0.00
B12	DDW	30	0.0	5.55	0.1	0.00
B13	DDW	90	-2.0	4.60	0.2	0.00
B14	DDW	180	-0.4	5.60	0.3	0.05
B15	DDW	360	-3.2	4.70	0.6	0.07
B16	SW	10	1.2	7.90	0.4	0.00
B17	SW	30	2.0	7.98	0.5	0.00
B18	SW	90	-0.4	7.64	1.1	0.12
B19	SW	180	-0.2	7.80	1.0	0.00
B20	SW	360	-2.8	8.20	1.7	0.10

Appendix 4. The Calculation Methods of Elemental Mobility During the Palagonitization

The gains and losses of the oxide components during the first step of palagonitization, assuming constant Ti, can be calculated according to equation,

$$L1_i = [C^g_{TiO2}/C^{gp}_{TiO2}] \times C^{gp}_i - C^g_i \quad \text{.....(1)}$$

and the percentage of the gain loss is

$$X1_i\% = L1_i/C^g_i \times 100\% \quad \text{.....(2)}$$

Where

$L1_i$ = total amount of component i, lost or gained in the first step;

$X1_i$ = percentage of change of component i,

C^g_{TiO2} = weight fraction of TiO_2 in glass,

C^{gp}_{TiO2} = weight fraction of TiO_2 in gel-palagonite,

C^g_i = weight fraction of component i in glass, and

C^{gp}_i = weight fraction of component i in gel-palagonite.

Elemental mobility during the second step of palagonitization is difficult to calculate. This is because that isovolumetric calculation requires the densities for both reactant and product. However, mechanic separation of gel-palagonite from fibrous-palagonite is not feasible and the difference in their densities are not known. A further approximation is to assume the two material have same density. Although this assumption is the density difference will be probably small and the error introduced by this assumption

will be acceptable. Thus we calculate the gains and losses of oxide components using a simple equation,

$$L2_i = C^{FP}_i - C^{GP}_i \quad \text{.....(3)}$$

and the persentage of the change,

$$X2_i\% = L2_i/C^{GP}_i \times 100\% \quad \text{.....(4)}$$

where

$L2_i$ = total amount of component i, lost or gained in second stages;

$X2_i$ = percentage of change of component, i, in second stages;

C^{FP}_i = weight fraction of component i in FP; and

C^{GP}_i = weight fraction of component i in GP

The overall gains or losses of oxide components, L_i, is the resultant effect of steps 1 and 2, and can be calculated according to equation,

$$L_i = L1_i + (C^{g}_i + L1_i) \times X2_i\% \quad \text{.....(5)}$$

and the percent of change, X_i, is

$$X_i\% = L_i/C^{g}_i \times 100\% \quad \text{.....(6)}$$

References

Aagard, P. and Helgeson, H.C., 1982. Thermodynamic and kinetic constraints on reaction rates among minerals and aqueous solution. I. Theoretical considerations. Am. Jour. Sci, v. 282, pp.237-285.

Abrajano, T.A., Jr. and Bates, J.K., 1987. Transport and reaction kinetics at the glass/solution interface region: results of repository-oriented leaching experiments. In Scientific Basis for Nuclear Waste Management X, Eds. J.K. Bates and W.B.Seefeldt, MRS, Pittsburgh, PA. pp.533-546.

Adams, P.B., 1984. Glass corrosion: a record of the past? a predictor of the future? J. Non-Cryst. Solids, v. 67, pp.193-205.

Ailin-Pyzik, I.B. and Sommer, S.E.,1981. Microscale chemical effects of low temperature alteration of DSDP Basaltic glasses. Jour. Geophys. Res., v.86, No. B10, pp.9503-9510.

Akabane, N. and Kurosawa, A., 1958. Sidicic acid solutions, 1, system of SiO_2, NaOH, $CaCl_2$ and H_2O. Chem. Society (Japan) Journal, v.61, pp.303.

Allen, C.C., 1982. Stability and alteration of naturally occuring low-silica glasses: Implications for the long-term stability of waste from glasses. In Scientific Basis for Nuclear Waste Management V, ed. W. Lutze, North Holland, NY.

Andrews, A.J., 1977. Low temperature fluid alteration of

oceanic layer 2 basalts, DSDP Leg 37. Can. J. Earth. Sci. v.14, pp.991-926.

Andrews, A.J., 1978. Petrology and geochemistry of alteration in layer 2 basalts. Ph.D. Dissertation, University of Western Ontario.

Apted, M.J., Mcvay, G.L., and Wald, J.W., 1986. Release of actinides from defense waste glass under simulated repository conditions. Nuclear Tenchnology, v.73, pp.165-178.

Bacon, F.R. and Raggon, F.C., 1959. Promotion of Attack on glass and silica by citrate and other anions in neutral solutions. Jour. Am. Ceram. Soc., v.42, No.4, pp.199-205.

Balshaw, K.M., 1980. Cenozoic clay-mineral stratigraphy in the South Philippine Sea, DSDP Leg 59. In L. Kroenke, R. Scott et al., Init. Repts. DSDP, 59: Washington (U.S. Govt. Printing Office), pp.597-602.

Banba, T. and Murakami, T., 1985. The leaching behavior of a glass waste form - Part II: the leaching mechanisms. Nucl. Tech., v.70, pp.243-248.

Banba, T., Murakami, T., and Kimura, H., 1987. The leaching behavior of a glass waste form - Part III: the mathematical leaching model. Nucl. Tech., v.76, pp.84-90.

Banfield, J.F. and Eggleton, R.A. 1989, The weathering of granitic plagioclase, included muscovite lamellae, and K-feldspar: an electron microscope study. Clays and Clay Minerals, in press.

Baragar, W.A., Plant, A.G., Pringle, G.J., and Schau, M.,

1977. The petrology of alteration in three discrete flow units of Sites 332 and 335, In Initial Reports of Deep-sea Drilling Project vol.37, eds. F. Aumento, W.G. Melson, et al. Washington (U.S. Government Printing Office) pp.811-820.

Barkatt, A., Boulos, M.S., Barkatt, Alisa, Sousanpour, W., Boroomand, M.A., Maccdo, P.B., and O'Keefe, J.A., 1984. The chemical durability of tektites - A laboratory study and correlation behavior. Geochimica et Cosmochimica Acta, v.48, pp.361-371.

Barkatt, A., Gibson, B.C., Macedo, P.B., Montrose, C.J., Sousanpour, W., Barkatt, Alisa, Boroomand, M-A., Roders, V., and Penafiel, M. 1986, Mechanism of defense waste glass dissolution. Nucl. Tech. v.73, pp.140-164.

Berner, R.A. and Holdren, G.R.,Jr., 1977. Mechanisms of feldspar weathering: some observational evidence. Geology 5, pp.369-372.

Blum, A. and Lasaga, A. 1988. Role of surface speciation in the low-temperature dissolution of minerals. Nature, v.331, pp.431-433.

Boksay, Z. and Bouquet, G., 1980. The pH dependence and an electrochemical interpretation of the dissolution rate of a silicate glass network. Physics and Chemistry of Glass, v.21, No.3, pp.110-113.

Bonatti, E., 1965. Palagonite, hyaloclastites and alteration of volcanic glass in the ocean. Bull. Volc. v.28, pp.3-15.

Bradley, D.J., Harvey, C.O., and Turcatte, R.P., 1979.

Leaching of actinites and tecnetium from simulated high-level waste glass PNL-3152, Pacific Northwest Laboratory, Richland, WA.

Braithwaite, J.W., 1980. Brine chemistry effects on the durability of a simulated waste glass, In Scintific Basis for Nuclear Waste Management II, eds. Clyde, J.M., Northrup, Plenum Press, New York, pp.199-207.

Brindley, G.W., 1955. Stevensite, a montmorillonite-type mineral showing mixed-layer characteristics. Am. Miner. v.40, pp.239-247.

Brookins, D.G., 1984, Geochemical aspects of radioactive waste disposal, Springer-Verlag, N.Y. 347p.

Budd, S.M., 1961. The mechanisms of chemical reaction between silicate glass and attacking agents, Part 1., Electrophilic and Nuclephilic Mechanisms of Attack. Phys. Chem. Glasses, vol.2, pp.111-115.

Bunker, B.C., Arnold, G.W., Beauchamp, E.K., and Day, D.E., 1983. Mechanisms for alkali leaching in mixed-Na-K silicate glasses. J. Non-Cryst. Solids, v.58, pp295-322.

Bunker, B.C., 1986. Solution chemistry of silicate and borate materials . In Better Ceramics Through Chemistry II, Eds. C.J. Brinker, D.E. Clark, and D.R. Ulrich, MRS. Pittsburgh, PA, pp.49-56.

Bunker, B.C., 1987. Waste glass leaching: chemistry and kinetics. In Scientific Basis for Nuclear Waste Management X, Eds. J.K. Bates and W.B. Seefeldt, MRS, Pittsburgh, PA, pp.493-507.

Byerly, G.R. and Sinton, J.M., 1979. Compositional trends in natural basaltic glasses from DSDP holes 417D and 418A. In: Initial Reports of the Deep Sea Drilling Project 53., Donnelly, T., Franchetau, J., et al. Eds., U.S. Govt. Printing Office, Washington, D.C., Part 2, pp.957-971.

Byers, C.D., Jercinevic, M.J., Ewing, R.C., and Keil, K., 1985. Basalt glass: An analogue for the evaluation of the long-term stability of nuclear waste from borosilicate glasses, Mat. Res. Soc. Symp. Proc., vol.44, pp.583-590.

Byers, C.D., Jercinovic, M.J., and Ewing, R.C., 1987. A study of natural glass analogues as applied to alteration of nuclear waste glass. NUREG/CR-4842, Argonne National Laboratory.

Chick, L.A. and Pederson, L.R., 1984. The relationship between reaction layer thickness and leach rate for nuclear waste glasses. Mat. Res. Soc. Symp. Proc.26, Elsevier Science Publishing Co., Inc. pp.635-642.

Chou, L. and Wollast, R., 1985. Steady-state kinetics and dissolution mechanisms of albite. A.J.Sci., v.285, pp.963-993.

Christensen, H., Hermansson, H.P., Clark, D.E., and Werme, L., 1984. Surface reactions occurring on simulated nuclear waste glass immersed in aqueous solutions containing bentonite, granite, and stainless-steel corrosion products. In Advances in Ceramics vol.8, Eds. G.G. Wicks and W.A. Ross, The American Ceramic Soc. Columbus, Ohio, pp.346-357.

Clark, D.E., Dilmore, M.F., Ethridge, E.C., and Hench, L.L.,

1976. Aqueous corrosion of soda-silica and sods-lime-silica glass. J. Am. Ceram. Soc., pp.62-65.

Clark, D.E. and Hench, L.L., 1983. Theory of corrosion of alkali-borosilicate glass. Mat. Res. Soc. Symp. Proc. v.15, Elsevier Science Publishing Co., Inc. Pittsburgh, PA, pp.113-124.

Conradt, R., Roggendorf, H., and Scholze, H., 1985. Investigations on the role of surface layers in HLW glass leaching. Mat. Res. Soc. Symp. Proc. v.50, Pittsburgh, PA, pp.203-210.

Crovisier, J.L., Thomaosin, J.H., Juteau, T., Eberhart, J.P., Touray, J.C., and Baillif, P., 1983. Experimental seawat.. basaltic glass interation at 50°C: Study of early developed phases by electron microscopy and x-ray photoelectron spectrometry. Geochi. Cosmochi. Acta v.47, pp.377-387.

Crovisier, .L., Fritz, B., Grambow, B., and Eberhart, J.P., 1986. Dissolution of basaltic glass in seawater: experiments and thermodynamic modelling. In Scientific Basis For Nuclear Waste Management IX, ed. L.Werme, MRS, Pittsburgh, PA, pp.273-280.

Davis, J.A. and Hayes, K.F., 1986. Geochemical processes at mineral surfaces. ACS Symposium Series, No.323, pp.672.

Dickin, A.P., 1981. Hydrothermal leaching of hyolite glass in the environment has implication for nuclear waste disposal. Nature, v.294, pp.342-347.

Dlouhy, Z., 1982, Disposal of radioactive wastes, Elsevier Sci. Pub. Co., N.Y., 264p.

Doremus, R.H., 1975. Interdiffusion of hydrogen and alkali ions in a glass surface. J. Non-Cryst. Solids., v.19, pp. 137-144.

Douglas, R.W. and El-shamy, T.M.M., 1967. Reaction of glass with aqueous solutions. Jour. Am. Ceram. Soc., vol.50, No.1, pp.1-8.

Dugger, D.L., Stanton, J.H., Irby, B.N., McConnell, B.L., Cummings, W.W., and Maatman, R.W., 1964, The exchange of twenty metal ions with the weakly acidic silanol group of silica. Jour. Phy. Chem. V.68, pp.757-760.

Eggleton, R.A., and Keller, J., 1982. The palagonitization of limburgite glass-A TEM study. N. Jb. Miner. Mh. H.7, pp. 321-336.

Ewing, R.C., 1979. Natural glasses: Analogues for radioactive waste forms, in: Scientific Basis for Nuclear Waste Management vol.I, ed. McLarthy, G.J., Plenum Press, N.Y., pp.57-68.

Ewing, R.C. and Jereinovic, M.J., 1987. Natural analogues: their applications to the prediction of the long-term behavior of nuclear waste forms. Mat. Res. Soc. Symp. Proc. v.84, pp.67-83.

Eyring, H., 1935. The activated complex in chemical reactions. Jour. Chem. Phy., v.3, pp.107-115

Faust, G.T. and Murata, K.J., 1953. Stevensite, redefined as a member of the montmorillonite group. Amer. Mineral., v.38, pp973-987.

Feng, X. and Barkatt, A., 1988. Structural thermodynamic

model for the durability and viscosity of nuclear waste glasses. Mat. Res. Soc. Symp. Proc., v.112, Pittsburgh, PA, pp.732-742.

Feng, X., Barkatt, A., and Jiang, T., 1988. Systematic composition studies on the durability of waste glass WV205. Mat. Res. Soc. Symp. Proc. v.112, Pittsburgh, PA, pp.673-683.

Fisher, R.V. and Schmincke, H-U, 1984. Pyroclastic Rocks, Springer-Verlag, Berlin, Heideberg, 472p.

Fournier, R.O. and Rowe, J.J., 1977. The solubility of amorphous silica in water at high temperatures and high pressures. Am. Mineral., v.62, pp.1052-1056.

Freude, E., Grambow, B., Lutze, W., Rabe, H., and Ewing, R.C., 1985. Long-term release from high level waste glass Part IV: the effect of leaching mechanism. Mat. Res. Soc. Symp. Proc. v.44, Pittsburgh, PA, pp.99-106.

Furnes, H., 1974. Volume relations between palagonite and authgenic minerals in hyaloclastites and its bearing on the rate of palagonization. Bull. Volc., v.38, pp.173-186.

Furnes, H., 1975, Experimental palagonitization of basaltic glasses of varied composition. Contrib. Mineral. Petrol., vol.50, pp.105-113.

Furnes, H., 1978. Element mobility during palagonitization of a subglacial hyaloclastite in Iceland. Chemical Geology, v.22, pp.249-264.

Furnes, H., 1980. Chemical changes during palagonitization of an alkali olivine basaltic hyaloclastite, Santa Maria,

Azores. N. Jb. Min. Abh., v.138, pp. 14-30.

Furnes, H., and Mohamed, I.H.El-Anbaawy., 1980. Chemical changes and authigenic mineral formation during palagonitization of a basanite hyaloclastite, Gran Canaria, Canary Islands. Neues Jahrbuch Fur Mineralogic Abhandlangen, v.139, No.3, pp. 279-302.

Goto, K., 1955. Solubility of amorphous silica. J. Chem. Soc. Japan, v.76, pp.1364-1366.

Grambow, B., 1984. Geochemical modeling of the reaction between glass and aqueous solution. In Advances in Ceramics Vol.8, Eds. G.G.Wicks and W.A.Ross, The Am.Ceram.Soc., Columbus, Ohio, pp.474-489.

Grambow, B., 1985, A general equation for nuclear waste glass corrosion, In Scientific Basis for Nuclear Waste Management VIII, eds. C.M. Jantzen, J.A. Stone and R.C. Ewing, MRS, Pittsburgh, PA, pp.15-27.

Grambow, B., Jercinovic, M.J., Ewing, R.C., and Byers, C.D., 1986. Weathered basalt glass: a natural analogue for the effects of reaction progress on nuclear waste glass alteration. Mat. Res. Soc. Symp. Proc. v.50, pp.263-272.

Grambow, B., 1987. Nuclear waste glass dissolution: mechanism, model and application. JSS Project 87-02, SKB, Stockholm, 68p.

Grauer, R., 1985. Synthesis of recent investigations on corrosion behavior of radioactive waste glasses. EIR-Report No.538, Swiss Federal Institute for Reactor Research.

Gresens, R.L., 1967. Composition-volume relationships of

metasomatism. Chem. Geol., v.2, pp.47-65.

Harvey, K.B., Litke, C.D., and Boase, C.A., 1984. Diffusion-based leaching models for glassy waste forms. In Advances in Ceramics Vol.II, eds. Wicks, G.G. and Ross, W.A., The American Ceramic Society, Columbus, Ohio, pp.496-508.

Hay, R.L. and Iijima, A., 1968. Nature and origin of palagonite tuffs of the Honolulu Group on Oahu, Hawaii. Geol. Soc. Amer. Mem(oirs)., v.116, pp. 338-376.

Hay, R.L. and Iijima, A., 1968. Petrology of palagonite tuffs of KOKO Craters, Oahu, Hawaii. Contr. Mineral. and Petrol., v.17, pp.141-154.

Hein, J.R. and Scholl, D.W., 1978. Diagenesis and dissolution of late Cenozoic volcanic sediment in the southern Bering Sea. Geo. Soc. Am. Bull., v.89, pp.197-210.

Hermansson, H.P., Hilbert, C., Clark, D.E., and Werme, L., 1983. Effects of solution chemistry and atmosphere on leaching of alkali borosilicate glass, In Scientific Basis for Nuclear Waste Management VI, Ed. D.G. Brookins, North Holland Pub. Co. N.Y., pp.143-145.

Hollister, C.D., Anderson, D.R., and Heath, G.R., 1981. Subseabed disposal of nuclear wastes, Science, v.213, pp.1321-1325.

Honnorez, J., 1972. La palagonitization, l'alteration sous marine du verre volcanique basique de palagonia(sicile). Birkhauser verlag basel and styttgart, 132p.

Honnorez, J., 1978. Generation of phillipsites by palagonitization of basaltic glass in SEA water and the origin of

K-rich deep-sea sediments. In Natural Zeolites-Occurrence, Properties, Uses, eds. Sand, L.B. and Mumpton, F.A., Pergamon Press, Oxford and New York, pp.245-258.

Honnorez, J., 1981. The aging of the oceanic lithosphere. In The Oceanic Lithosphere, Eds. E.Emiliani, The Sea, vol.7, J. Wiley, N.Y., pp.525-567.

Hyndman, R.D., Von Herzen, R.P., Erickson, A.J., and Jolivet, J., 1977. Heat flow measurement, DSDP Leg 37, In Initial Reports of the DSDP vol.37, eds. F.Aumento, W.G. Melson, et al., Washington (U.S. Government Printing Office) pp.347-362.

Iler, R.K., 1973, Effect of adsorbed alumina on the solubility of amorphous silica in water. J. Colloid. Interface Sci., v.43, pp.399-408.

Isard, J.O. and Muller, W., 1986. Influence of alkaline earth ions on the corrosion of glasses. Phys. Chem. Glasses, vol.27, pp.55-58.

Jakobsson, S.P. 1978, Environmental factors controlling the palagonitization of the Surtsey Tephra, Iceland. Bull.Geol. Soc. Denmark, v.27 (spec. iss.), pp.91-105.

Jakobsson, S.P. and Moore, J.G., 1986. Hydrothermal minerals and alteration rates at Surtsey Volcano, Iceland. Geol. Soci. Am. Bull, v.97, pp.648-655.

Jantzen, C.M. and Plodinec, M.J., 1984. Thermodynamic model of natural and nuclear waste and medieval and nuclear waste glass durability. J. Non-Cryst. Solids, v.67, pp.207.

Jenne, E.A., 1979. Chemical modeling-goals, problems,

approaches, and priorities. In Chemical Modeling in Aqueous Systems, Eds. E.A. Jenne, ACS symposium series, ACS, Washington, D.C., pp.1-21.

Kenna, B.T. and Murphy, K.D., 1980. Mechanism for elevated temperature leaching. In Scientific Basis for Nuclear Waste Management II, ed. C.J.M. Northrup, Jr., Plenum, New York, pp.191-198.

Kuhn, W.L. and Peters, R.D., 1983. Leach models for a commercial nuclear waste glass, Mat. Res. Soc. Symp. Proc., vol.15, pp.167-174.

Kullenberg, G., 1986. The role of the oceans as a waste disposal option. NATO ASI Series, D.Reidel Publishing Company, Holland, pp.725.

Langseth, M. G., and Mrozowski, C.L., 1980. Geophysical survey for Leg 59 Sites, DSDP. In Kroenke, L., Scott, R., et al., Init. Repts. DSDP, 59: Washington(U.S. Govt. Printing Office), pp.487-501.

Lanza. F. and Parnisari, S., 1979. Evaluation of long-term leaching of borosilicate glass in pure water CONF-790420, U.S. Department of Energy, Washington, D.C.

Lee, S.Y., Jackson, M.L., and Brown, J.L., 1975. Micaceous inclusions in kaolinite observed by ultramicrotomy and high resolution electron microscopy. Clay and Clay Minerals, v.23, pp.125-129.

Lee, C.T. and Clark, D.E., 1985. Electrokinetics, adsorption and colloid study of simulated nuclear waste glasses leached in aqueous solutions. Mat. Res. Soc. Symp. Proc.

v.44, pp.221-228.

Lokken, R.O. and Strachan, D.M., 1984. Long-term leaching of two simulated waste glasses, in :Advances in Ceramics, v.8, Nuclear Waste Management, The American Ceramic Soc. Columbus, Ohio, pp.39-48.

Lutze, W., Malow, G., Ewing, R.C., Jercinovic, M.J.,and Keil, K., 1985. Alteration of basalt glasses: Implications for modelling the long-term stability of nuclear waste glasses. Nature, v.304, pp.252-255.

Lutze, W., Grambow, B., Ewing, R.C., and Jercinovic, M.J., 1987. The use of natural analogues in the long-term extrapolation of glass corrosion processes. In Natural Analogues in Radioactive Waste Disposal. Eds. B.Come and N.A.Chapman, Graham and Trotman, Oxford, 192p.

Malow, G and Ewing, R.C., 1981. Nuclear waste glasses and volcanic glasses: A composition of their stabilities, in: Scientific Basis for Nuclear Waste Management. Moore, J.G., Ed., v.3, Plenum Press.

Malow, G., 1982. The mechanisms for hydrothermal leaching of nuclear waste glasses: properties and evaluation of surface layers. In Scientific Basis for Nuclear Waste Management V, Eds. W. Lutze, MRS, North-Holland, N.Y., pp.25-36.

Malow, G., Lutze, W., and Ewing, R.C., 1984. Alteration effects and leach rates of basaltic glasses: Implications for the long-term stability of nuclear waste from borosilicate glasses. J. Non-Crystalline Solids, v.67, No.1-3, pp.305-322.

Marshall, W.L. and Warakomski, J.M., 1980. Amorphous silica solubility-II. Effect of aqueous salt solutions at 25°C. Geochimica et Cosmochimica Acta, v.44, pp.913-921.

McGrail, B.P., Sodium diffusion and leaching of simulated nuclear waste glass, Journal of American Ceramic Soc., v. 67(7), pp.463-467.

Melson, W.G. and Thompson, G. 1973. Glassy abyssal basalts, Atlantic sea floor near St. Paul's Rock: petrography and composition of secondary clay minerals. Geol. Soc. Am. Bull., v.84, pp.703-716.

Mendel, J.E., et al., 1981. A state-of-the-art review of materials properties of nuclear waste forms. PNL-3802, Pacific Northwest Laboratory, Richland, Washington.

Mendel, J.E., et al., 1984. Final report of the defense high -level waste leaching mechanism program. PNL-5157, Pacific Northwest Laboratory, Richland, Wa, USA.

Miles, G.A. and Howe, R.C., 1977. Biostratigraphic Summary, Deep Sea Drilling Project Leg 37. in Aumento, F., Melson, W.G. et al., Initial Reports of DSDP Vol. 37, Washington (U.S. Government Printing Office). pp.968-977.

Moore, J.G., 1966. Rate of palagonitization of submarine basalt adjacent to Hawaii. U.S.G.S. Prof. Paper, 550D, D163-D171.

Morgenstein, M. and Riley, T.J., 1975. Hydration-rind dating of basaltic glass: a new method for archeological chronologies. Asian Perspectives, v.17, pp.154-159.

Muehlenbachs, K. and Clayton, R.N., 1972. Oxygen isotope

geochemistry of submarine greenstones. Can. J. Earth Sci., v.9, pp.471-478.

Muehlenbachs, K., 1977. Oxygen isotope geochemistry of rocks from DSDP Leg37., Can. J. Earth Sci., v.14, pp.771-776.

Muir, I.J., Bancroft, G., and Nesbitt, H.W., 1989. Characteristics of altered labradorite surfaces by SIMS and XPS. Geochimica et Cosmochimica Acta, In press.

Murakami, T. and Banba, T., 1984. The leaching behavior of a glass waste form - Part I: the characteristics of surface layers. Nucl. Tech., v.67, pp.419-428.

Nesbitt, H.W. and Muir, I.J., 1988. SIMS depth profiles of weathered plagioclase and processes affecting dissolved Al and Si in some acidic soil solutions. Nature, v.334, pp. 336-338.

Oka, Y., Ricker, K.S., and Tomozawa, M., 1979. Calcium deposition on glass surface as an inhibitor to alkaline attack. J. Am. Ceram. Soc., v.62, pp.631-632.

Parkhurst, D.L., Thorstenson, D.C., and Plummer, L.N., 1980. PHREEQE - a computer program for geochemical calculations. U.S. Geological Survey, Water-Resources Investigations, Reston, Virginia, pp.80-96.

Paul, A., 1977. Chemical durability of glasses: a thermodynamic approach. J. Mat. Sci., v.12, pp.2246-2268.

Paul, A., 1982. Chemistry of glasses. Chapman and Hall, New York, 126p.

Peacock, M.A., 1926. The petrology of Iceland, Part1, the basic tuffs. Royal Society of Edinburgh, Transactions,

v.55, pp.53-76.

Peacock, M.A. and Fuller, R.E., 1928. Chlorophaeite, sideromelance and palagonite from the Columbia River Plateau. Am. Mineral. v.13, pp.306-382.

Pederson, L.R., Buckwalter, C.Q., McVay, G.L., and Riddle, B.L., 1983. Glass surface area to solution volume ratio and its implications to accelated leach testing. in Scientific Basis for Nuclear Waste Management VI, ed. Brookins, D.G. North-Holland, N.Y., pp47-54.

Pentreath, R.J., 1980, Nuclear power, man and the environment, London: Taylor and Francis.

Plodinec, M.J., Wicks, G.G., and Bibler, W.E., 1982. An assessment of Savannah River borosilicate glass in the repository environment, DP-1629.

Ramanaidou, E. and Noack, Y., 1987. Palagonites of the Red Sea: a new occurrence of hydroxysulphate. Min. Magazine, v.51, pp.139-143.

Rautenschlein, M., Jenner, G.A., Hofmann, A.W., Kerrich, R., Schmincke, H.-U., and White, W.M., 1985. Isotopic and trace element composition of volcanic glasses from the akaki Canyon, Cyprus: implications for the origin of the Troodos Ophiolite. Earth and Plan. Sci. Lett., v.75, pp.369-383.

Robinson, R.A. and Stokes, R.H., 1965, Electrolyte solutions, 2nd ed. Butterworth, London, 571p.

Robinson, P.T., Flower, M.F.J., Schmincke, H., and Ohnmacht, W., 1977. Low temperature alteration of oceanic basalts, DSDP Leg 37. In F. Aumento, W.G. Melson et al., Init. Repts

of DSDP, v.37. Washington (U.S. Govnt. Printing Office), pp.775-794.

Robinson, P.T., Melson, W.G., O'Hearn, T., and Schmincke, H-U., 1983. Volcanic glass compositions of the Troodos Ophiolite, Cyprus. Geology, v.11, pp.400-404.

Ross, W.A., et al., 1978. Annual report on the characterization of high-level waste glasses, PNL-2625, Pacific Northwast Laboratory, Richland, Washington.

Salter, P.F. and Jacobs, G.K., 1982. Evaluation of radionuclide transport: effect of radionuclide sorption and solubility. In Scientific Basis for Nuclear Waste Management V, ed. W. Lutze, pp.801-810.

Scheetz, B.E., Freeborn, W.P., Smith, D.K., Anderson, C., Zolensky, M., and White, W.B., 1985. The role of boron in monitoring the leaching of borosilicate glass waste forms. Mat. Res. Soc. Symp. Proc. vol.44, pp.129-134.

Schmincke, H-U., 1981. Ash from vitric muds in deep sea cores from the mariana trough and fore-arc regions (South Philippine Sea) (Sites453, 454, 455, 458, 459), in: Init. Repts. Deep Sea Drilling Project, v.60, pp.473-481.

Scott, R.B. and Hajash, A. JR, 1976. Initial submarine alteration of basaltic pilliow lavas: a microprobe study. Am. J. of Sci. v.276, pp.480-501.

Shade, J.W., Pederson, L.R., and McVay, G.L., 1984. Waste glass-metal interations in brines. In Advances in Ceramics vol.8, Eds. G.G.Wicks and W.A.Ross, The Am. Ceramic. Soc. Columbus, Ohio, pp.358-367.

Shido, F., Miyashiro, A. and Ewing, M., 1974. Compositional variation in pillow lavas from the Mid-Atlantic Ridge. Marine Geol., v.16, pp. 177-190.

Singer, R, A., 1974. Mineralogy of palagonitic material from the Golan Heights, Israel. Clay and Clay Minerals, v.22, pp. 231-240.

Smets, B.M.J. and Lommen, T.P.A., 1983. The role of molecular water in the leaching of glass. Phys. Chem. Glasses, v.24, pp.35.

Smets, B.M.J. and Tholen, M.G.W., 1985. The pH dependence of the aqueous corrosion of glass. Phys.Chem.Glasses, vol.26, pp.60-63.

Sombret, C.G., 1985. The vitrification of high level radioactive wastes in France. Nucl. Energy, v.24, pp.85-98.

Staudigel, H., Fray, F.A., and Hart, S.R., 1979. Incompatible trace element geochemistry and $^{87}Sr/^{86}Sr$ in basalts and correspoding glasses and palagonites. in: Initial Reports of the Deep Sea Drilling Project 51, 52, 53, Donnelly, T. Franchetau, J., et al.) U.S. Govt. Printing Office, Washington, D.C., v.2, pp.1137-1143.

Staudigel, H., Hart, S.R., and Richardson, S.H., 1982. Ateration of oceanic crust: processes and timing. Earth Plant. Sci. Lett., v.52, pp.311-327.

Staudigel, H. and Hart, S.R., 1983. Alteration of basaltic glass: mechanisms and significance for the oceanic crust -sea water budget. Geochimica et Cosmochimica Acta, v.47, pp.337-350.

Stokes, K.R., 1971. Further investigations into chlorophaeite and palagonite. Mineralogical Magazine, v.38, pp. 205-214.

Strachan, D.M., Turcotte, R.P., and Barnes, B.O., 1982. MCC-1: A standard test for nuclear waste forms. Nucl.Tech., v.56, pp.306.

Strachan, D.M., 1983. Results from long-term use of the MCC-1 static leach test method. Nucl. Chem. Waste Manag. v.4, pp.177-188.

Strachan, D.M., Pederson, L.R., and Lokken, R.O., 1985. Results from the long-term interation and modelling of SRL -131 glass with aqueous solutions. Mat. Res. Soc. Symp. Proc., v.50, pp.195-202.

Stumm, W. and Morgan, J.J., 1981. Aquatic chemistry. 2nd Ed. John Wiley and Sons, New York, 780p.

Thompson, G., 1983. Basalt-seawater reaction. In Hydrothermal Processes at Seafloor Spreading Centers, P.A. Rona, K. Bostrom, L. Laubier and K.L. Smith eds. NATO Conf. Ser.4, v.12, New York, Plenum Press, pp.225-278.

Trichet, J., 1969. Contribution a l'alteration experimentale des verres volcaniques. Ph.D. thesis, Faculty of Sciences, Paris.

Trichet, J., 1972. Contribution a l'Etude de l'Alteration Experimentale des verres volcaniques. Publ.4, Ecole Normale Superieure, Paris.

Tsong, T.S.T., Houser, C.A., Yusef, N.A., Messier, R.F., White, W.B., and Michells, J.W., 1978. Obsidian hydration profiles measured by sputter-induced optical emission.

Science, v.201, pp.339-340.

van der Gaast, S.J., Mizota, C., and Jansen, J.H.F., 1986. Curved smectite in soils from volcanic ash in Kenya and Tanzania: a low-angle x-ray powder diffraction study. Clays and Clay Minerals, v.34, pp.665-671.

Wallace, R.M. and Wicks, G.G., 1983. Leaching chemistry of defense borosilicate glass, in: Scientific Basis for Nuclear Waste Management VI, Brookins, D.G., Ed., North Holland Publishing Company, New York, p.23.

Wsatsik, J.H., Jr., and Harvey, C.O., 1979. High temperature leaching of a simulated high-level waste glass, PNL-3172, Pacific Northwest Laboratory, Richland, WA.

Wentworth, C.K., 1938. Ash formations on the island Hawaii. Hawaii Volcano Observatory 3rd Special Report, Honolulu, Hawaiian Volcano Research Association, 173p.

Wicks, G.G., O'Rourke, P.E., and Whitkop, P.G., 1982. The chemical durability of Savannah River Plant waste glass as a function of groundwater pH, DPMS-81-104, Sawannah River Laboratory.

Wiley, J.R., 1979. Leach rates of high activity waste borosilicate glass. Nucl. Tech., vol.43, pp.268-272.

Wisw, S.W., Weaver, F.M., and Guven, N., 1973. Early silica sedimentary rocks: Devitification and replacement phenomena. In: Proceedings, 31st Ann. Mett. of the Electron Microscopy Soc. Am. Claitor's Publishing Division, Baton Rouge, Louisiana, Arceneaux, C.J., Ed., pp.206-207.

Wise, Jr., S., and Weaver, F., 1979. Volcanic ash: examples

of devitrification and early diagensis. In: Scanning Electron Microscopy, I. SEM Inc., AMF O'Hare, Illinois, pp.511-518.

Zhou, Z., Fyfe, W.S., and K. Tazaki, 1987. Glass Stability in Marine Environments. In Natural Analogues of Radioactive Waste Disposal, eds. B. Come and N.A. Chapman, Graham & Trotman, CEC, pp.153-163.

Zhou, Z. and Fyfe, W.S., 1988, A comparative experimental study on glass stability in distilled water and sea water. In Scientific Basis for Nuclear Waste Management XI, eds. M.I. Apted and R.E. Westerman, North Holland, N.Y., pp725-735.

Zhou, Z. and Fyfe, W.S., 1989. Palagonitization of basaltic glass from DSDP Site 335: texture, chemical composition, and mechanism of formation. Am. Mineral., in press.

Zhou, Z., Fyfe, W.S., van der Gaast, S.J., and Tazaki, K., 1989. The micro-structure of palagonite of DSDP Site 335, Leg 37, to be submitted to Clays and Clay Minerals.